Electronic Theses and Dissertations

Theses, Dissertations, and Major Papers

2012

Numerical Investigation on Heat Transfer and Fluid Flow Behaviors of Viscous Fluids through Minichannel Heat Exchanger

Mohammed Ismail
University of Windsor

Follow this and additional works at: https://scholar.uwindsor.ca/etd

Numerical Investigation on Heat Transfer and Fluid Flow Behaviors of Viscous Fluids
through Minichannel Heat Exchanger

by

Mohammed Ismail

A Thesis
Submitted to the Faculty of Graduate Studies
through Mechanical, Automotive, and Materials Engineering
in Partial Fulfillment of the Requirements for
the Degree of Master of Applied Science at the
University of Windsor

Windsor, Ontario, Canada

2012

Numerical Investigation on Heat Transfer and Fluid Flow Behaviors of Viscous Fluids

through Minichannel Heat Exchanger

by

Mohammed Ismail

APPROVED BY:

_____
Dr. Sreekanta Das
Department of Civil and Environmental Engineering

_____
Dr. Biao Zhou
Department of Mechanical, Automotive and Materials Engineering

_____
Dr. Amir Fartaj, Advisor
Department of Mechanical, Automotive and Materials Engineering

_____
Dr. David Ting, Chair of Defense
Department of Mechanical, Automotive and Materials Engineering

June 15, 2012

DECLARATION OF ORIGINALITY

I hereby certify that I am the sole author of this thesis and that no part of this thesis has been published or submitted for publication.

I certify that, to the best of my knowledge, my thesis does not infringe upon anyone's copyright nor violate any proprietary rights and that any ideas, techniques, quotations, or any other material from the work of other people included in my thesis, published or otherwise, are fully acknowledged in accordance with the standard referencing practices. Furthermore, to the extent that I have included copyrighted material that surpasses the bounds of fair dealing within the meaning of the Canada Copyright Act, I certify that I have obtained a written permission from the copyright owner(s) to include such material(s) in my thesis and have included copies of such copyright clearances to my appendix.

I declare that this is a true copy of my thesis, including any final revisions, as approved by my thesis committee and the Graduate Studies office, and that this thesis has not been submitted for a higher degree to any other University or Institution.

ABSTRACT

Miniature heat exchanger concept is gaining popularity in automotive and other industrial applications due to enhanced heat flux, light weight, and larger heat transfer area density compared to conventional heat exchangers. Heat transfer and flow characteristics of different viscous liquids, such as engine oil, automatic transmission fluid, 50% ethylene glycol, and Deionized water were numerically analyzed through a multi-port serpentine minichannel heat exchanger (MICHX). Hot liquids of different flow rates at constant temperature of 76°C were cooled by a constant air temperature of 14°C and flow rate of 507g/s. The heat transfer performance of engine oil was found poor compared to other fluids. Pressure drop in MICHX for engine oil was also found extremely higher compared to water. However, the distribution of temperature, mass flow rate, and heat transfer rate in each channel is more even for high-viscosity fluids compared to low-viscosity fluids. The entrance region effects in thermal and flow fields for high-viscosity fluids were observed negligible.

DEDICATION

Dedicated to my beloved

Father: Late Md Abdul Jalil,

Mother: Zohara Khatoon,

Wife: Shamima Akhter, and

Sons: Aljami Ismail and Miraj Ismail

who are the source of my inspiration and strength.

ACKNOWLEDGEMENTS

First and foremost, I am greatly thankful to the Almighty for the wisdom and perseverance that He has been bestowed upon me through this research work. It is my pleasure to express deep appreciation to Dr. Amir Fartaj for his sincere guidance, advice, and continuous support throughout the research works. Without his expert guidance, successful completion of this research would not be possible.

I would also like to express my sincere gratitude to Dr. Biao Zhou and Dr. Sreekanta Das for accepting to be my thesis committee members. University of Windsor is acknowledged for the financial support through the GA and scholarship opportunities. I am deeply acknowledging the cordial support and services of Ms. Rose Gignac and Ms. Barbara Tattersall during the research work with the Department of Mechanical, Automotive, and Materials Engineering.

Appreciation and intense acknowledgement go to Serena Askar and Mo Karimi for reviewing my thesis and putting their valuable comments and directions in write-up. I would also like to extend my heartfelt appreciation to my colleagues Engr Sarbadaman Dasgupta, Abdul Quaiyum, Shahram Fotowat, and Mohammad Saadi for their assistance and cooperation.

Finally, I am sincerely indebted to my wife and children for their encouragement, inspiration and continuous support to my research.

TABLE OF CONTENTS

LIST OF TABLES

LIST OF FIGURES

NOMENCLATURE

A	Area, m^2
Br	Brinkman number
C_p	Specific heat capacity at constant pressure, $j/(kgK)$
D_{ch}	Hydraulic diameter of channel, m
D_h	Hydraulic diameter, m
d	Diameter of the tube, m
Da	Darcy number
De	Dean number
dN	Nozzles diameter, m
e/d	Relative roughness value
f	Fanning friction factor
G_l	Liquid mass flux, kg/ m²s
h_l	Liquid side heat transfer coefficient, $w/(m^2K)$
H_p	Porous fins height
H	Tube height, m
h	Heat transfer coefficient, $w/(m^2K)$
j	Colburn factor
j_a	Air-side Colburn factor
k_l	Thermal conductivity of liquid, $w/(mK)$
k	Thermal conductivity, $w/(mK)$
L_f	Fin spacing, m
L	Characteristic length, m

$\dot{m}_a$	Mass flow rate of air, kg/s
$\dot{m}_{ch}$	Mass flow rate of liquid in each channel, kg/s
$\dot{m}_L$	Mass flow rate of liquid, kg/s
$\dot{m}$	Mass flow rate, kg/s
M	$\dfrac{\mu_{eff}}{\mu}$
max	Maximum
min	Minimum
Nu	Nusselt number
Nu_a	Air-side Nusselt number
Nu_l	Liquid-side Nusselt number
n	Index behavior of shear thinning power law fluid
N	Number of channels
P	Pressure, kPa
Pr	Prandtl number
Q	Heat transfer rate, w
Re_a	Air-side Reynolds number
Re_l	Liquid-side Reynolds number
R_k	Thermal conductivity ratio
Re	Reynolds number
T	Temperature, $°C$
V	Velocity, m/s
W	Tube width, m

GREEK SYMBOLS

μ_{eff}	Effective viscosity, kg/ms
Δ	Difference
μ	Dynamic viscosity, kg/ms
ρ	Density, kg/m³
α	Tube aspect ratio $(= H/W)$

SUBSCRIPTS

a	Air
atf	Automatic transmission fluid
avg	Average
b	Bulk
eff	Effective
f	Fin
g	50% ethylene glycol
i	Inlet
l	Liquid
o	Outlet
m	Mean
s	Wall surface
ser	Serpentine
w	Water

ABBREVIATIONS

ATF	Automatic Transmission Fluid
CFD	Computational Fluid Dynamics
CMC	Carboxymethyl Cellulose
DAQ	Data Acquisition System
DFM	Digital Flow Meter
FS	Fused Silica
HB	Heat Balance
LBGK	Lattice Boltzmann Bhatnagar Gross Krook
MB	Mass Balance
MCHX	Microchannel heat exchanger
MICHX	Minichannel Heat Exchanger
PTD	Differential Pressure Transducer
RTD	Resistance Temperature Detector
SMCHX	Serpentine Meso-channel Heat Exchanger
SS	Stainless Steel
VLSI	Very Large Scale Integrated

CHAPTER I

INTRODUCTION

Researchers are very concerned regarding two important issues, namely energy and environment. Therefore, production and proper utilization of energy is the key to sustainable cost-effective development. The sources of energy, such as wind, hydroelectric, solar, biomass, geothermal, uranium (for nuclear power generation), coal, and ocean energy, are available in large quantities. However, the reserves of energy sources have been diminished day by day due to its continuous usages in domestic, industrial, and other sectors in everyday life. The highest impact on environment of any human activity has been made by the supply and implementation of energy that is the fundamental importance to society. Even though, energy and environment concerns were initially associated with local character, such as extraction, transportation, or noxious emissions, they have now extended to face national, regional, and global issues, such as acid rain and the greenhouse effect.

1.1 Background

One of the most important fields of energy is heat, which has a wide application in power generation, automotive and HVAC industries, nuclear industries, aerospace application, space research, marine and mining applications, chemical processing, petroleum, and many other areas. When heat energy is in use, heat transfer occurs either in heating or in cooling mode due to the temperature differences in the physical systems. Heat transfer is the most widespread phenomenon in various real world applications in energy conversion, transmission, and consumption. Appropriate devices allow easy heat transfer. Heat exchangers are the devices that exchange heat energy between two or more

fluids at different temperatures and in thermal contact in order to remove or to add heat as quickly as possible. In many heat exchangers, two fluids are separated by a wall through which the heat transfer occurs. Heat transfer can be defined as the transport of thermal energy from a hotter object to a cooler object. Some of the examples about heat exchangers are cooling towers, evaporators, condensers, car radiators, and pre-heaters.

Heat exchangers can be classified based on the working principles, geometry of construction, heat transfer mechanisms, fluid flow arrangements, and transfer processes. They can also be classified based on sizes and surface area to volume ratio. Based on channel dimensions, especially the characteristic length or hydraulic diameter, two main classification schemes are available in open the literature. One scheme was proposed by Mehendale et al (2000) as microchannels ($D_h = 1\mu m \sim 100\mu m$), meso-channels ($D_h = 100\mu m \sim 1mm$), compact ($D_h = 1mm \sim 6mm$), and conventional passage ($D_h > 6mm$). Another scheme was proposed by Kandlikar et al (2006) as conventional channels ($D_h > 3mm$), minichannels ($3mm \geq D_h > 200 \mu m$), microchannels ($200\mu m \geq D_h > 10\mu m$), transitional Microchannels ($10\mu m \geq D_h > 1\mu m$), transitional nanochannels ($1\mu m \geq D_h > 0.1\mu m$), and nanochannels ($0.1\mu m \geq D_h$). The heat exchanger used in the current study is classified as a mini-channel heat exchanger (MICHX) according to S. G. Kandlikar (2006) as the diameter of each channel falls within the range of 200μm to 3mm.

The MICHX used in the current study is built up by multi-port flat slab. There is no gap in between adjacent channels for fluid interaction. Flat heat transfer surfaces at the top and the bottom faces of each slab offer the air flow an excellent contact with the heating surfaces, which leads to elevated heat transfer over the conventional heat

exchangers of isolated tube rows. Flow, in a cross-flow orientation, over tubes in inline or staggered arrangement, which is widely used in many conventional heat exchangers applications forms a wake region at the rear of each tube when fluid is flowing over the tube. Where as, the effects of wake region behind the channels are very insignificant when air flows over the multi-port MICHX slab. Figures 1.1 and 1.2 illustrate the differences between tubes and monolithic channels structures inside heat exchanger core.
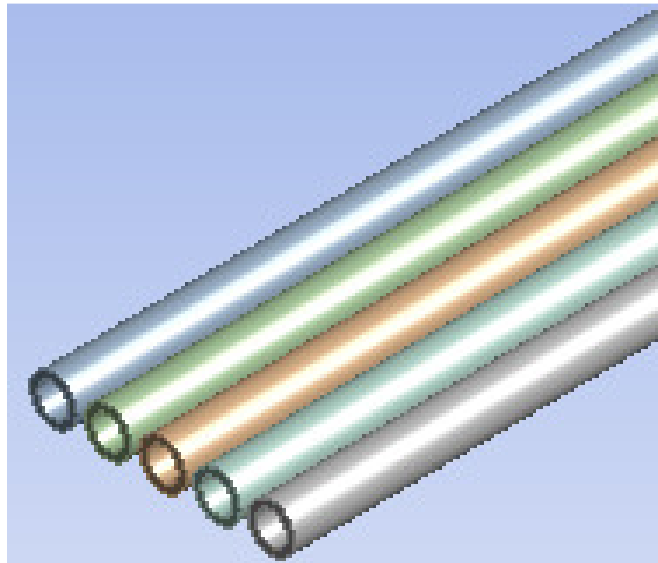
Figure 1.1. Circular tubes flow passages in heat exchanger core
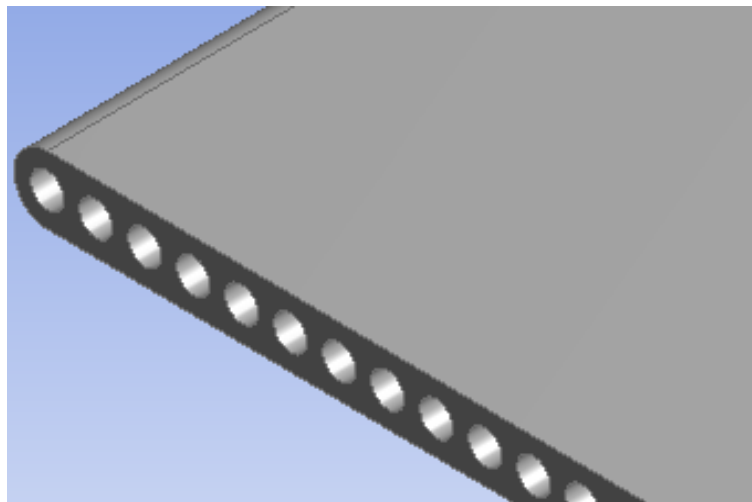
Figure 1.2. Circular channels inside the MICHX slab

Research and development in technology have been substituting existing equipment with lightweight, smaller, portable, thinner, and faster devices. Nevertheless, in fluid mechanics, these technological research and developments have need of more compact thermal solutions. As a result, the air conditioning industries have been experiencing continuous challenges to obtain higher efficiency levels and greater equipment reliability. However, these challenges become more difficult to meet the energy efficiency when the goal is simultaneously to reduce equipment size, and limit the cost (Keogh, 2007). In the past, manufacturers were used to meet the efficiency levels by improving and increasing the overall heat transfer area of the individual components, such as compressors, condensers, and evaporators (Ozdemir, 2009). Once Tuckerman and Pease (1981) first introduced a high-performance heat sink for a very-large-scale integrated (VLSI) circuits to remove heat from electronic circuits quickly and effectively, miniature heat exchangers became an emerging and innovative method in thermal applications.

Nowadays, in many specialized areas, such as microelectronics, robotics, aerospace, biomedical, and automotive applications, miniature heat exchangers with viscous fluids are widely used (Dehghandokht et al., 2011). Miniature heat exchangers have been becoming popular in engineering and industrial applications because of its enhanced heat transfer flux, light weight, larger heat transfer area density, less pollutant emission, less energy consumption, and increased reliability when compared to other traditional methods of heat exchange (Khan and Fartaj, 2011).

A wide range of studies have reported experimental results of heat transfer and fluid flow on meso-channel, mini-channel, and micro-channel heat exchangers or heat

sinks. Although non-circular cross-section in narrow size heat exchangers or heat sinks are available in open literature as provided in, the study of a full-size heat exchanger with narrow-circular channels in multi-port flat slabs with serpentine bend is still rare. Many researchers have studied different heat transfer and fluid flow characteristics through narrow channel heat exchangers and compared with conventional ones in recent years.

Many investigations on different liquids including water and ethylene glycol-water mixture in narrow channel heat exchangers are performed in recent years. Harms et al. (1999) presented experimental results for single-phase forced convection in deep rectangular microchannels of 251μm wide, 1000μm deep and 119μm thick. Deionized water was tested for the Reynolds number ranged from 173 to 12900. Wang et al. (1999) demonstrated a general heat transfer and friction correlations for louver fin round tube heat exchangers with different geometrical parameters including louver pitch, louver height, longitudinal tube pitch, transverse tube pitch, tube diameter, and fin pitch.

Garimella et al. (2001) in a single tube heat exchanger and Oliet et al. (2007) and Jokar et al (2010) in complete heat exchangers, investigated glycol-water mixture flow using non-circular cross-sections. Qu and Mudawa (2002) presented numerical results for a rectangular micro-channel heat sink consisted of 1cm2 silicon wafer. They used water as the cooling fluid inside the 57μm x 180μm micro-channels separated by a 43μm wall.

Qu and Mudawar (2002) carried out another study about pressure drop and heat transfer in a single-phase micro-channel heat sink using DI-water at $139 \leq \text{Re}_w \leq 1672$ both experimental and numerically. 231μm x 713μm rectangular micro-channels heat sink was fabricated from oxygen-free copper and fitted with a polycarbonate plastic cover

plate. Qu et al. (2006) also studied on flow development and pressure drop for adiabatic single-phase water flow in a single 222μm x 694μm x 12cm rectangular micro-channel at $196 \leq Re \leq 2215$. Peng et al. (2011) carried out both experimental and numerical investigation on convection heat transfer in a channel with 90° and V-shaped ribs. Khan and Fartaj (2011) experimentally investigated a 50:50 ethylene glycol-water mixture flow through a microchannel heat exchanger (MCHX) with air in a cross-flow orientation.

Even though, many studies have been conducted on water and ethylene glycol, study on highly viscous fluids, such as automatic transmission fluid (ATF) and engine oil are still very rare in the open literature. Engine oil, automatic transmission fluid (ATF), ethylene glycol, and water are widely used in automotive and industrial applications. Therefore, Research on these commercially important fluids in miniature heat exchanger is still required.

1.2 Motivation

Sources of energy are limited, while energy demands are continuously increasing. As a result, the necessity of thermal system equipment which can provide a very high performance in a smaller space is paramount for many industries. In thermo-fluid applications, the heat transfer intensification that refers to the practice of achieving elevated heat transfer using miniature heat exchangers has become an increasingly demanding and growing research area (Luo et al., 2007).

The following motivating considerations exist for a comprehensive CFD analysis of the heat exchanger used in current study:

- For a given volume, the area density (surface area to volume ratio) of minichannel heat exchanger (MICHX) is more than that of conventional heat exchangers, which leads to higher volumetric heat flux.

- The small hydraulic diameter channels result in a high heat transfer coefficient.

- Higher heat transfer coefficient and greater volumetric heat flux make the MICHX lightweight and mobile. It is very important for systems where space availability is restricted.

- Multi-port flat slabs allows the air flow to be a very good contact with the heating surfaces and leads to higher heat transfer over the conventional heat exchangers of isolated tube rows.

- Monolithic structure of multi-port slab minimizes leakage, diminishes noise, extends the life time, and helps the environment.

- Due to the reduced volume or miniature size, less material being used, and hence the minimal material cost is possible.

- Numerical simulations are very useful supplement to the interpretation of the experimental data, where temperature fields and heat fluxes are very difficult or impossible to measure.

- Numerical study is a cost effective technique, which avoids the need of numerous prototype tests.

1.3 Objectives

Numerous studies have been performed in straight multi-port narrow channel heat exchangers using water and ethylene glycol as working fluids. However, studies of multi-port slab serpentine heat exchanger (i.e. with a bend in the channel paths with parallel channels inside the slab core) using highly viscous fluids, such as automatic transmission fluid (ATF) and engine oil are still very limited in the open literature. Engine oil is widely used in many industrial applications, such as automotive and aircraft engines, agricultural and construction equipment, locomotives and electrical generators for lubrication, corrosion prevention, and engine cooling. ATF is extensively used in vehicles with self shifting or automatic transmissions, power assisted steering systems, and 4WD transfer cases for the special requirements of a transmission, such as valve operation, brake band friction, torque converter, and gear lubrication. Therefore, study on these commercially important fluids in narrow channels is still required to fill in the gaps in research.

The main goal of current study is to investigate the heat transfer characteristics of high-viscosity fluids in MICHX. It is desired to compare the performance of the heat exchanger using high viscosity fluid with that using low viscosity fluid in order to provide information to the fulfillment of the potentiality of MICHX in the real-world applications. The main objectives of current study are included below:

- Perform numerical investigation on different fluids, such as engine oil, ATF, ethylene glycol, and water to evaluate heat transfer and fluid flow characteristics

- Compare the numerical results with available experimentally measured data

- Compare the heat transfer and flow behaviors of different viscous fluids

- Evaluate the temperature and flow distributions through in MICHX

- Investigate the effect of serpentine slab on heat transfer performance

- Provide information, which may be a great source for future works to the fulfillment of the potentiality of MICHX in automotive, HVAC, and other real-world industrial applications.

In order to achieve those objectives, numerical simulations were conducted on engine oil, ATF, 50% ethylene glycol, and DI-water. A commercial CFD code, namely ANSYS FLUENT was used in order to perform numerical simulations.

CHAPTER II

REVIEW OF LITERATURE

It is necessary to have a good understanding about the concept of heat transfer and fluid flow through narrow channels before starting to develop a computational model. Therefore, a number of previous researches are studied, and a detailed review on narrow channel heat exchangers is done. It is noted that scientists and researchers first experimentally investigated the heat transfer and fluid flow behaviors in micro-and mini-channels and then compared their results with conventional correlations obtained in the past couple of decades. In recent years, a wide range of numerical studies have been done to obtain more inclusive results. Some of the important previous investigations related to current study are extensively summarized in this chapter.

2.1 General Overview

A heat exchanger is one of the most important devices in many engineering and biomedical applications. Numerous extensive studies have been conducted on compact heat exchangers to improve the performance of such devices. Researchers have been looking for compact, energy efficient and environmentally friendly heat exchangers for the last couple of decades. Tuckerman and Pease (1981) designed and tested a very compact, water-cooled integral microchannel heat sink to remove heat from the silicon integrated circuits. They reported that heat flux of about 790 W/cm2 can be dissipated by flowing water through microchannels, while maintaining temperature increase below 71$^{\mathrm{o}}$C. Consequently, a wide range of studies have been performed to study the heat transfer and flow characteristics in narrow channel heat exchangers.

Mehendale et al. (1999) and Kandlinkar et al. (2006) reported the classifications based on hydraulic diameter of the channel as shown in Table 2.1 and 2.2.

Table 2.1. Channel classification according to Mehendale et al. (1999)	
Microchannels	1-100μm
Meso-channel	100μm -1mm
Compact passages	1-6mm
Conventional passages	> 6mm

Table 2.2. Channel classification according to Kandlinkar et al. (2006)	
Conventional passages	> 3 mm
Minichannels	3mm ≥ D > 200μm
Microchannels	200μm ≥D >10μm
Transitional Microchannels	10μm ≥ D > 1μm
Transitional Nanochannels	1μm ≥D > 0.1μm
Nanochannels	0.1μm ≥ D

An approximate solution for determining the pressure drop of fully developed, laminar, single-phase flow in smooth singly connected microchannels of a wide variety of channel cross-sections was studied by Bahrami et al. (2007). Studies have reported experimental results of heat transfer and fluid flow on meso-channel, mini-channel, and micro-channel heat exchangers or heat sinks.

Many studies have indicated that both the channel geometry and fluid viscosity have a very significant effect on the pressure drop and heat exchanger performance. Even though, a wide range of investigations on different liquids including water and ethylene

glycol-water mixture in narrow channel heat exchangers have been performed in recent years, studies on highly viscous liquids like automatic transmission fluid (ATF) and engine oil are very rare in the open literature. Followed are some of the important investigations related to the current study available in the open literature.

2.2 Experimental Studies on Narrow Channel Heat Exchangers

Due to the importance of miniature heat exchangers in many specialized areas including microelectronics, robotics, aerospace, biomedical, and automotive applications, a wide range of experimental researches have been conducted in recent years. The first experimental investigation on micro scale technology for cooling of very-large-scale integrated (VLSI) circuits was designed and established by Tuckerman and Pease (1981). They have found a maximum substrate temperature rise of 71°C above the input water temperature at power density of 790 W/cm2.

Adams et al (1998) carried out turbulent, single-phase forced convection of water through circular channels with diameters of 0.76 and 1.09 mm. They found that Nusselt numbers for the microchannels higher than those predicted by traditional large channel correlations including Gnielinski correlation. The diameter, Reynolds number, and Prandtl number ranges were (0.102 - 1.09mm), (2.6×10^{3} - 2.3×10^{4}), and (1.53 - 6.43), respectively. Another experimental study about flow characteristics of water via microtubes of fused silica (FS) and stainless steel (SS) with diameters range from 50μm to 254μm was carried out by Mala and Li (1999). Almost the same pressure gradient as predicted by the Poiseuille flow theory for low Reynolds number (Re) has been found. However, as Re increased, a significant increase in the pressure drop was observed compared to that predicted by the Poiseuille flow theory. As a result, higher friction

factor was found compared to the one given in the conventional theory. The results also showed that FS microtubes needed a higher pressure drop than SS microtubes for the same flow rate and diameter due to either the effects of surface roughness of the microtubes or an early transition from laminar to turbulent flow.

A study on the effect of the number of tube rows, fin pitch and tube diameter on the heat transfer and fluid flow behaviors was conducted by Wang and Chi (2000). They found that heat transfer performance to be increased with the decrease of fin pitch for the number of tubes row equals to 1 or 2 and negligible for number of tubes row ≥ 4 and Re > 2000. They also found a very small effect of the number of tube rows on the friction performance for the same fin pitch. Pressure drops for the fin collar outside diameter (Dc) = 10.23 mm were found to be approximately 10 - 15% higher than those of Dc = 8.51 mm. Wu and Cheng (2003) carried out another research on convective heat transfer and pressure drop of water in the laminar regime through different trapezoidal silicon microchannels. Their results showed that the Nusselt number (Nu) and friction factor (f) increased with increasing surface roughness and surface hydrophilic property. Adding to that Nu increases almost linearly with Reynolds number at Re < 100, while it increases very little at Re >100.

Kandlikar et al. (2003) investigated the effect of surface roughness on pressure drop and heat transfer in $500 \leq Re \leq 2600$ for 1.067mm diameter and $900 \leq Re \leq 3000$ for 0.62mm diameter circular tubes. For the 1.067 mm diameter tube, the effects of the roughness from $e/d = 0.00178\ to\ 0.00225$ on heat and pressure drop were found to be insignificant. Whereas, for the 0.62 mm tube, the highest heat transfer and pressure drop were observed with higher e/d (=0.00355). They reported that above 1.067mm diameter

tubes with e/d = 0.003 can be considered as smooth tubes. On the other hand, enhanced heat transfer and pressure drop were observed for the smaller diameter (< 0.62mm) tubes of the same roughness value. Another finding is that for the small diameter tubes, a roughness value > 0.003 has a significant effect on transition to turbulence.

Khan et al. (2004) compared the thermo-hydraulic performances of two traditional tube heat exchangers (circular and elliptical) and one circular shape meso-channel heat exchanger to compare their thermo-hydraulic performances. Their results show that the meso-channel heat exchanger exhibits superior thermo-hydrodynamic performance over the other two, and the elliptical tube heat exchanger shows higher performance compared to the circular tube. Owhaib and Palm (2004) also studied experimentally the heat transfer characteristics of single-phase forced convection R-134a in single circular micro-channels with 1.7mm, 1.2mm, and 0.8mm inner diameters. They reported that in the turbulent regime, the results were in a good agreement with the classical correlations. However, their results did not agree with any of the suggested correlations for microchannels. Adding to that the heat transfer coefficients were almost identical for all the three diameters in the laminar region.

Nuntaphan et al. (2005) performed a study on 23 heat exchangers with crimped spiral configurations to investigate the effect of tube diameter, fin spacing, transverse tube pitch, and tube arrangements. The pressure drop was found to be increasing but the heat transfer coefficient decreasing with the increase of tube diameter and fin height for the inline arrangement. Whereas, the pressure drop due to the fin height, is very small for the staggered arrangement compared to that of the inline arrangement. They also found that the fin spacing has a strong influence on the air side performance for both inline and

staggered arrangements. Hetsroni et al. (2005) carried out both experimental and theoretical investigations on single-phase heat transfer in micro-channels using circular, triangular, rectangular, and trapezoidal micro-channels with hydraulic diameters ranging from 60µm to 2000µm. They performed their experiment using distilled water in the laminar regime to investigate the effects of geometry, energy dissipation, and axial heat flux due to thermal conduction through the working fluid and channel walls.

Saitoh et al. (2005) presented another study discussing the boiling heat transfer of refrigerant R-134a flow in horizontal tubes with 0.51mm, 1.12mm, and 3.1mm inner diameters. They found that the flow inside a tube approached homogeneous flow for the smaller tube diameter. They reported that the effect of heat flux was strong in all the three tubes. Results showed that the local heat transfer coefficient and the effect of mass flux on the local heat transfer coefficient drops with the decrease of tube diameter. It was also reported that the measured pressure drop for the 3.10mm and 0.51mm inner diameter tubes were in a good agreement with the Lockhart–Martinelli correlation and the homogenous pressure drop model respectively. Bintoro et al. (2005) designed and experimentally investigated a closed-loop electronics cooling system for a single phase computer chip by adopting impinging jet and a mini channels heat exchanger. A channel diameter of 1.27mm and nozzles diameter (dN) of 0.5mm and 0.8mm were used. The cooling capacity of the system was reported to be 200w over a single chip with a hydraulic diameter of 12 mm which was equivalent to the heat flux of 177w/cm^2 with a coefficient of performance of the system of 21.4.

Another investigation regarding the heat transfer characteristics of a single-row aluminum fin-and-tube crossflow heat exchanger was carried out by Tang and Yang

(2005). They emphasized on the regime of low flow rate of the in-tube fluid (water). They reported that the thermal resistance of both liquid-side and air-side were almost equal for $500 \leq Re \leq 1200$. However, for $1200 \leq Re \leq 6000$, the air-side thermal resistance was much higher than that on the liquid-side. They also found that the liquid-side thermal resistance is less than 10% of the overall thermal resistance. Brandner et al. (2006) studied various micro-structured cross flow heat exchangers to compare their thermal performance. They used two heat exchangers with different layouts of micro column arrays (aligned and staggered). They showed that the heat transfer in a micro-heat exchanger can be enhanced by decreasing the hydraulic diameter of the microchannels. In their investigation, they used a ''bottom-up'' approach and showed that Poiseuille number depends only on the geometrical parameters of the cross-section for constant fluid properties and flow rate in fixed cross-section channels. The arbitrary cross-sections included rectangular, trapezoidal, triangular, hyper-ellipse, trapezoid, sine, square duct with two adjacent round corners, rhombic, annular, circular, rectangular with semi-circular ends and moon-shaped channels. Their results showed the square root of the cross-sectional area $\sqrt{A}$, as the characteristic length scale, is superior to the conventional hydraulic diameter, D_h.

Qu et al. (2006) carried a study on the flow development and pressure drop for an adiabatic single-phase water flow in a single 222μm x 694μm x 12cm rectangular micro-channel at $196 \leq Re \leq 2215$. They reported that the quick entrance effects have created observable vortices in the inlet region that had a very significant influence on the downstream flow development. Cross-flow heat exchangers with wavy fins and flat tubes were experimentally investigated by Junqi et al. (2007). The experiment was carried out

at a constant tube-side water flow for air side Reynolds number in the range of 800–6500 with different fin pitches, fin lengths and fin heights. The results showed that for $800 \leq Re \leq 6500$, Colburn factor, j and Fanning friction factor, f factors decreased with increasing Re, and j and f factors increased with fin space increasing at the same Re. Results also showed that the j factor increased with fin height, while the effect of fin height on f factor is insignificant.

Tang et al. (2009) carried out both experimental and numerical studies on air-side heat transfer and friction characteristics of different types of fin-and-tube heat exchangers of 18mm tubes in diameter with $4000 \leq Re \leq 10000$. Higher heat transfer and pressure drop were found for the crimped spiral fins compared to the other fins. The performance of the heat exchanger with mixed fins (front vortex-generator fin and rear slit fin) was also found to be better than that for fins with delta-wing vortex generators. They also reported that the slit fin offers the best heat transfer performance at high Reynolds numbers. Stignor et al. (2009) carried out an investigation on liquid-phase heat transfer in three multiport minichannel tubes of rectangular geometry with different cross-sections. The study was conducted on laminar flow regime using four different secondary refrigerant liquids: water, propylene glycol, Hycool 20, and Temper-20. In spite of the shape of the minichannels, a better agreement has been found with the Gnielinski's correlation for laminar flow, developing temperature profile, and fully developed velocity profile in circular tubes with constant wall temperature boundary condition.

Jokar et al. (2010) experimentally investigated heat transfer and flow characteristics through five different meso-channel compact heat exchangers of 2.6mm – 4.1mm hydraulic diameters. R-134a and 50% glycol-water were used and a modified

Wilson plot technique was applied to obtain the heat transfer coefficients and the Fanning equation in order to calculate the pressure drop friction factors. They showed that the heat transfer and pressure drop correlations for the macro-channels are not directly applicable for meso-channels compact heat exchangers. Dasgupta et al. (2011) conducted another study of MCHX having 15 slabs of 2mm in thickness with 68 circular channels of 1mm diameter each. They have maintained the air-side Reynolds number range from 750 to 3165 at a constant liquid-side Reynolds number of 200. Results show higher air-side Nusselt number compared to other studies.

Dang and Teng (2011) studied both numerically and experimentally one microchannel and two minichannel heat exchangers having length of 32mm and the same total rectangular cross-sectional area of $1mm^2$ for all channels,. Results show that both the heat transfer rate and pressure drops obtained from microchannel heat exchanger are higher than those obtained from the minichannel heat exchangers. Peng et al. (2011) carried out both experimental and numerical investigation of convection heat transfer in a channel with 90° and V-shaped ribs. They found that for both the 90o ribs and V-shaped ribs showed an enhanced convection heat transfer in expense of increased pressure drop compared to a flat wall without ribs. They also reported that the overall thermo-hydraulic performance of the V-shaped ribs was superior to that of the 90o ribs. A study on air side heat transfer and fluid flow behaviors of multi-port serpentine cross-flow mesochannel heat exchanger was performed by Siddiqui et al (2012). Their experiment on ethylene glycol–water mixture was conducted in air-to liquid cross-flow orientation on a wavy finned 68-port mesochannel heat exchanger at air-side Reynolds number ranged between

$752 \leq Re_a \leq 3165$. In comparison with other studies, they found that the air-side Nusselt number (Nu_a) and Colburn factor (j_a) are higher.

2.3 Numerical Simulations on Narrow Channel Heat Exchangers

Numerical simulations are considered as a very useful supplement to the interpretation of the experimental data, where measurements of temperature fields and heat fluxes are obviously very difficult or impossible to obtain. It becomes an economical prediction technique by avoiding the need of numerous prototype tests. As a result, computational fluid dynamics (CFD) has been becoming a very significant research technique in heat exchanger studies. Ryu et al. (2002) conducted a numerical optimization of the thermal performance of a microchannel heat-sink of 1cm x 1cm square horizontal surface. The height, channel width, and fin thickness of the microchannel heat-sink are 453µm, 45.3µm, and 35.3µm respectively. They used water as a coolant and silicon as heat-sink material. Gamrat et al. (2004) performed a numerical investigation on heat transfer of rectangular micro-channels using three channel heights 0.3mm, 0.6mm, and 1mm. Based on hydraulic diameter, they maintained $300 \leq Re \leq 2360$ and found low thermal resistance at small channel height. They have concluded that the heat transfer performance can be improved by decreasing the channel height.

Wang et al (2004) studied the frictional performance of the highly viscous fluid in minichannels having diameters of 0.198 – 2.01mm. They used water and lubricating oil as the working fluids with Reynolds number of 0.1 to 1500 and found a negligible influence of viscosity on the friction factor for the hydraulic diameter greater than 1.0mm. Albakhit and Fakheri (2005) numerically investigated the flow and heat transfer in parallel flow microchannel heat exchangers for thermally developing laminar flow in

two parallel rectangular channels. Their result shows that the developing velocity profiles led to higher values of the overall heat transfer coefficient in the entrance region. A thermo-fluid–dynamic investigation was numerically performed by Carluccio et al. (2005) in an air-oil cross flow aluminum compact heat exchanger in order to estimate the effect of the air channel geometry at different flow regimes. The highest heat flux zones were reported in correspondence with the changes of air-flow direction. The geometrical configuration permitted an enhanced thermal gain in presence of a higher pressure drop.

Gamrat et al. (2005) performed both 3-D and 2-D numerical simulations in rectangular microchannels heat sink to investigate the conduction and entrance effects on heat transfer for $200 \leq \text{Re} \leq 3000$. In contrast to the uniform inlet velocity and temperature profiles reported by Shah and London (1998), they found that the entrance effects to be dependent on the Reynolds number and the channel spacing separately. They also reported that viscous heating was not taken into account in numerical simulations, which could cause a decrease in Nusselt number. Zhuo et al. (2006) carried out numerical simulations of the fluid flow and heat transfer of water in silicon micro-channels with non-circular cross-sections. The authors investigated the effect of the geometric parameters of the micro-channels and discussed the variations of Nusselt number with Reynolds number from the field synergy principle.

Ngo et al. (2007) used three-dimensional computational fluid dynamics (3D CFD) FLUENT code to investigate the thermal hydraulic performance of a microchannel heat exchanger (MCHX) with S-shaped and zigzag fins using a supercritical carbon dioxide loop. Their results show that the MCHX with s-shaped fins can provide a pressure drop 6-7 times lower preserving almost the equivalent heat transfer performance compared to a

conventional MCHX with zigzag fins. Cheng (2007) used stacked rectangular two-layer microchannel heat sink with embedded passive microstructure in his numerical investigation by three-dimensional conjugated model of CFD. The ratio of embedded structure height to microchannel height has been varied from 0.13 to 0.26 at a fixed Reynolds number of 14.8. The stacked microchannel with passive structures shows better performance than the smooth microchannels. Liu et al. (2007) carried out a 2-dimensional numerical investigation for fluid flow and heat transfer in microchannel cooling passages for low Reynolds number flow of water in a 100μm single channel. They found a significant role in the variation of viscosity and the induced cross-flow velocity to the convective heat transfer. However, the enhancement of heat transfer due to the variation of conductivity in the thermal developing process was reported relatively insignificant except for the cases with very low Reynolds numbers.

Lao and Jen (2008) carried out a three-dimensional numerical simulation in a square duct with a curvature ratio of $0.05-1.0$ and Dean Number (De) of $0-200$ in the fully developed fluid flow and heat transfer. The researchers used the D3Q27 incompressible LBGK model and found that the onset of transition from single-pair vortex to double-pair vortex depends on both the curvature ratio and Dean Number for the square duct with high curvature ratio. Kahalerras and Targui (2008) performed a numerical analysis of a double pipe heat exchanger with porous fins attached at the external wall of the inner cylinder by using the finite volume method (FVM). Numerical analysis was performed for Darcy number ($10^{-6} \leq Da \leq 10^{-1}$), porous fins height ($0 \leq H_p \leq 1$), spacing ($0 \leq L_f \leq 39$), and thermal conductivity ratio ($1 \leq R_k \leq 100$).

Chen et al. (2009) performed a three-dimensional model using noncircular microchannel heat sinks including triangular, rectangular, and trapezoidal microchannels to investigate heat transfer and fluid flow characteristics. Their results show that the triangular microchannel has the highest thermal efficiency among the three geometries. Li et al. (2010) performed another 3D numerical simulation in an aluminum heat exchanger with integrated fins and micro-channels to investigate the air-side heat transfer and flow characteristics. They reported that for Re number below 2000, both the Colburn factor (j) and Fanning friction factor (f) increase when increasing fin height and fin thickness, and decrease when increasing fin pitch. With the increase in the flow depth, j factor decreases but f factor increases. The best performance of the heat exchanger was found for fin pitch of 1.0 mm, flow depth of 26 mm, fin height of 6.6mm and fin thickness of 0.1 mm. The air-side performance of the integrated fins and micro-channel heat exchanger was reported and compared to the multi-louver and the wavy fin flat tube heat exchanger for high and low Reynolds number.

The wall heat transfer mechanisms for a vapor bubble inside a 200µm x 200µm square cross section microchannel was numerically studied by Mukherjee et al. (2011). They used SIMPLER method to solve the Navier-Stokes equations along with continuity and energy equations. They found that the wall heat transfer can be improved by increasing the wall superheat and the bubble growth rates without any affect from the change in the incoming liquid flow rates. They also found longer and thinner bubbles to be produced due to a small effect of the liquid surface tension on the bubble growth. Moreover, the bubble with the lowest contact angle exhibited the highest growth rate and the highest wall heat transfer. Furthermore, they identified the increasing the wall heat

transfer mainly due to the motion of evaporating liquid–vapor interface. The growth of the thermal boundary layer was found to be prevented by the bubble growths which pushed the liquid against the microchannel walls. However, no significant effect of surface tension on wall heat transfer was obtained.

Dehghandokht et al. (2011) numerically analyzed fluid flow and heat transfer characteristics of water and ethylene glycol-water mixture in a multi-port serpentine meso-channel heat exchanger (SMCHX). The numerical results for predictions of heat transfer rate, pressure and temperature drops in the coolants, and the core surface temperature around the serpentine bend are validated with the experimental data found from the SMCHX. They carried out another 3-D numerical simulation, for forced convection of hot water in a serpentine MSCHX with a cold air flowing across and found the elevated heat transfer rate due to the existence of serpentine bend in the meso-channel heat exchanger. They reported that the air-flow in contact with the multi-port slab flat surfaces was maintained a uniform temperature distribution on the top and bottom faces. The fairly uniform distribution of heat through all the channels was reported due to the parallel channels located inside the meso-channel slab core.

Another investigation about heat transfer in simultaneously developing flow for rectangular tubes was presented by Garimella et al. (2001) for $118 < \text{Re} < 10,671$. They employed three different typical dimensions used in automotive heat exchangers tube sizes and shapes of $D_h = 2.21mm$, $\alpha = 0.050$; $D_h = 3.02mm$, $\alpha = 0.108$, and $D_h = 1.74mm$, $\alpha = 0.029$. They found higher Nusselt numbers in the developing regime, especially for short tubes. They reported that the effect of aspect ratio was not very significant.

2.4 Effect of Viscosity on MICHX Performance

The performance of viscous fluids, especially highly viscous fluids like engine oil and ATF are extremely dependent on temperature. This is due to the rapid response in variation of viscosity with temperature. Few numerical studies have been performed to investigate the effect of viscosity of liquid and axial conduction of wall in order to investigate heat transfer performance of MICHX.

Obot et al. (1997) reported the Prandtl number range of $0.7 \leq Pr \leq 125.3$ working on ethylene glycol, water, and ethylene glycol-water mixture. They found that the friction factor is independent of Pr in smooth pipes. Tso and Mahulikar (2000) conducted a study on water flow in microchannels in the laminar regime to observe the behavior of the local Nusselt number (Nu) and the Brinkman number (Br) for the constant wall heat flux boundary condition. They found a strange behavior of local Nu which decreases with increasing local Re along the flow. The Brinkman number was found to be 10^{-8}–10^{-5}.

Thermal effectiveness and entropy generation of parallel and counter-flow heat exchangers with highly viscous fluids was numerically investigated by Bagalagel and Sahin (2002). Their results showed that viscous friction with variable viscosity has a very significant effect on heat exchanger performances for lower inlet temperatures of highly viscous fluid. The entropy generation number was also found to be higher when the viscous friction was considered. In addition, they also found that the effect of viscosity on both counter-flow and parallel flow heat exchangers is similar. On the other hand, the counter-flow heat exchanger performance showed a smaller tendency of deviation between the no viscous friction behavior and the viscous friction behavior which made it more attractive than the parallel flow exchanger.

Nield et al. (2003) studied the effects of axial conduction and viscous dissipation in thermally developing forced convection through parallel plate channel in a porous medium with walls at constant temperature. The authors reported that viscous dissipation is negligible when Brinkman number (Br) is zero while the viscous dissipation has a very significant effect on the developing Nusselt number. They added that in the absence of viscous dissipation, the developing Nusselt number (Nu) differs little with the Darcy number (Da) whereas Nu significantly increases with the decrease in Peclet number (Pe).

Especially for a very small Darcy number, a small quantity of viscous dissipation $(Br \neq 0)$ also plays a role to jump the fully developed Nu to a value which is independent of Br they added. Another investigation on the effect of viscous dissipation in fully developed forced convection through a parallel plate channel at uniform temperature and uniform heat flux was performed by Nield et al. (2004). They established an expression for Nusselt number (Nu) as a function of Bn. At uniform-flux boundary conditions, the relationship between Nu and Bn for a very large Darcy number $(Da = 10^4)$ and $M = 1$ is

$$Nu = \frac{70}{17} + \frac{54}{14} Bn \qquad (2.1)$$

where

$$Br = \frac{\mu V^2}{(T_m - T_w)k} \qquad (2.2)$$

They also claimed that for a very small Darcy number $(Da = 10^{-4}, slug\ flow)$, the Nu is equal to 6 and independent of the Brinkman number and the viscous dissipation. Koo and Kleinstreuer (2004) studied on viscous dissipation effects on temperature and friction factor in microtubes and microchannels. In their experiment, they used water, methanol, and iso-propanol as working fluids in different conduit geometries. They

claimed that, for microconduits, viscous dissipation a strongly depends on the channel aspect ratio, Reynolds number, Eckert number, Prandtl number, and hydraulic diameter of the conduit. Their results showed that temperature increased significantly due to viscous dissipation even in a very low Reynolds number flow for high-viscous and low heat capacity fluids. Results also showed that for water flow in a tube with D < 50μm, viscous dissipation becomes significant. They claimed that the viscous dissipation increased rapidly with a decrease in channel size.

Wang et al. (2004) experimentally examine the frictional performance of water and lubricant oil (SUNISO 4GS having kinematic viscosity, $v = 54.9 mm^2/s$ at 40°C) in round and rectangular minichannels of hydraulic diameter, $D_h = 0.198-2.01 mm$. The experiment was conducted with Reynolds number for water about from 100 to 30,000 and for the lubricant oil about from 0.1 to 1500. They found a negligible influence of viscosity on the friction factor when hydraulic diameter is greater than 1mm. The measured friction factors for lubricant oil were found 10-30% lower than those of predicted values, which could be attributable to the viscous heating.

Nonino et al (2007) carried out a parametric investigation on the effects of temperature-dependent viscosity and viscous dissipation in simultaneously developing flows in microchannels with convective boundary conditions. The finite element method was conducted in circular tube and parallel plate channel considering an exponential relationship of viscosity with temperature as

$$\mu = \mu_a exp[-\beta(t - t_a)] \tag{2.3}$$

$$with \ \beta = -\frac{\left(\frac{d\mu}{dt}\right)}{\mu} = constant$$

which can be cast in the following dimensionless forms of

$$\frac{\mu}{\mu_a} = exp(-\beta T) = \left(\frac{\mu_e}{\mu_a}\right)^T \tag{2.4}$$

where, dimensionless temperature, $T = \frac{t-t_a}{t_e-t_a}$ and

dimensionless viscosity parameter, $\beta = -ln\left(\frac{\mu_e}{\mu_a}\right)$.

Their numerical results confirmed that larger hydrodynamic entrance length and lower asymptotic Nusselt number compared to constant viscosity flows because of viscous heating. They also found that, in the case of fluid heating, viscous dissipation and temperature dependent viscosity influenced the radial temperature profiles.

Yataghene et al. (2009) analyzed the heat transfer in a scraped surface heat exchanger for Newtonian and non-Newtonian fluids both experimentally and numerically. Viscous dissipation was taken into account and controlled with the Brinkman number, the rotating velocity and the thermal boundary conditions. For the viscous Newtonian fluid, the effects of viscous dissipation were reported as very significant in both boundary conditions. It was found that the temperature of the fluid increases due to viscous friction or viscous dissipation rise due to the increase of rotor speed. Whereas, for non-Newtonian shear thinning fluid (2wt% CMC solution), viscous dissipation was found negligible. The temperature distribution in the fluid was found to be heterogeneous instead of homogeneous due to the geometrical configuration of the apparatus. For index behavior of shear thinning power law fluid (n) < 0.3, the effect of viscous dissipation was found to be negligible. However, for n > 0.5, the effect of viscous dissipation led to boost up the temperature.

2.5 Effect of Axial Conduction

Maranzana et al. (2004) studied the effect of axial conduction in the walls in two 10mm long and 500µm thick blocks of silicon. Water flow was passed through the 100µm thick channel with a Reynolds number of 15.4. They imposed a 30kw/m^2 uniform heat flux on the upper face of the top block, while the lower face of the bottom block was maintained adiabatic. A dimensionless number M was introduced to quantify the relative part of axial conduction through walls. They noticed that axial conduction can be neglected if the values of M become less than 102. They also reported that the wall heat flux density, for small Re (15.4), cannot be strongly uniform because most of the flux is transported to the fluid flow at the entrance of the mini–micro-channel. It is shown that the axial conduction through the walls of a mini–micro heat exchanger results in a loss of efficiency. They added that axial conduction in the walls has also to be taken into account when designing mini–micro counter-flow heat exchangers in order to find out an optimal conductivity for the wall to get the highest efficiency of heat exchanger.

Another study on the consequences of axial conduction in a parallel plate microchannel heat transfer and fluid flow with a fully-developed velocity distribution was performed by Cole and Cetin (2011). The authors included fluid axial conduction for a low range of Pe (0.1 < Pe < 100). A uniform heat flux was applied to the outside of the channel wall. Their results showed that the effect of the axial conduction in the channel wall is significant for (i) the small microchannel length-over-height ratio; (ii) the small Pe; (iii) the large wall thickness relative to the channel height and (iv) the high conductivity of the wall material relative to the thermal conductivity of the working fluid. They also stated that the effect of the axial conduction in the wall is negligible for high Pe flow (e.g. Pe > 100) and low thermal conductivity of the wall materials.

2.6 Scope of current study

A wide range of studies have been performed using different working fluids in order to investigate heat transfer and fluid flow behaviors in various types of macro- and micro-scale heat exchangers. Various investigations have been reviewed very carefully and observed especially which are focused on different types of heat exchangers, fins and fluids, flow arrangements, channel sizes and geometry. Some researchers have studied straight multi-port narrow channel heat exchangers using water and ethylene glycol as the working fluids. However, studies of multi-port slab serpentine heat exchanger (i.e. with a bend in the channel paths with parallel channels inside the slab core) using highly viscous fluids like engine oil and ATF are very rare. Even though a few studies have been conducted on viscous fluids in order to capture their thermo-physical properties, heat transfer and fluid-flow performances on engine oil and ATF cooling studies, especially in a MICHX were not found in the open literature. Experiments cannot predict the complex measurements and thermal fields.

Therefore, numerical simulations may be very helpful as a supplement to those investigations of heat flux, temperature and convection fields. Four liquids, including water, 50% ethylene glycol, typical engine oil and ATF have been used through a MICHX in the current numerical study. It is predicted that the findings of the current study will be an addition source to the industry-based information in the heat transfer and fluid flow areas. Hence, the current study may be evaluated as a novel one since it provides a comprehensive investigation on the highly viscous fluids, such as engine oil and ATF cooling approaches through the use of a MICHX.

CHAPTER III

DESIGN AND METHODOLOGY

In the current study, numerical simulations are conducted in a multiport serpentine Minichannel Heat Exchanger (MICHX). DI-water, 50% ethylene glycol, engine oil, and automatic transmission fluid (ATF) are used individually as liquid-side working fluids while air is blown at a constant temperature and velocity in an across flow orientation. The numerical results for water and 50% ethylene glycol are validated with the experimental results of Khan and Fartaj (2001). Comparisons between the numerical and experimental results are made for the liquid-side outlet temperature and pressure drop, air-side outlet temperature, and average surface temperature around the serpentine of the SMCHX slab as a function of mass flux. Details of experimental setup, the physical devices, geometry modeling, and the numerical method used in this study are presented in this section. Consequently, the working fluids and their physical properties are described briefly.

3.1 Experimental Setup

To conduct the heat transfer and fluid flow research, the experimental facility used for this study was designed and assembled by Khan and Fartaj (2011), as shown schematically in Figure 3.1. The working liquid fluid is circulated by a gear pump and passed through an electrical pre-heater to maintain the inlet temperature. A 230μ filter is placed to prevent the small particles from entering the MICHX. After that, the fluid passes through channels and returns back to the reservoir. Two resistance temperature detectors, RTD 1 & RTD 2, and two pressure transducers, PTD 1 & PTD 2, are placed at

the inlet and outlet of the test section to measure the temperatures and the pressures respectively.
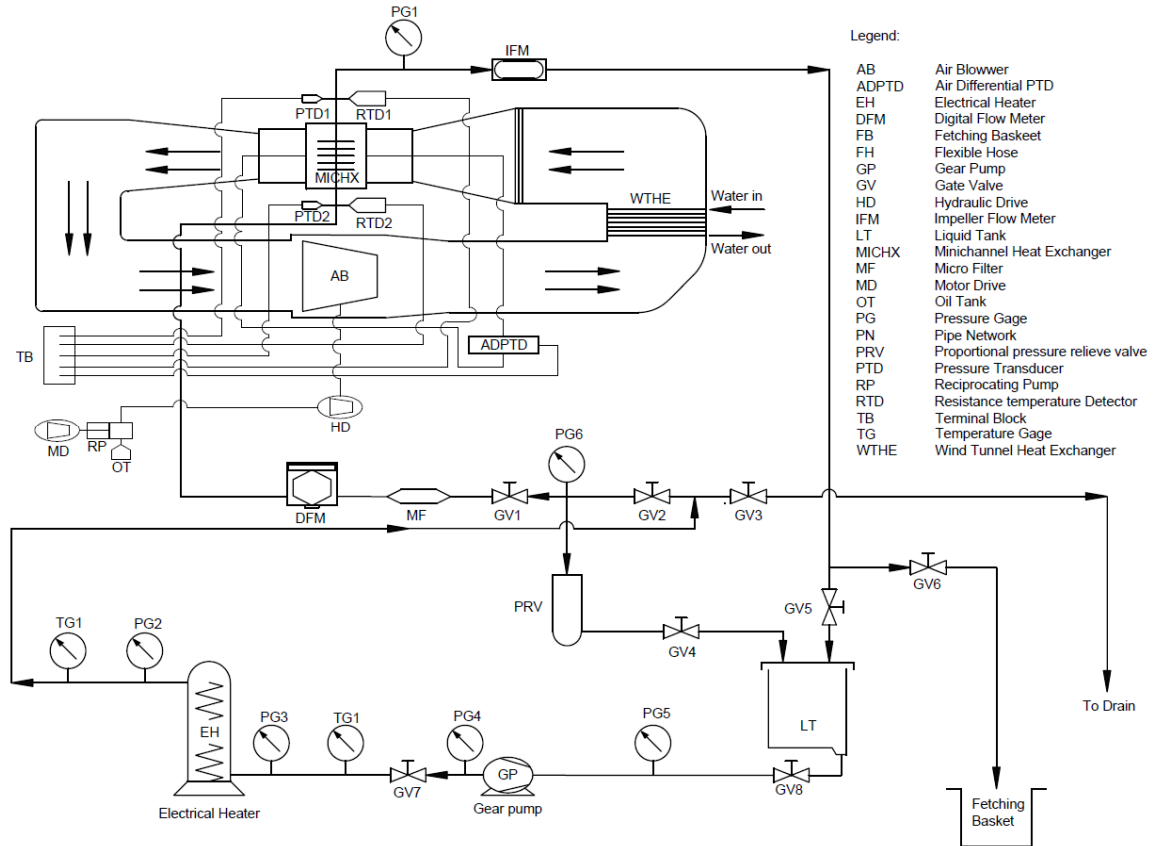
Figure 3.1. Schematic of the experimental set up for heat transfer and fluid flow research

The MICHX is set up inside a test chamber of the wind tunnel. The air is circulated across the heat exchanger through fins inside a closed loop thermal wind tunnel by an air blower, which extracts the heat from the working fluid. To measure the inlet and the outlet temperatures of the air, two thermal grids with nine (3 x 3) and twenty five (5 x 50) type-T thermocouples are installed in the test section. The flow of air is controlled by an air blower with a mass flow rate of 0.507kg/s. To measure the air inlet and outlet pressures, a FlowKinetics FKT series is used. The water flowing through tubes of a built-in heat exchanger in the wind tunnel controls the inlet air temperature. A 16-bit

NI Data Acquisition (DAQ) system is incorporated to monitor and record all the experimental data.

The devices and instruments used in the experimental setup are presented in Appendix A.1.

3.1.1 Minichannel Heat Exchanger (MICHX) Test Specimen

A photograph of the minichannel heat exchanger (MICHX) test specimen used in the current study is presented in Figure 3.2.
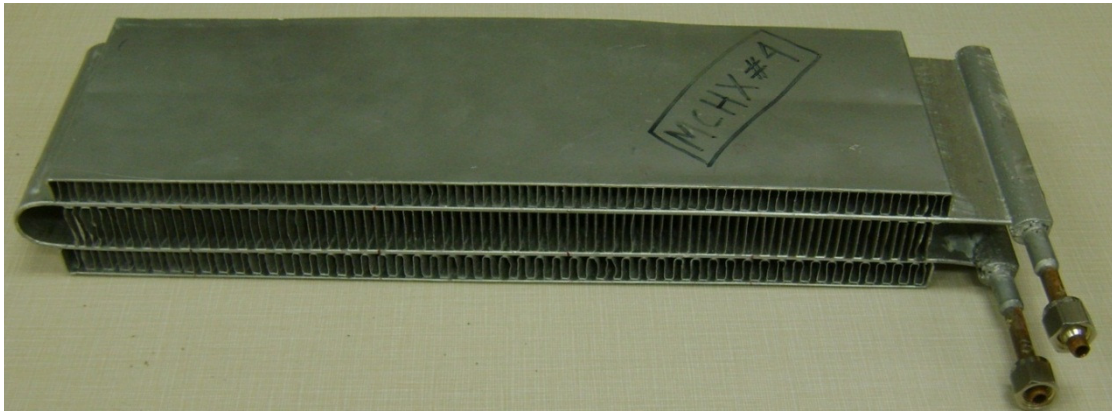
Figure 3.2. MICHX-test specimen

Inlet and outlet manifolds, serpentine slabs, and fins are made of aluminum alloy 3003. The equally spaced 68 circular channels, each one of 1mm diameter, inside a 2mm thick and 100mm width slab were constructed using micro-fabrication. Liquid flows through the inlet tube to the inlet header and distributes to the 68 ports or channels along the slabs and serpentines. Serpentine refers to the curved portion of the channels, through which flow will reverse in direction. The fluid exits from the multi-port slabs into the outlet tube through the outlet header. The air side fins are placed between above and underneath of the multi-port mini-channel slabs.

The detailed specifications of MICHX are shown in Table 3.1.

Table 3.1. Specifications of test specimen (MICHX)	
Parameters	Magnitudes
Material	Aluminum alloy 3003
Number of slabs	2
Number of serpentine	1
Slab length along X-axis (mm)	304
Slab thickness along Y-axis (mm)	2
Slab width along Z-axis (mm)	100
Number of channels inside each slab	68
Channel diameter inside the slab (mm)	1
Port to port distance (mm)	1.463
Inner diameter of serpentine curve (mm)	20
Type	wavy
Number of fins per 25.4mm	8
Height of middle fins (mm)	20
Height of top and bottom fins (mm)	10
Fin thickness (mm)	0.1
Inner diameter of header (mm)	4.76
Outer diameter of header (mm)	6.35

The test specimen used in the current study is place in a 305mm x 305mm x 610mm test chamber. The walls are of the test chamber are made of Plexiglas of low

thermal conductivity and are thick enough to prevent heat loss to the outside environment. Extra insulations are placed around the test chamber to avoid any heat transfer to the surroundings. Hence, heat transfer takes place only through the slabs of the MICHX in the test chamber; as the hot liquid flowing inside the channels transfer heat to the colder air over the slab.

3.2 Geometry Modeling

The first step of the computational modeling is to define an idealization of problem of interest, which includes an appropriate geometry of the physical model and a set of relevant quantities, which are interested to measure. The geometry of computational domain and meshing details are shown in Figs 3.3-3.6c.
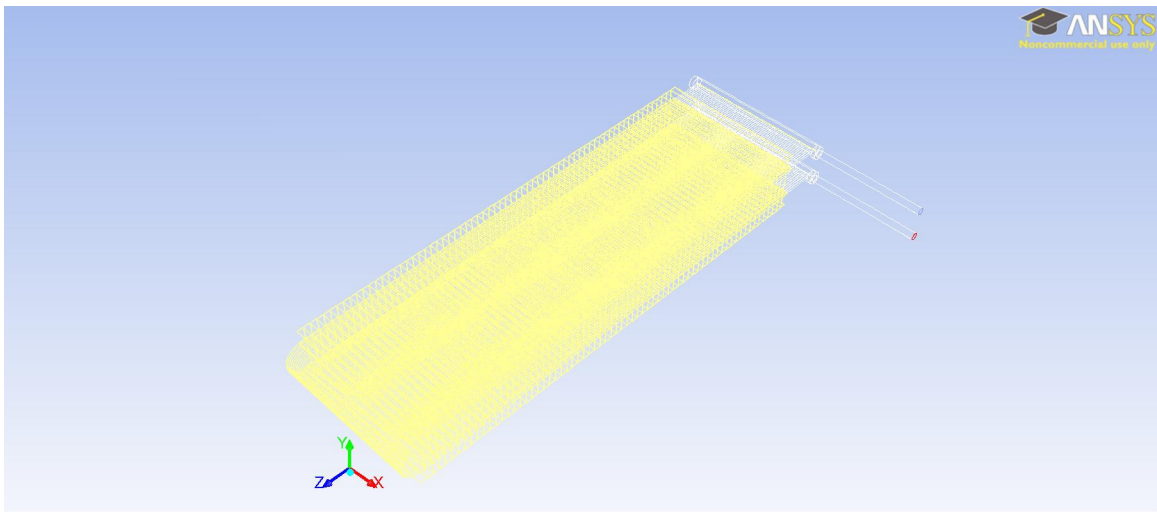
Figure 3.3. Serpentine MICHX with manifolds used in simulation
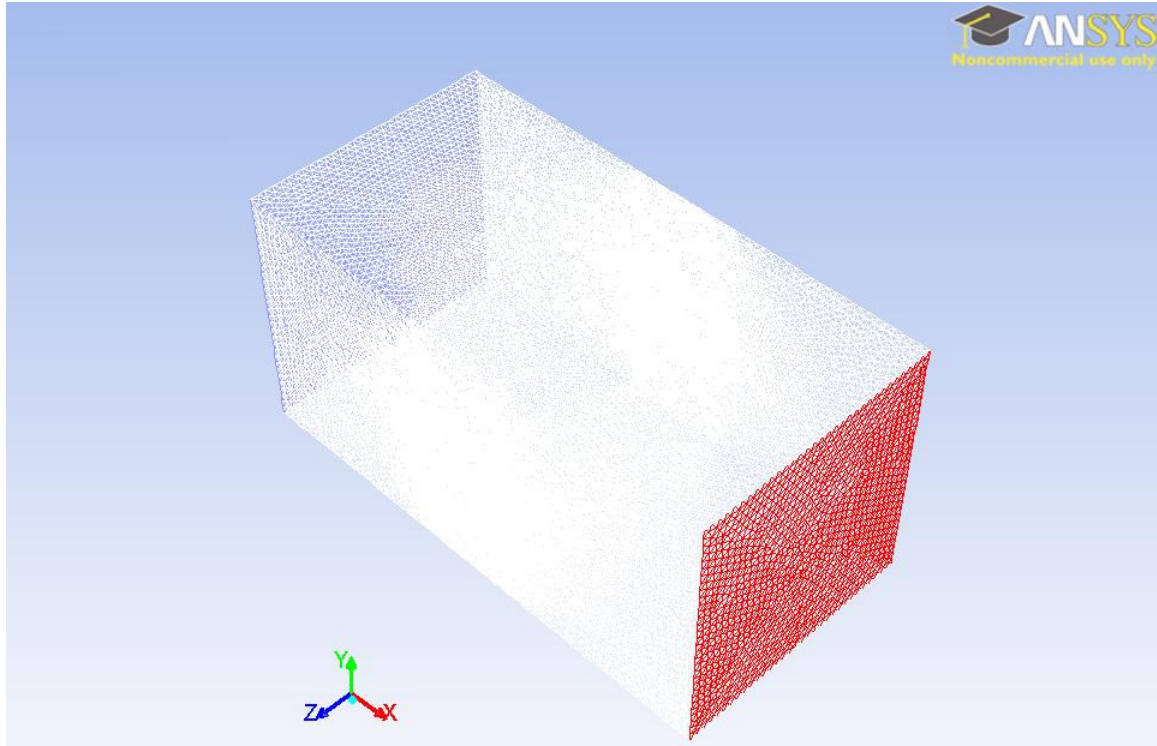
Figure 3.4. Test chamber (Air) used in simulation
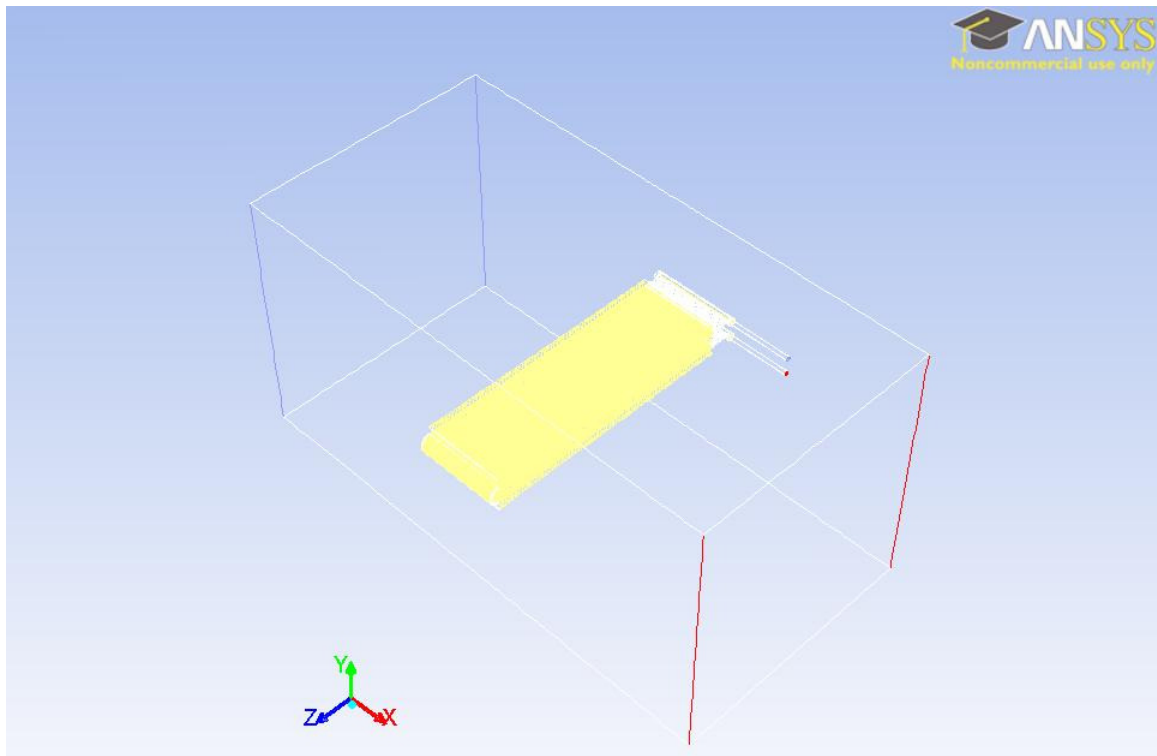
Figure 3.5. Computational domain (305mm x 305m x 610mm) with MICHX
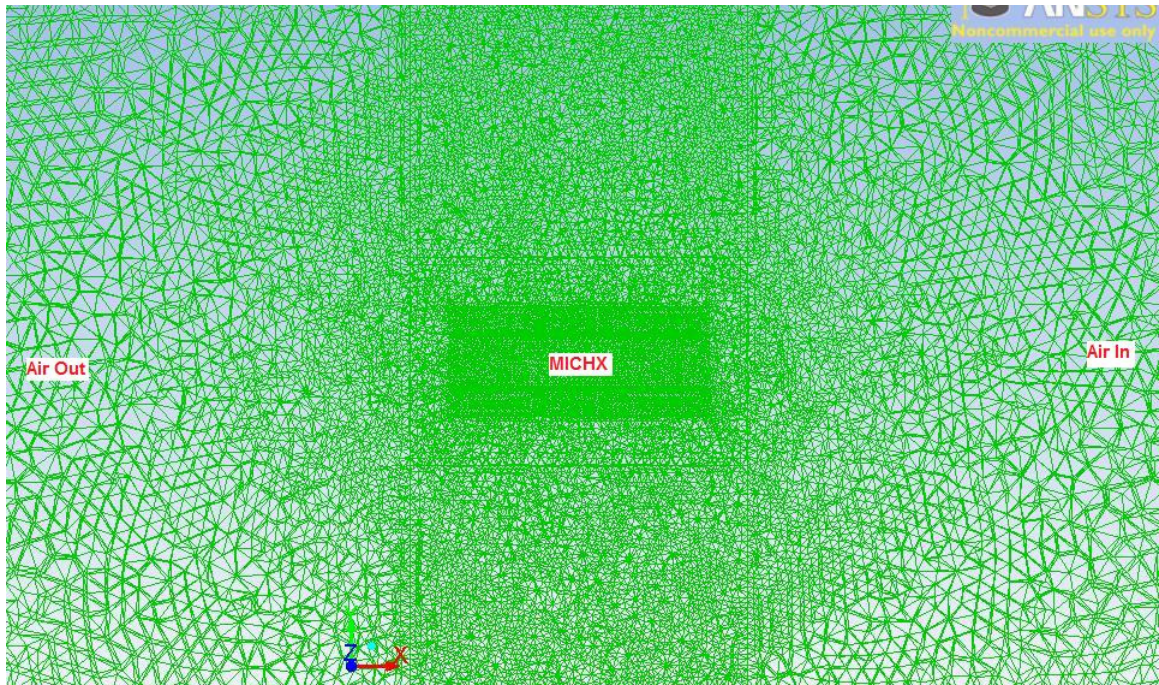
Figure 3.6a. Mesh in computational domain (XY plane)
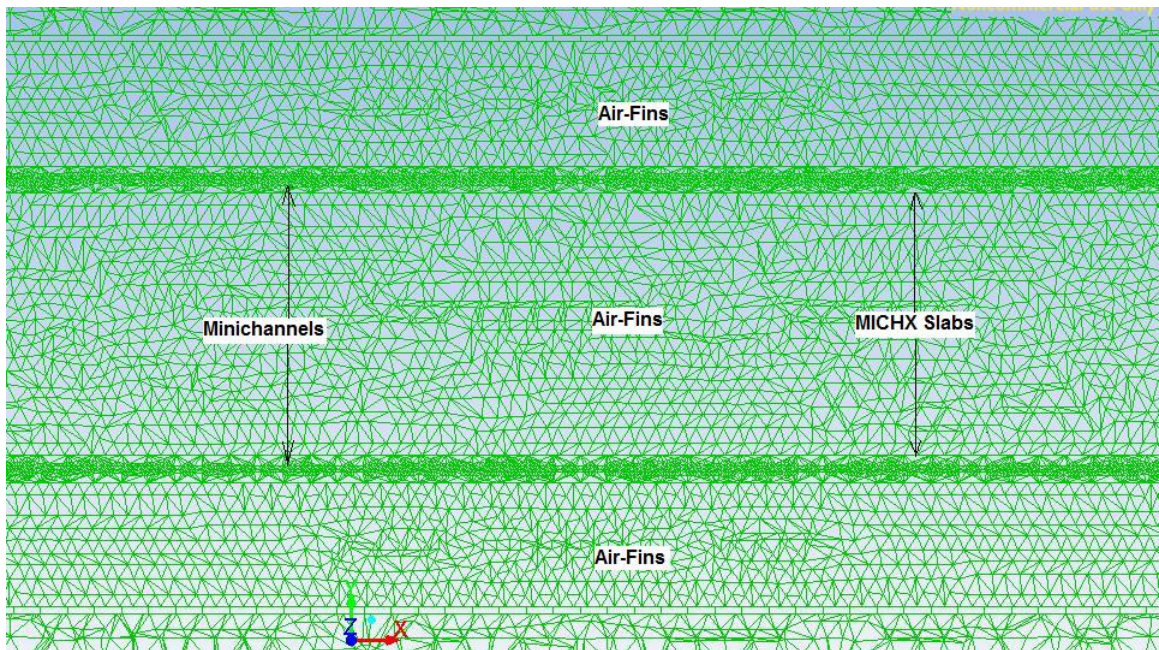
Figure 3.6b. Mesh in Test Specimen
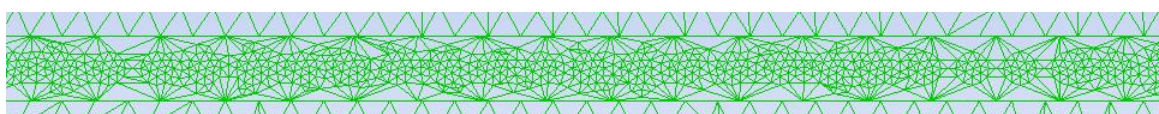
Figure 3.6c. Mesh in minichannels

Gambit 2.4, a commercial code of geometry modeling was used as a preprocessing tool to create physical model of the MICHX and generated mesh for FLUENT CFD solution. Type of meshing is a very important issue in Gambit operation, which directly affects the numerical results and convergence time. It was difficult to use a particular structured mesh for the entire domain due to the complexity of physical model with regard to the computational domain. Therefore, the whole computational domain was divided into some sub-domains and discretized with the unstructured tetrahedral elements. Clustering also plays a very significant role in numerical simulations in heat transfer and fluid flow analysis. In order to increase the accuracy of the results, the channel regions adjacent to the walls were clustered carefully. The detailed grid systems of computational domain are presented below.

- Domain Extents:

  x-coordinate: min (mm) = -305, max (mm) = 305

  y-coordinate: min (mm) = -163, max (mm) = 142

  z-coordinate: min (mm) = -333.65, max (mm) = 11.5

- Volume statistics:

  Minimum volume (mm^3): 6.27e-5

  Maximum volume (mm^3): 411.02

- Face area statistics:

  Minimum face area (mm^2): 2.265e-03

  Maximum face area (mm^2): 122.31

- Zones: 6 cell zones and 102 face zones.

- Mesh Details: Details of mesh are presented in Table 3.2.

Table 3.2 Details of mesh

Zone	Cell type	Number of cells
Solid_fins	Hexahedral	87300
Solid_slab	Wedge	949836
Fluid channels	Wedge	641784
Air	Tetrahedral	3143855
Fluid manifold_above	Mixed	315220
Fluid manifold_below	Mixed	315220
Total number of cells		5453215
Number of Faces		16135759
Number of Nodes		2097279
Maximum aspect ratio		1.73e+02

3.3 Numerical Method

The best method to know absolutely how a mathematical model will behave under any circumstances is the analytical solution. In this method, calculus, trigonometry, and other math techniques are used to find a solution to the set of equations. However, this method is likely to work only for simple models. For more complex models, the calculations become extremely complicated.

In those circumstances, numerical methods are the replacement of solving the equations. For a differential equation that defines behavior over time, the numerical

method starts with the initial values of the variables, and momentarily uses the equations to solve the changes in these variables. Thousands of repetitive calculations are involved with this method. A computer is essential to execute these calculations. The result is a long list of numbers, not an equation. It is just an approximation, while it can be a very good estimation under certain conditions.

The geometry of the minichannel heat exchanger (MICHX) model used in current study is very complex. Making an allowance for the complexity of the model, numerical method was carried out to find out the behavior of thermal and flow fields.

The computations were carried out with two Quad-Core CPUs having Random Access Memory (RAM) of 8GB. Three-dimensional double precision (3DDP) pressure-based absolute velocity formulation was utilized. Even though, the flow regime in liquid-side was both laminar and turbulent, the flow regime in air-side was turbulent. It is anticipated to choose an appropriate turbulent model to solve the heat transfer and fluid flow problems. In fact, unfortunately there is not a single turbulence model that is universally accepted as being superior for all types of problems. The standard k-ε turbulent model was considered to solve the fluctuating velocity fields for air-side turbulent flow.

3.3.1 Selection of Numerical Method

The selection of numerical method and model generally depends on many factors, such as complexity of the flow, specific type of problem, expected accuracy of results, availability of computational resources, and the amount of time for the simulation. It is desired to understand the capabilities, competences and limitations of various options to make the most suitable and appropriate choice of model for a specific application. Peiro

and Sherwin (2005) stated that there are many situations where obtaining an exact solution of a partial differential equation (PDE) is not possible

In computational modeling of any physical process, there are three conventional methods for numerical solution of PDEs, namely the finite difference method (FDM), the finite element method (FEM), and the finite volume method (FVM).

Finite difference method (FDM): Finite difference method is the oldest method, which is capable of handling complex geometries in multiple dimensions. It is based on the application of a local Taylor expansion to approximate the differential equations and uses a topologically square network of lines to generate the discretization of the PDE. From the inspiration of the use of an integral form of the PDEs, the finite element (FE) and finite volume (FV) techniques are developed.

Finite Element Method (FEM): Finite Element Method (FEM) is generally applied to structural analysis, which works on weighted residual technique. In FEM, nodal connectivity is important to come to be solution. Otherwise it may be fridge in solution domain. The code computes a length expansion and calculates the stress as the first derivation of the length. In order to do this, the FEM-Cell has to have at least a linear weight function, which may reduce the speed of the solution progress. The accuracy of results may be increased by using FE-methods in presence of a large overhead.

Finite Volume Method (FVM): Finite Volume Method (FVM) works on conservation principles. In FVM, nodal connectivity is not mandatory. Instead, face connectivity is necessary because flux between cell face has to be conserved. In computational fluid dynamics (CFD), calculation of a first derivation of a value is not required and accordingly only 1 node per cell (constant weight function) is sufficient in

FVM. To manage constant weight function instead of linear weight function leads to a lesser memory requirement. Eymard et al. (2006) confirmed that in FVM, the numerical flux is conserved from one discretization cell to its neighbour, which makes this method reasonably attractive for modeling of fluid mechanics, semi-conductor device simulation, heat and mass transfer problems.

Considering an allowance for the complexity of the geometry, limitation of processor speed, inadequacy of random access memory (RAM), and the type of problem dealing with, the simulations were performed with ANSYS FLUENT version 13.0, a widely used finite volume method (FVM) based commercial CFD code. This method has been extensively used in many engineering fields, such as fluid mechanics, heat and mass transfer or petroleum engineering.

3.3.2 Key Assumptions

The Navier-Stokes and energy equations were used to model the convective heat transfer and fluid flow process with the following assumptions:

(i) Steady fluid flow and heat transfer

(ii) Incompressible fluid flow

(v) Heat transfer between the heat exchanger and the surroundings by radiation or conduction is negligible due to appropriate thermal insulation

(vi) No heat loss or gain by the air to or from the outside surroundings near the test chamber

(vii) Thermo-physical properties of all liquid working fluids are temperature dependent

(viii) Turbulence effects are accounted for using the standard k-ε turbulent model with standard wall function.

3.4 Setup of Computational Parameters

In order to solve any problem by using numerical simulation, an accurate setup of computational parameters, such as model, boundary conditions and solver settings are very significant. Simulation process, time and accuracy depend on these issues. In current study, the computational simulations were carried out in 3-dimentional, double precision, pressure-based, absolute velocity formulation and implicit scheme. Detailed physical and numerical key issues and computational parameters are presented in this chapter.

3.4.1 Model Setup

Setting an appropriate model for solving heat transfer problems is very important for consistency and accuracy of results. Different settings of numerical model for this study are presented in Table 3.3.

Table 3.3 Model setting

Model	Settings
Space	3D
Time	Steady
Viscous	Standard k-epsilon turbulence model
Viscous heating	Enabled
Energy	Enabled
Radiation	None
Other parameters	Disabled
Model constants	$C_\mu = 0.09$, $C_{1\varepsilon} = 1.44$, and $C_{2\varepsilon} = 1.92$
	TKE Prandtl number = 1
	TDR Prandtl Number = 1.3
	Wall Prandtl number = 0.85
	Energy Prandtl number = 0.85

3.4.2 Material Properties

An appropriate setup of material thermo-physical properties in CFD simulations is a very significant matter, especially for heat transfer cases. Properties of all materials, such as air, liquids, and solid are illustrated in this chapter.

(i) Material: air (fluid)

In all cases the numerical simulation is performed using air as the gaseous medium flowing over the heat exchanger. This is a good representation of most typical applications where a flow of air is used to remove heat from a device. As the thermo-physical properties of air changes very little with a little changes in air-side temperature,

the thermo-physical properties of air are considered constant and used the default values of ANSYS FLUENT as presented in Table 3.4.

Table 3.4 Thermo-physical properties of air			
Property	Units	Method	Value(s)
Density	kg/m3	constant	1.225
Cp (Specific Heat)	j/kg-k	constant	1006.43
Thermal Conductivity	w/m-k	constant	0.0242
Viscosity	kg/m-s	constant	1.7894e-05
Molecular Weight	kg/kgmol	constant	28.966
L-J Characteristic Length	angstrom	constant	3.711
L-J Energy Parameter	k	constant	78.6
Thermal Expansion Coefficient, 1/k		constant	0
Degrees of Freedom		constant	0
Speed of Sound	m/s	n/a	

(ii) Material: Liquid (fluid) – Engine oil, automatic transmission fluid (ATF), 50% ethylene glycol, and water

Inside the channels four liquids, namely engine oil, ATF, 50% ethylene glycol, and water are considered. These liquids are of interest as they have applications in cooling in many industries, for example in automotive applications. The thermo-physical properties including the thermal conductivity (k), specific heat (C_p), density (ρ), and dynamic viscosity (μ) of liquids vary considerably with temperature. As the physical properties of the working fluids especially liquids are temperature dependent, relevant correlations are utilized to account for these properties.

Thermophysical properties of liquids were composed from Ashrae (1997), CAN-AM Instruments Ltd, Kemp and Linden (1990), and Shell Nederland. The piece-wise linear relationship are considered for thermal conductivity (k), specific heat (C_p), and density (ρ) of the liquid fluids with temperature. Whereas, a polynomial approaches of FLUENT is considered for the viscosity (μ) of the each liquid with temperature. The relationships among the thermo-physical properties of liquid fluids and temperature are shown in Figs 3.7-3.11.
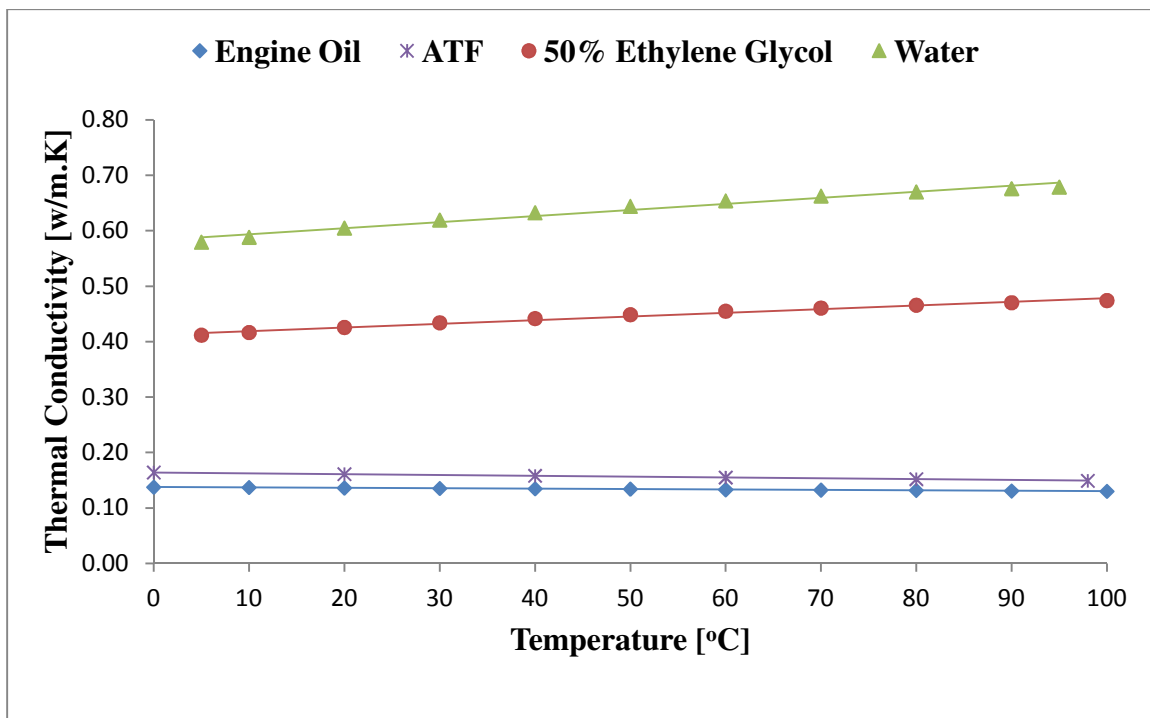
Figure 3.7. Variations of thermal conductivity of different liquids with temperature
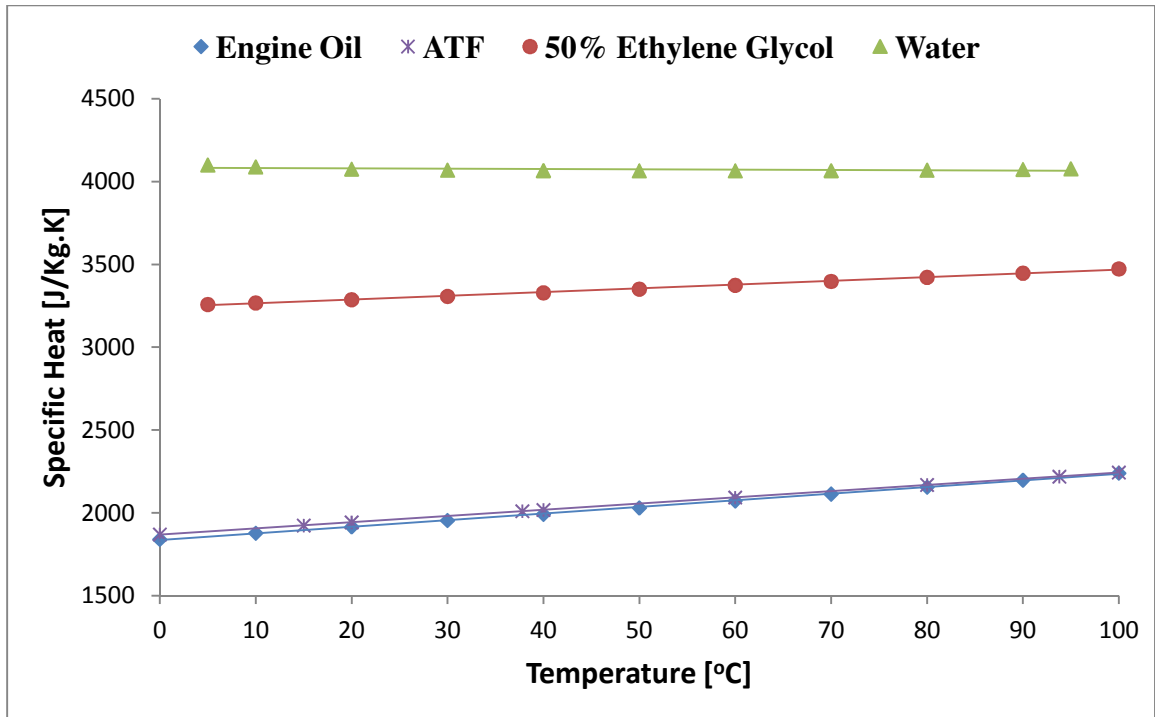
Figure 3.8. Variations of specific heat of different liquids with Temperature
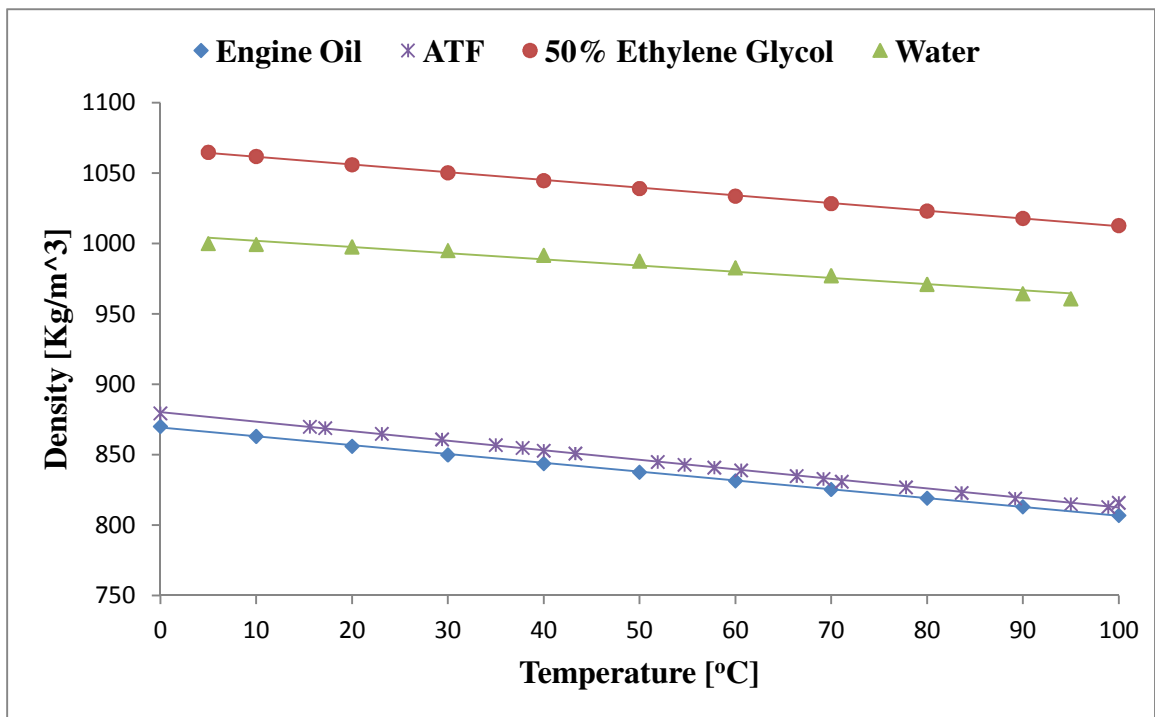
Figure 3.9. Variations of density of different liquids with temperature
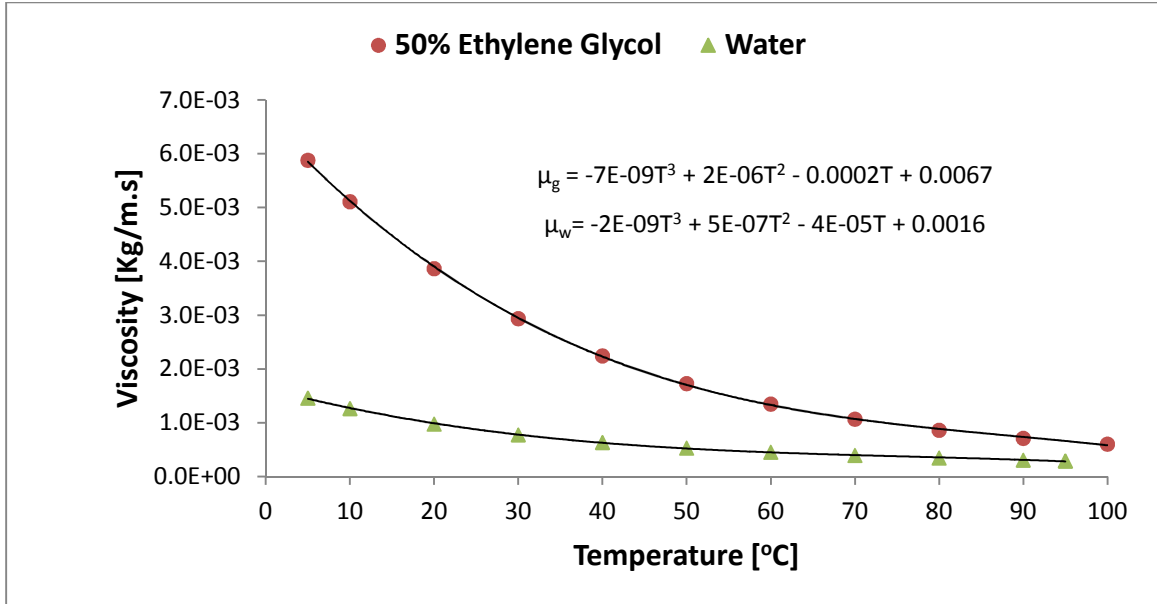
Figure 3.10. Variations of viscosity of water and 50% ethyline glycol with temperature

$$\mu_g = -7E\text{-}09T^3 + 2E\text{-}06T^2 - 0.0002T + 0.0067$$

$$\mu_w = -2E\text{-}09T^3 + 5E\text{-}07T^2 - 4E\text{-}05T + 0.0016$$
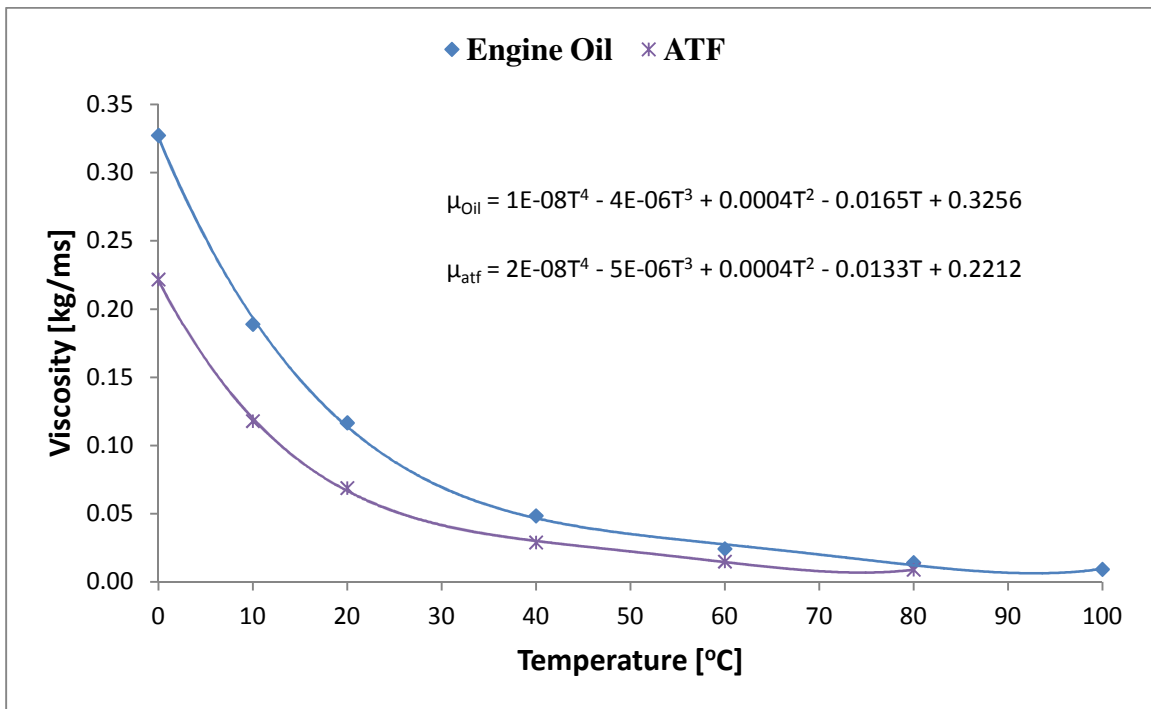
Figure 3.11. Variations of viscosity of engine oil and ATF with temperature

$$\mu_{Oil} = 1E\text{-}08T^4 - 4E\text{-}06T^3 + 0.0004T^2 - 0.0165T + 0.3256$$

$$\mu_{atf} = 2E\text{-}08T^4 - 5E\text{-}06T^3 + 0.0004T^2 - 0.0133T + 0.2212$$

(iii) Material: aluminum (solid)

There is no significant change in physical properties, such as density, specific heat, and thermal conductivity of aluminum with temperature within the range of the operating conditions in the current study. Hence, the default values of aluminum properties in ANSYS FLUENT are considered, which are shown in Table 3.5.

Table 3.5. Thermo-physical properties of aluminum			
Property	Units	Method	Value(s)
Density	kg/m3	constant	2719
Cp (Specific Heat)	j/kg-k	constant	871
Thermal Conductivity	w/m-k	constant	202.4

3.4.3 Boundary Conditions

The following boundary conditions are applied for the computational domain:

- Inlet working fluids: Mass flow rates and temperature were specified for both liquid-side and air-side.

- Outlet liquids: Outflow boundary condition was specified.

- Outlet air: Outflow boundary condition was specified with following computational parameters.

- Inlet and outlet manifolds and headers: Zero heat flux was specified.

- Serpentine: Zero heat flux was specified at outer and inner surface at the serpentine bend.

- Walls: wall the boundary condition was for test chamber walls.

Inlet boundary conditions of working fluids and wall boundary conditions for test chamber walls are shown in Tables 3.6 and 3.7 respectively.

Table 3.6. Inlet Boundary Conditions of Working Fluids	
Parameters	Magnitudes
Inlet liquid temperature (^{o}C)	76
Inlet liquid mass flow rates (g/s)	
DI-water	0.9, 1.3, 1.8, 2.2, 2.6, 3.1, 3.5, 18.8, 25.5, 33.7, 39.4, 47.3, 51.6, 59.7, 66.1, and 76.0
50 % Ethylene glycol	2.6, 3.9, 5.2, 6.5, 7.8, 9.1, 10.4, 18.8, 25.5, 33.7, 39.4, 47.3, 51.6, 59.7, 66.1, and 76.0
Automatic transmission fluid (ATF)	18.8, 25.5, 33.7, 39.4, 47.3, 51.6, 59.7, 66.1, and 76.0
Engine oil	18.8, 25.5, 33.7, 39.4, 47.3, 51.6, 59.7, 66.1, 76.0, 101.4, and 126.7
Inlet air temperature (^{o}C)	14
Inlet air mass flow rate (g/s)	507

Table 3.7. Wall Boundary Conditions	
Wall thickness	0
Heat generation rate	0
Convective heat transfer coefficient	0
Thermal BC Type	1
Free Stream Temperature (k)	300
Wall Motion	Stationary
Shear Boundary Condition	No slip
Wall Roughness Constant	0.5

3.4.4 Solver Settings

- Type: Pressure-based

- Velocity formulation: Absolute

Other important computational parameters are presented in Table 3.8 and 3.9.

Table 3.8. Solver Setting	
Relaxation	
Variables	Relaxation Factor
Pressure	0.3
Density and Body Forces	1
Momentum	0.7
Turbulent Kinetic Energy (TKE)	0.8
Turbulent Dissipation Rate (TDR)	0.8
Turbulent Viscosity and Energy	1

Table 3.9. Linear Solver			
Linear Solver			
Variable	Solver	Termination	Residual
	Type	Criterion	Reduction Tolerance
Pressure	V-Cycle	0.1	
X, Y, and Z Momentum	Flexible	0.1	0.7
Turbulent Kinetic Energy (TKE)	Flexible	0.1	0.7
Turbulent Dissipation Rate	Flexible	0.1	0.7
Energy	Flexible	0.1	0.7
Pressure-Velocity Coupling	SIMPLE		
Discretization Scheme			
Pressure	Standard		
Momentum	First Order Upwind		
Turbulent Kinetic Energy (TKE)	First Order Upwind		
Turbulent Dissipation Rate (TDR)	First Order Upwind		
Energy	First Order Upwind		
Solution Limits			
Minimum Absolute Pressure	1		
Maximum Absolute Pressure	5e+10		
Minimum Temperature	1		
Maximum Temperature	5000		
Minimum Turbulent Kinetic Energy	1e-14		
Minimum Turbulent Dissipation Rate	1e-20		
Maximum Turbulent Viscosity Ratio	1e+12		

3.4.5 Residuals

The sum of the normalized absolute residuals in each control volume for the flow and energy variables were reduced to 1e-04 and 1e-08 respectively when successive iteration was stopped.

3.4.6 Solution Initialization: Standard Initialization

3.5 Governing Equations

Computational fluid dynamics (CFD) is basically based on the governing equations of fluid dynamics. The physical phenomena of the fluid motion can generally be defined in fundamental mathematical equations, usually in partial differential form, which govern a process of interest and are often called governing equations in CFD. They represent mathematical statements of the conservation laws of physics [Tu et al. 2008].

One of the most important steps of the modeling process is to characterize the idealization of the physical reality by the governing equations of the problem. In fluid dynamics, the Navier–Stokes equations are considered to be an appropriate representation of the irrotational (without vorticity) flow of an incompressible fluid flow [Peiro and Sherwin, 2005]. In current study, time-averaged instantaneous (exact) governing equations of continuity, momentum, energy, turbulence kinetic energy, k, and rate of dissipation, ε, are used to the convective heat transfer and fluid flow problems based on the key assumptions. In this section, a brief explanation of each equation is presented.

3.5.1 Continuity or Mass Conservation Equation

The continuity or mass conservation equation used in ANSYS FLUENT is

$$\frac{\partial \rho}{\partial t} + \nabla.(\rho \vec{v}) = S_m \tag{3.1}$$

where, ρ is density, t is time, $\vec{v}$ is velocity, and S_m is mass source i.e. the mass added due to vaporization of liquid droplets or condensation of air.

Based on the assumptions, the simplified form of continuity equation (Eq. 3.1) becomes

$$\frac{\partial}{\partial x_i}(\rho u_i) = 0 \tag{3.2}$$

3.5.2 Momentum Equation

The conservation of momentum in an inertial (non-accelerating) reference frame used in ANSYS FLUENT is

$$\frac{\partial}{\partial t}(\rho \vec{v}) + \nabla.(\rho \vec{v}\vec{v}) = -\nabla P + \nabla.(\bar{\bar{\tau}}) + \rho \vec{g} + \vec{F} \tag{3.3}$$

where P is the static pressure, $\rho \vec{g}$ is the gravitational body force, and $\vec{F}$ is external body force.

$\bar{\bar{\tau}}$ represents the stress tensor and may be defined as

$$\bar{\bar{\tau}} = \left[(\nabla \vec{v} + \nabla \vec{v}^T) - \frac{2}{3} \nabla.\vec{v}I \right] \tag{3.4}$$

where μ, I, and the term $\left(\frac{2}{3} \nabla.\vec{v}I \right)$ represent the molecular viscosity, the unit tensor, and the effect of volume dilation respectively.

According to the assumptions, the simplified form of momentum equation (Eq. 3.3) is

$$\frac{\partial}{\partial x_i}(\rho u_i u_k) = \frac{\partial}{\partial x_i}\left(\mu \frac{\partial u_k}{\partial x_i} \right) - \frac{\partial P}{\partial x_i} + \frac{\partial}{\partial x_i}(-\rho \overline{u_i' u_j'}) \tag{3.5}$$

3.5.3 Energy Equation

The energy equation is modeled according to the concept of Reynolds analogy to turbulent momentum transfer used in ANSYS FLUENT is

$$\frac{\partial}{\partial t}(\rho E) + \frac{\partial}{\partial x_i}[u_i(\rho E + P)] = \frac{\partial}{\partial x_j}\left(k_{eff}\frac{\partial T}{\partial x_j} + u_i(\tau_{ij})_{eff}\right) + S_h \qquad (3.6)$$

where E, k_{eff}, and $(\tau_{ij})_{eff}$ are the total energy, effective thermal conductivity, and deviatoric stress tensor respectively.

The effective thermal conductivity, k_{eff} is calculated as

$$k_{eff} = k + \frac{C_p}{Pr_t} \qquad (3.7)$$

where k, is the thermal conductivity. The default value of the turbulent Prandtl number, Pr is 0.85.

The deviatoric stress tensor, $(\tau_{ij})_{eff}$ represents the viscous heating and may be defined as

$$(\tau_{ij})_{eff} = \mu_{eff}\left(\frac{\partial u_j}{\partial x_i} + \frac{\partial u_i}{\partial x_j}\right) - \frac{2}{3}\mu_{eff}\left(\frac{\partial u_k}{\partial x_k}\delta_{ij}\right) \qquad (3.8)$$

Based on assumptions, the simplified energy equation (Eq. 3.6) can be written as

$$\frac{\partial}{\partial x_i}(\rho u_i T) = \frac{\partial}{\partial x_j}\left(k_{eff}\frac{\partial T}{\partial x_j} + u_i(\tau_{ij})_{eff}\right) \qquad (3.9)$$

3.5.4 Turbulent Kinetic Energy Equation, k

The general equation of turbulence kinetic energy, k used in ANSYS FLUENT is

$$\frac{\partial}{\partial t}(\rho k) + \frac{\partial}{\partial x_i}(\rho k u_i) = \frac{\partial}{\partial x_j}\left[(\mu + \frac{\mu_t}{\sigma_k})\frac{\partial k}{\partial x_j}\right] + G_k + G_b - \rho\epsilon - Y_M + S_k \qquad (3.10)$$

where, G_k represents the generation of turbulence kinetic energy due to the mean velocity gradients,

G_b is the generation of turbulence kinetic energy due to buoyancy,

Y_M represents the contribution of the fluctuating dilatation in compressible turbulence to the overall dissipation rate,

σ_k the turbulent Prandtl numbers for k and

S_k is the user-defined source term.

Based on assumptions, the simplified form of the turbulent kinetic energy equation, k (Eq. 3.10) may be written as

$$\frac{\partial}{\partial x_i}(\rho k u_i) = \frac{\partial}{\partial x_j}\left[(\mu + \frac{\mu_t}{\sigma_k})\frac{\partial k}{\partial x_j}\right] + G_k - \rho \epsilon \tag{3.11}$$

The term, G_k may be defined from the exact equation for the transport of k as

$$G_k = -\rho \overline{u_i' u_j'}\frac{\partial u_i}{\partial x_i} \tag{3.12}$$

3.5.5 Turbulent Energy Dissipation, ε

The turbulent energy dissipation rate, ε, used in ANSYS FLUENT is

$$\frac{\partial}{\partial t}(\rho \epsilon) + \frac{\partial}{\partial x_i}(\rho \epsilon u_i) = \frac{\partial}{\partial x_j}\left[(\mu + \frac{\mu_t}{\sigma_\epsilon})\frac{\partial \epsilon}{\partial x_j}\right] + C_{1\epsilon}\frac{\epsilon}{k}(G_k + C_{3\epsilon}G_b) - C_{2\epsilon}\rho\frac{\epsilon^2}{k} + S_\epsilon \tag{3.13}$$

where, $C_{1\epsilon}, C_{2\epsilon}$, and $C_{3\epsilon}$ are constants

σ_ϵ the turbulent Prandtl numbers for ϵ and

S_ϵ is user-defined source terms.

According to the key assumptions, the equation for the turbulent energy dissipation (Eq. 3.13), may be simplified as

$$\frac{\partial}{\partial x_i}(\rho \epsilon u_i) = \frac{\partial}{\partial x_j}\left[(\mu + \frac{\mu_t}{\sigma_\epsilon})\frac{\partial \epsilon}{\partial x_j}\right] + C_{1\epsilon}\frac{\epsilon}{k}G_k - C_{2\epsilon}\rho\frac{\epsilon^2}{k} \tag{3.14}$$

The turbulent (or eddy) viscosity, μ_t is computed by combining k and ϵ as

$$\mu_t = \rho C_\mu \frac{k^2}{\epsilon} \tag{3.15}$$

where, C_μ is a constant.

3.6 Heat Transfer and Fluid Flow Fundamental Equations

3.6.1 Heat Transfer Rate (Q)

The steady state heat transfer between the hot liquid fluids and the cold air through MICHX slab wall due to the forced convection is calculated as

$$Q_l = \dot{m}Cp_l(T_{i,l} - T_{o,l}), \text{ for liquid-side heat transfer rate} \qquad (3.16)$$

and

$$Q_a = \dot{m}Cp_a(T_{o,a} - T_{i,a}), \text{ for air-side heat transfer rate} \qquad (3.17)$$

where, Cp is specific heat and T is temperature. The subscripts *l, a, i,* and *o* stand for liquid, air, inlet, and outlet respectively.

3.6.2 Heat Transfer Coefficient (h)

The heat transfer coefficient of the liquids, h_l, is estimated as

$$h_l = \frac{Q_l}{A_s(T_b - T_s)} \qquad (3.18)$$

where, A_s is the heat transfer surface area, T_b is the liquid bulk temperature, and T_s is the inner surface or wall temperature of the channel.

3.6.3 Heat Balance and Mass Balance

In numerical computations, errors may occur because of round-off, truncation, and discretization errors. Errors arise due to the storage and processing of numerical data. It is impossible to denote all real numbers, which have infinitely many digits, exactly on a machine with finite memory. Once an error is made, it may accumulate in certain cases and usually propagates through the calculation.

The errors in heat balance (HB%) and mass balance (MB%) are evaluated as

$$HB\% = \frac{(Q_l - Q_a) \times 100}{Q_{avg}} \qquad (3.19)$$

and

$$MB\% = \frac{(\dot{m}_{i,l} - \dot{m}_{o,l}) \times 100}{\dot{m}_{i,l}} \qquad (3.20)$$

where, Q_l is the liquid-side heat transfer rate in w,

Q_a is the air-side heat transfer rate in w,

Q_{avg} is the average heat transfer rate,

$\dot{m}_{i,l}$ is the inlet-liquid flow rate in kg/s, and

$\dot{m}_{o,l}$ is the outlet-liquid flow rate in kg/s.

The effective or mean heat transfer rate (Q_{avg}) is defined as the arithmetic average of liquid-side and air-side heat transfer rates which is calculated as

$$Q_{avg} = \frac{Q_l + Q_a}{2} \qquad (3.21)$$

3.6.4 Mean Average Errors (%Error)

The errors in simulation results with compared to experimental results for above mentioned parameters are calculated as

$$\%Error\ in\ T_{o,l} = \frac{1}{N}\sum \frac{|T_{o,l\_exp} - T_{o,l\_num}|}{T_{o,l\_exp}} \times 100\% \qquad (3.22)$$

$$\%Error\ in\ T_{o,a} = \frac{1}{N}\sum \frac{|T_{o,a\_exp} - T_{o,a\_num}|}{T_{o,a\_exp}} \times 100\% \qquad (3.23)$$

$$\%Error\ in\ T_{ser} = \frac{1}{N}\sum \frac{|T_{ser\_exp} - T_{ser\_num}|}{T_{s\_exp}} \times 100\% \qquad (3.24)$$

$$\%Error\ in\ \Delta P_l = \frac{1}{N}\sum \frac{|\Delta P_{l\_exp} - \Delta P_{l\_num}|}{\Delta P_{l\_exp}} \times 100\% \qquad (3.25)$$

where, T is temperature, ΔP is pressure drop, and subscript o, l, a, ser, exp, and num stand for outlet, liquid, air, serpentine region respectively.

3.7 Dimensionless Fluid Flow and Heat Transfer Parameters

Many dimensionless parameters are generally used in fluid mechanics to characterize the heat transfer and fluid flow behavior. Some important dimensionless parameters associated with heat transfer and fluid flow, which are used in current study, are briefly described in this chapter.

3.7.1 Reynolds Number (Re)

Reynolds number (Re) is a very significant parameter in fluid mechanics. It is named after the British engineer and physicist, Osbourne Reynolds. It is defined as the ratio of inertia force to the viscous force and used to characterize the nature and flow regime of fluids. The general expression of Reynolds number is

$$Re = \frac{Inertia\ force}{viscous\ force} = \frac{\rho V^2 A}{\frac{\mu V A}{L}} = \frac{\rho V L}{\mu} = \frac{\rho V D_{ch}}{\mu} \tag{3.26}$$

For circular channel with diameter, D_{ch}, Eq. 3.26 can be rewritten as

$$Re = \frac{\rho V D_{ch}}{\mu} = \frac{4\dot{m}_l}{N\mu_{i,ch}\pi D_{ch}} \tag{3.27}$$

It specifies the flow characteristics, such as laminar, transitional, or turbulent regime. In a flow, usually the fluid viscous force acts for managing stability of flow, while fluid inertia is liable for disorganizing the flow. For small Reynolds numbers, the inertial is not that significant, therefore the flow is laminar and smooth. On the other hand, for high Reynolds number, the inertia plays an important role, and it is dominant. As a result, the flow is turbulent.

3.7.2 Prandtl Number (Pr)

The Prandtl number (Pr) is a dimensionless number, which is widely used in heat transfer approximations. It is named after the German physicist Ludwig Prandtl. It is defined as the ratio of momentum diffusivity (kinematic viscosity) to the thermal diffusivity and expressed as

$$Pr = \frac{Momentum\ diffusivity}{Thermal\ diffusivity} = \frac{v}{\alpha} = \left(\mu/\rho\right)/\left(\frac{k}{\rho C_p}\right) = \frac{\mu C_p}{k} \qquad (3.28)$$

where, v = kinematic viscosity = $\frac{\mu}{\rho}$,

α = thermal diffusivity = $\frac{k}{\rho C_p}$,

$\mu = dynamic\ viscosity$,

$k = thermal\ conductivity$

C_p = specific heat, and

ρ = density.

The Pr is related to viscosity, specific heat, and thermal conductivity of fluid, and describes the development of thermal boundary layer thickness on the heat transfer surface. The thermal boundary layer is a barrier to the heat transfer. Smaller Pr means that the heat diffuses very quickly than the velocity (momentum).

3.7.3 Brinkman Number (Br)

The Brinkman number (Br) is a very significant dimensionless number for viscous fluids like engine oil and ATF. It is the measure of viscous heating relative to the conductive heat transfer of fluid flowing through the channel. It is defined as the ratio of the heat generated by viscous dissipation to the heat transferred from the wall to the fluid or vice versa depending on fluid heating or cooling. The Br is expressed as

$$Br = \frac{Viscous\ dissipation}{Thermal\ conduction} = \frac{\mu V^2}{k(T_{m,l} - T_s)} \tag{3.29}$$

Viscous heating is important, when $Br \geq 1$.

The Br shows the importance of the temperature rise in the fluid due to viscous dissipation. It has a significant influence on viscous dissipation, which may be very significant for high-viscosity and low specific heat capacity fluids even in relatively low Reynolds number flow [Koo and Kleinstreuer, 2004].

3.7.4 Nusselt Number (Nu)

Nusselt number (Nu) was named after a German Engineer Ernst Kraft Wilhelm Nusselt. It is a very important dimensionless parameter in convective heat transfer fields, and is generally expressed as

$$Nu = \frac{Convective\ heat\ transfer\ coefficient}{conductive\ heat\ transfer\ coefficient} = \frac{hL}{k} \tag{3.30}$$

It depends on channel geometry, fluid heat transfer coefficient, and conductivity. For a circular geometry channel, $L = D_{ch}$. Therefore, the expression for Nu becomes

$$Nu = \frac{hD_{ch}}{k} \tag{3.31}$$

where, L is the characteristics length, D_{ch} is the channel diameter, h is the heat transfer coefficient, and k is the thermal conductivity of liquid at bulk temperature.

CHAPTER IV

ANALYSIS OF RESULTS

The main goal of the current study is to numerically investigate the heat transfer and fluid flow key parameters of different viscous fluids, namely engine oil, automatic transmission fluid (ATF), 50% ethylene glycol, and DI-water. In order to successfully achieve the study goal, the fluid flow behavior and convective heat transfer phenomena of the four liquids were numerically examined very carefully. The important parameters of the heat transfer and flow fields, such as, flow and temperature distributions, heat transfer rate, Reynolds numbers, heat transfer coefficient, Nusselt numbers, and Prandtl number of all these liquids were computed cautiously. Pressure drop and friction factor of the MICHX were also investigated.

The numerical simulations were performed at constant inlet liquid and air temperature of 76°C and 14°C respectively. The hot liquids at different mass flux of engine oil, automatic transmission fluid (ATF), 50% ethylene glycol, and DI-water were varied from $353 - 3796$, $353 - 1423$, $49 - 1423$, and $17 - 1423$ respectively. The ranges of Reynolds numbers for the four liquids computed at their corresponding bulk temperature were as $17 - 235$, $27 - 131$, $33 - 1439$, and $34 - 3802$. All four liquids were cooled with a constant air flow rate of 0.507kg/s.

The Prandtl numbers of engine oil, ATF, 50% ethylene glycol, and DI-water at bulk temperature were varied from $261 - 334$, $152 - 180$, $7.3 - 11.1$, and 2.33 respectively.

4.1 Verification of Numerical Results

In order to ensure the model was a good representation of reality, two categories of checks were performed. That included a numerical verification where the model was checked numerically to ensure accuracy and consistency. Once that was ensured, a selected set of the results were compared with experimental measurements to ensure good real-world agreement. The numerical verification was performed in a few ways.

Firstly, a grid dependence study was performed in order to ensure that the grid was fine enough to properly capture the features of the fluid flow and thermal fields. Four different grid systems (GS) were generated and compared for the numerical simulations. The results are presented in Fig. 4.1.
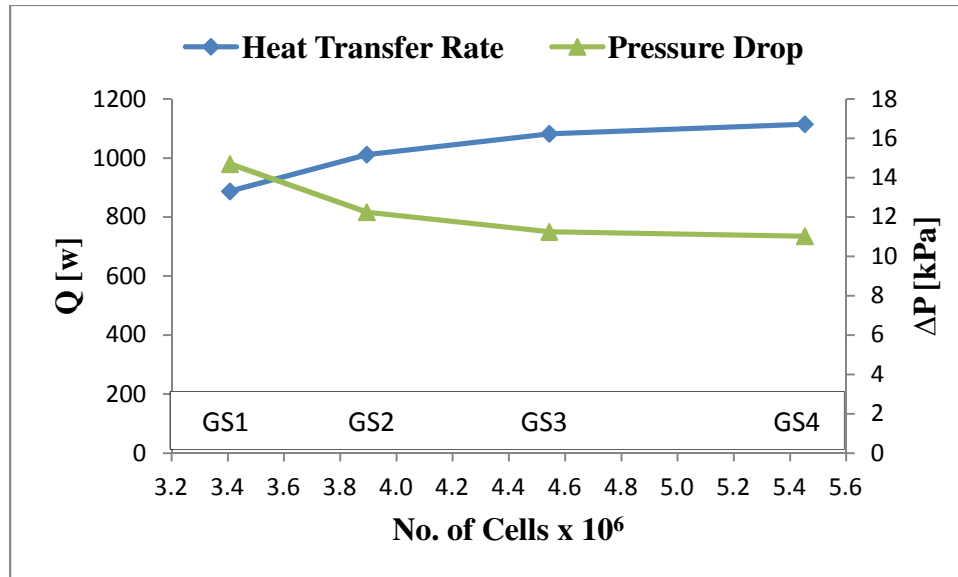

Figure 4.1. Heat transfer (Q) rate and pressure drop (ΔP) in different grid systems

The relative variations in the heat transfer and pressure drop between different grid systems are shown below;

Grid Systems	[%] Variations in Q	[%] Variations in ΔP
GS1 & GS2	12.28	20.00
GS2 & GS3	6.54	8.89
GS3 & GS4	2.91	2.04

Since the variations in heat transfer rate and pressure were found to be less than 3% between grid system 3 & 4, the GS4 which included about 5.45×10^6 grid cells was finally considered in all of the numerical simulations.

Other verification checked relate to overall mass and heat balance of the system. According to the law of conservation of mass and energy, the mass of an isolated system will remain constant over time and the heat transfer should ideally be the same for both liquid-and air-sides. Whereas, in numerical results it is observed the relationship are $\dot{M}_{i,l} \neq \dot{M}_{o,l}$ and $\dot{Q}_l \neq \dot{Q}_a$. The errors in heat balance and mass balance were calculated by using Eqs. 3.19 and 3.20. The errors observed in numerical simulations are mainly due to the rounding off the numbers because it is not possible to symbolize all real numbers exactly on a machine with finite memory. Some computational issues such as quality of meshes and residuals are also accountable for this error. The overall error in heat balance in all cases considered in this study was found in a range of ±1.03%, which is very acceptable. Similarly, the error in mass balance was calculated, which was found in the range of ±0.04%. This range of error is very acceptable as well. The computed results are shown in Figs. 4.2 and 4.3.
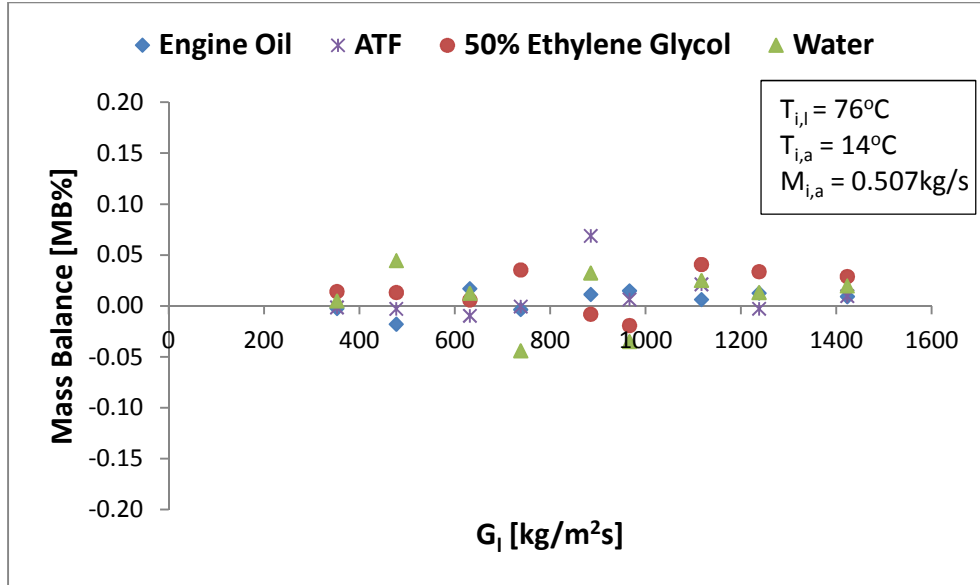
Figure 4.2. Percentage of errors in mass balance with mass fluxes
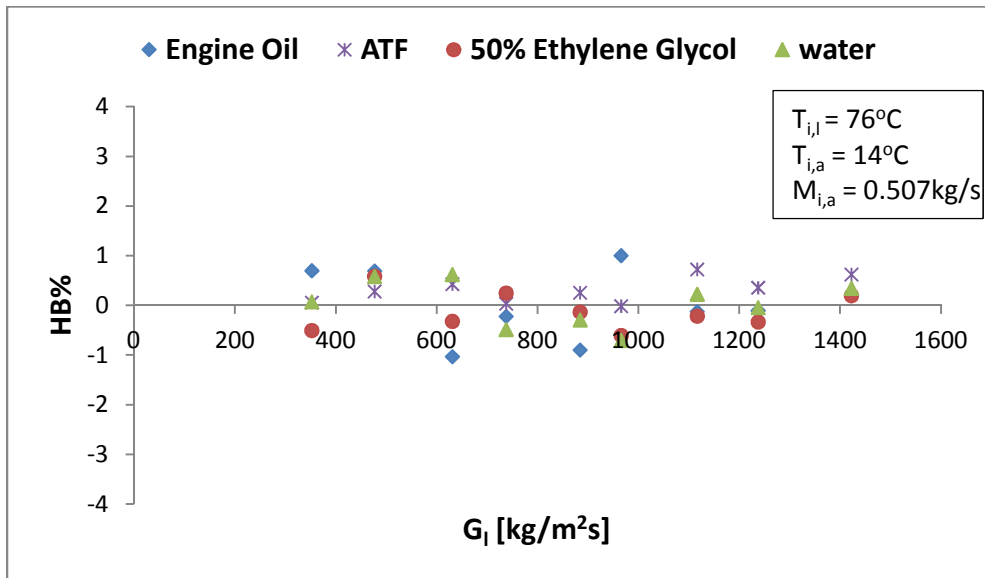
Figure 4.3. Percentage of errors in heat balance with mass fluxes

4.2 Validation of Numerical Results with Experimental Measurements

Once the model was shown to be numerically consistent, it was validated by comparing its predictions against experimental measurements. The heat transfer results in serpentine slab for 50% ethylene glycol and DI-water are compared. The comparisons between the numerical results and experimental measured data were evaluated for the

liquid-side outlet temperature, air-side outlet temperature, liquid-side pressure drop, and average surface temperature around the serpentine of the MICHX slab as a function of liquid-side Reynolds number. They are presented in Figs. 4.4-4.7.
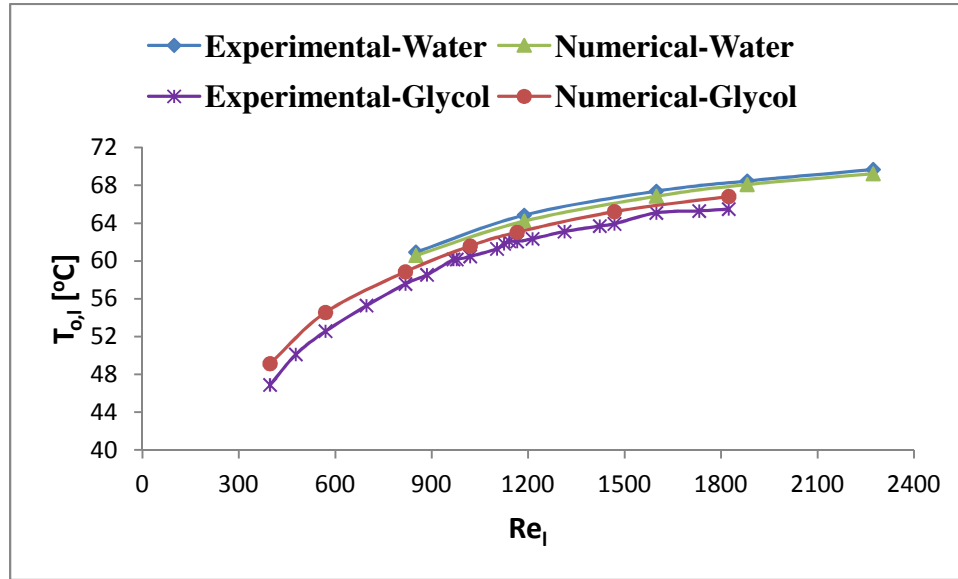
Figure 4.4. Variations of outlet temperature of liquid with Re_l
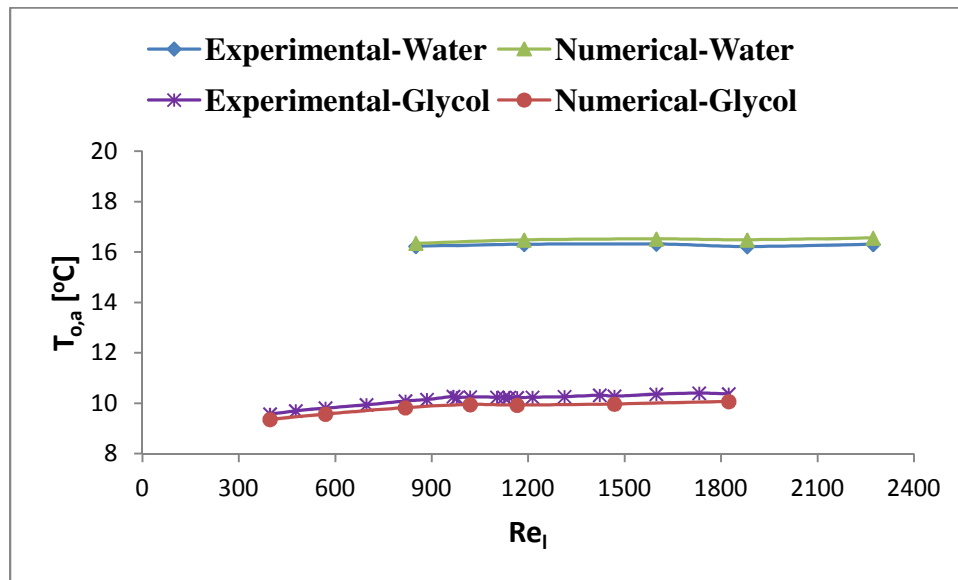
Figure 4.5. Variations of outlet temperature of air with Re_l
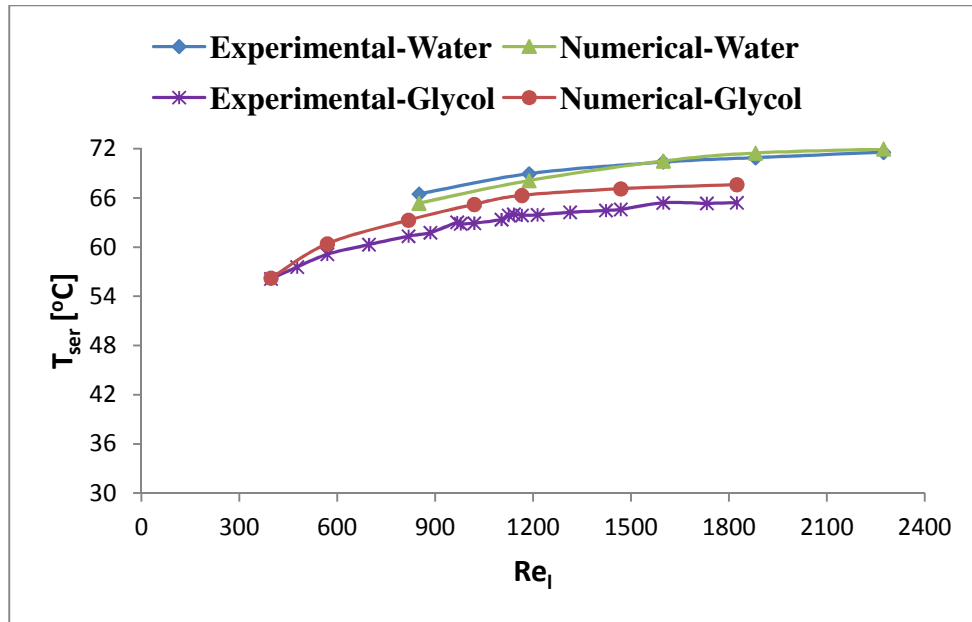
Figure 4.6. Variations of temperature around the serpentine region with Re_l
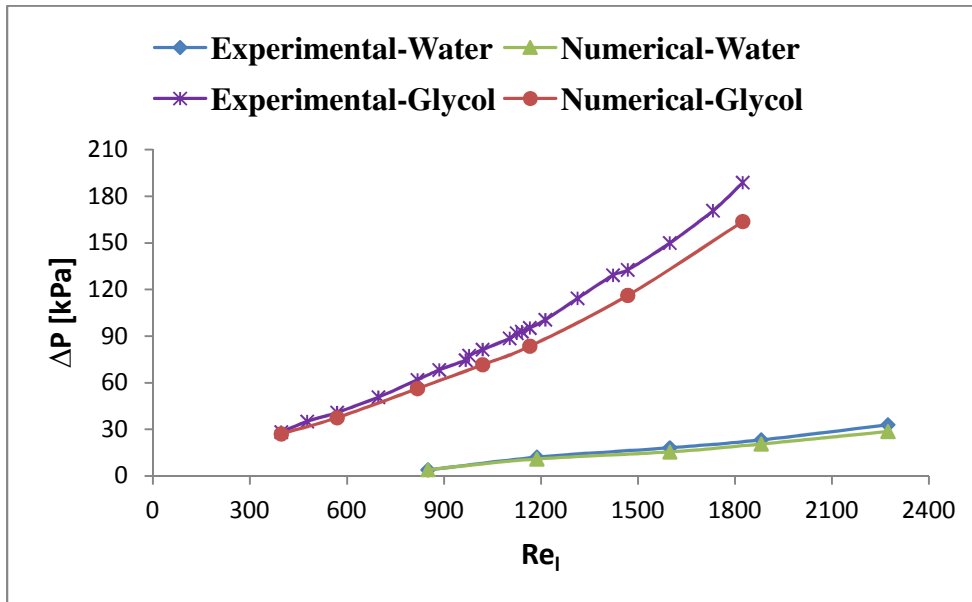
Figure 4.7. Variations of liquid-side pressure drop with Re_l

For water and ethylene glycol, percentage of mean average errors (%MAE) in simulation results were evaluated for liquid outlet temperature, air outlet temperature, temperature around the serpentine region and liquid-side pressure drop by using the Eqs. 3.22, 3.23, 3.24, and 3.25 respectively. Evaluated errors are shown in Figs. 4.8-4.11.
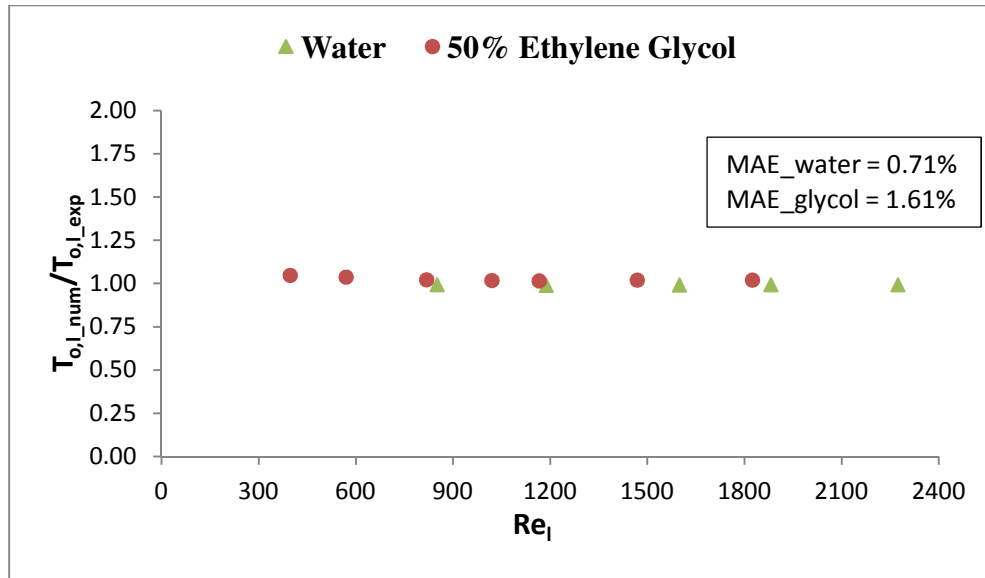
Figure 4.8. Percentage of mean average errors in liquid outlet temperature
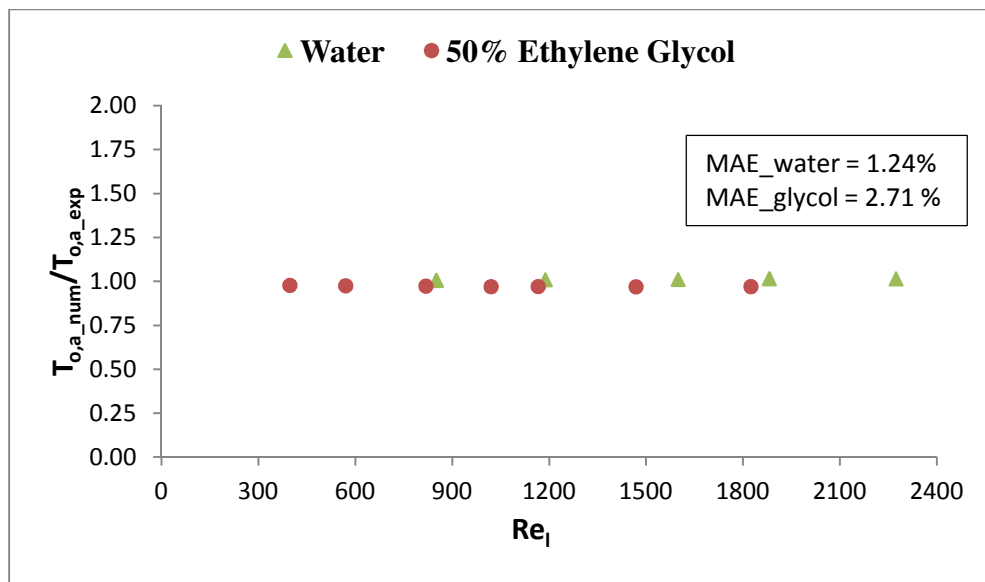
Figure 4.9. Percentage of mean average errors in air outlet temperature
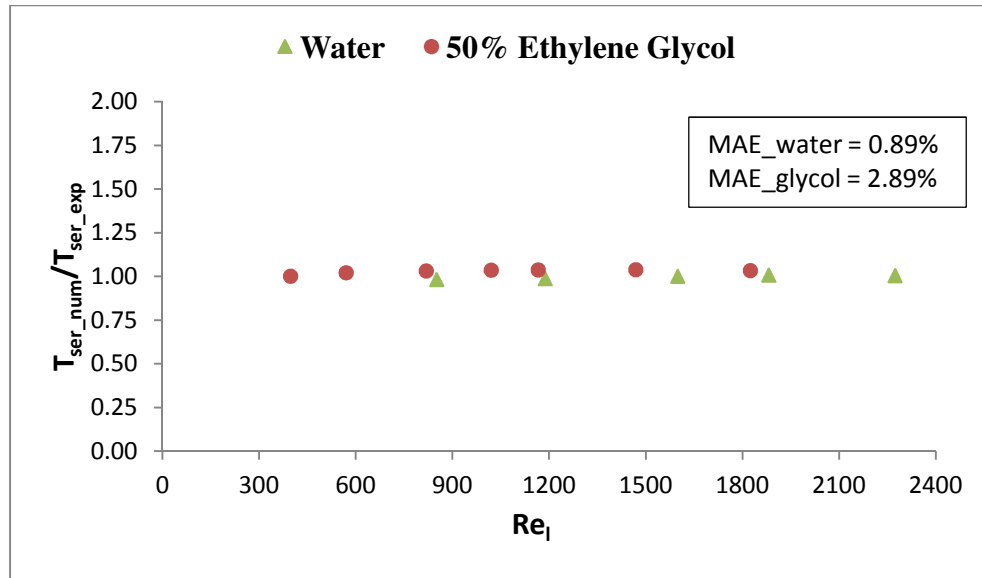
Figure 4.10. Percentage of mean average errors in serpentine temperature
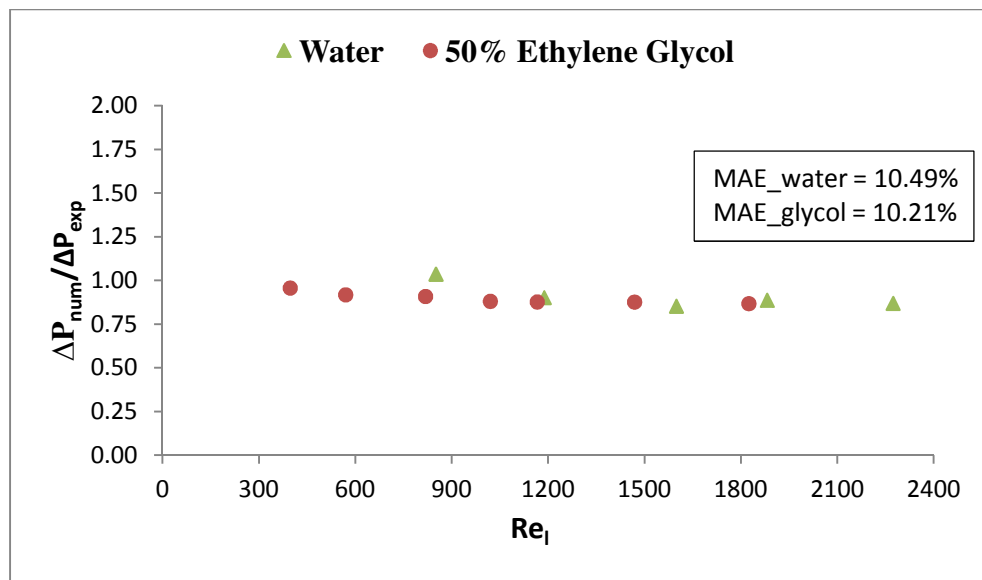
Figure 4.11. Percentage of mean average errors in liquid-side pressure drop

Mean average errors obtained from the model are summarized in Table 4.1.

Table 4.1. %Errors in numerical results compared to measured data		
Parameters	For DI-water	Glycol-water mixture
% Error in $\Delta T_{o,l}$	0.71	1.61
% Error in $\Delta T_{o,a}$	1.24	2.71
% Error in T_{ser}	0.89	2.89
% Error in $\Delta P_{o,l}$	10.49	10.21

The Table 4.1 shows that the error in pressure drops is about 10%. One of the main reasons of having such an error is the uncertainty of pressure transducers used in the experimental set up. For the same test specimen, Khan (2011) found that the uncertainties in pressure drops for water and glycol-water mixture were ± 5.7% and ±6.7% respectively.

Numerical results of above mentioned parameters show a very good agreement with experimental measured data, and one can easily rely on the consistency and accuracy of the model. Therefore, the results obtained from the numerical simulation can be used to study the thermal and fluid flow behaviors of MICHX.

4.3 Heat Transfer Basic Parameters

The heat transfer performance of any heat exchange process is related to some basic parameters, which govern the heat-transfer phenomena. Some of these are described in this section.

4.3.1 Liquid-side Inlet to Outlet Temperature Differences

The relationship between the liquid mass flux and inlet to outlet temperature difference are presented in Figure 4.12. Expectedly, the liquid-side temperature drop (ΔT_l) deceases with the increase of the liquid-side mass flux (G_l). The relationship followed a power law trend with a negative exponent with $R^2 > 0.988$ as

$$\Delta T_{oil} = 2221.4 G_{oil}^{-0.769} \tag{4.1}$$

$$\Delta T_{atf} = 2824.8 G_{atf}^{-0.815} \tag{4.2}$$

$$\Delta T_g = 3129.2 G_g^{-0.885} \tag{4.3}$$

and

$$\Delta T_w = 2969.9 G_w^{-0.898} \tag{4.4}$$

where, the subscripts *oil, atf, g,* and *w* represent engine oil, ATF, 50% ethylene glycol, and DI-water respectively.
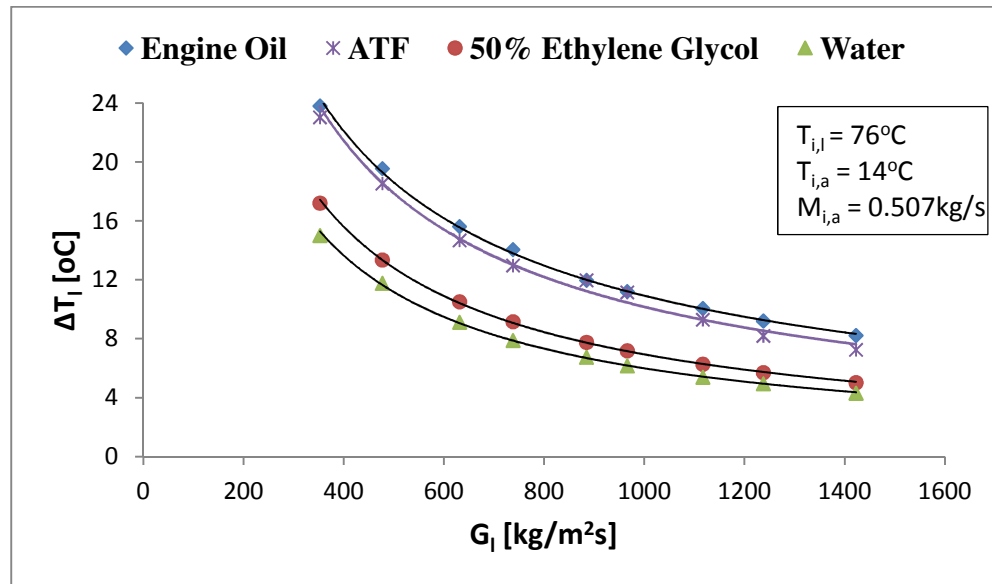

Figure 4.12. Variations of liquid-side temperature drop with liquid mass flux

In current study, both liquid-side and air-side inlet temperatures were maintained constant. As a result, the outlet temperature of the liquid was indicated by the heat

transfer mechanism. At lower G_l, the liquid residence time inside the channel is greater compared to the liquid residence time at higher G_l. The excessive residence time allows the liquid to drop more temperature at lower G_l than at higher G_l. Consequently, the outlet temperature becomes lower at lower G_l and higher at higher G_l triggering the inlet-to-exit temperature difference to be lower at higher G_l and vice versa.

From Fig. 4.12, for a particular liquid mass flux, it is obvious that $(\Delta T_l)_{oil} > (\Delta T_l)_{atf} > (\Delta T_l)_g > (\Delta T_l)_w$. Basically, this is due to the effect of the dynamic viscosity and its dependency on temperature. It is also apparent that for a constant liquid inlet temperature of 76°C, air inlet temperature of 14°C, and $353 \leq G_l \leq 1423$, the liquid-side temperature drop due to the cold air varies from 8-24°C, 7-23°C, 5-17°C, and 4-15°C for engine oil, ATF, ethylene glycol, and DI-water respectively as shown in Fig. 4.11. For the mass flux greater than approximately 1200kg/s, the temperature drop in engine oil, ATF, 50% ethylene glycol, and DI-water were found to be1.8, 2.0, 1.3, and 1.1°C respectively. It indicates that the liquids have already reached their maximum heat capacity i.e. they are almost thermally saturated.

4.3.2 Air-side Inlet to Outlet Temperature Differences

Figure 4.13 shows the variations of air-side inlet to outlet temperature with respect to liquid mass fluxes. From Fig. 4.13, it is evident that there is no significant change in the outlet temperature of the air with the change in the liquid mass flux, especially at higher mass fluxes of liquids. However, for the same liquid mass flux (G_l), $(\Delta T_a)_{oil} < (\Delta T_a)_{atf} < (\Delta T_a)_g < (\Delta T_a)_w$. As air flows at high velocity, it has a little time to stay in contact with the MICHX slab. As a result, the temperature rise in the air-side is very small. It is found that for a specified liquid mass flux of 1423kg/m^{2}s, the air-

side temperature rise due to engine oil, ATF, 50% ethylene glycol, and DI-water varies from 1.75-2.28°C, 1.79-2.30°C, 2.17-2.55°C, and 2.25-2.61°C respectively.
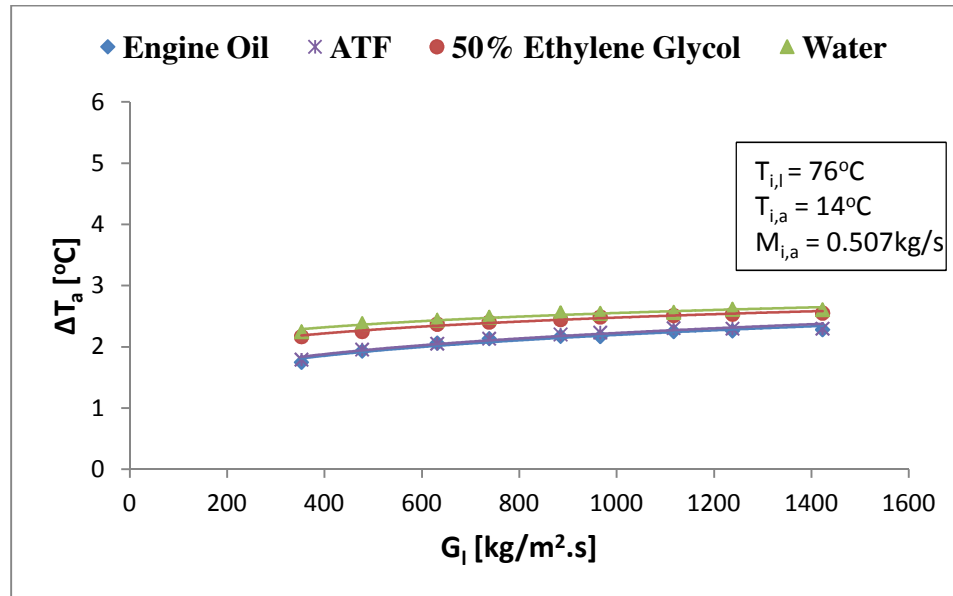

Figure 4.13. Air-side temperature differences with liquid mass flux

4.3.3 Non-dimensional Temperature
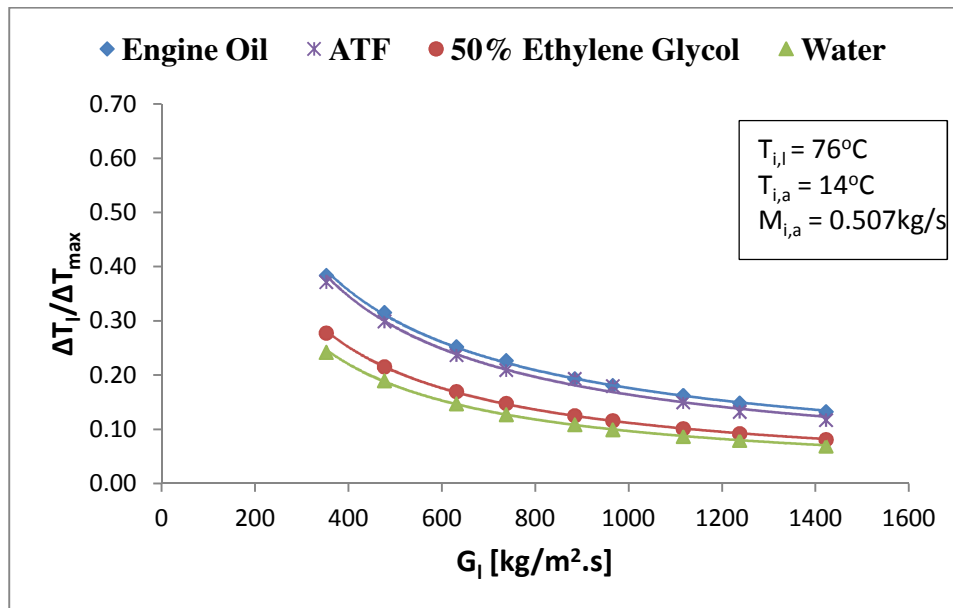
Figure 4.14. Variations of dimensionless temperature with liquid mass flux

The variations of liquid-side dimensionless temperature$\left(\frac{\Delta T_l}{\Delta T_{max}}\right)$ are plotted against liquid mass flux (G_l) as shown in Figure 4.14. The dimensionless temperature is defined as the ratio of the liquid-side temperature drop to the maximum temperature difference between liquid-side and air-side inlet temperatures. Therefore, the dimensionless temperature is evaluated as

$$\frac{\Delta T_l}{\Delta T_{max}} = \frac{T_{i,l} - T_{o,l}}{T_{i,l} - T_{i,a}} \tag{4.5}$$

Among the three temperatures, $T_{i,l}$, $T_{o,l}$, and $T_{i,a}$, in the right side of Eq. 4.5, $T_{i,l}$ and $T_{i,a}$, , are constant. Only the $T_{o,l}$ term is governed by the heat transfer. Figure 4.13 shows that the dimensionless temperature decreases with the increase in mass flow rate as well as liquid mass flux which follows a power law relationship with a negative exponent. Moreover, it is evident that at lower mass flow rate (lower G_l) , the curve slope is steeper compared to higher G_l. It indicates that at low mass flux of liquid, heat transfer performance is comparatively higher than high mass flux due to heat transfer saturation. For a particular liquid mass flux, the fluids behaves as $\left(\frac{\Delta T_l}{\Delta T_{max}}\right)_{oil} > \left(\frac{\Delta T_l}{\Delta T_{max}}\right)_{atf} >$ $\left(\frac{\Delta T_l}{\Delta T_{max}}\right)_g > \left(\frac{\Delta T_l}{\Delta T_{max}}\right)_w$ .thermo-physical properties, especially dynamic viscosity of liquid play the main role in this behavior.

4.3.4 Liquid-Side Pressure Drop

The overall pressure drop in a MICHX depends on the channel geometry and the fluid types. For a particular MICHX, viscosity of different liquid plays a very significant role on the pressure drop inside the channels. The variations of liquid-side pressure drop (ΔP) are plotted in Figure 4.15. Results show that the pressure drop in the liquid side is extremely higher in engine oil than DI-water. As expected, ΔP increases with increasing

liquid mass flux, and for a particular liquid mass flux, the relation is $\Delta P_{oil} > \Delta P_{atf} > \Delta P_g > \Delta P_w$. In addition, the curve slope for highly viscous fluids is steeper compared to low viscous fluid. The relationship between pressure drop and liquid mass flux follows power law as:

$$\Delta P_{oil} = 2.74 G_{oil}^{0.806} \tag{4.6}$$

$$\Delta P_{atf} = 4.60 G_{atf}^{0.617} \tag{4.7}$$

$$\Delta P_g == 0.007 G_g^{1.291} \tag{4.8}$$

and

$$\Delta P_w = 5 \times 10^{-4} G_w^{1.597} \tag{4.9}$$
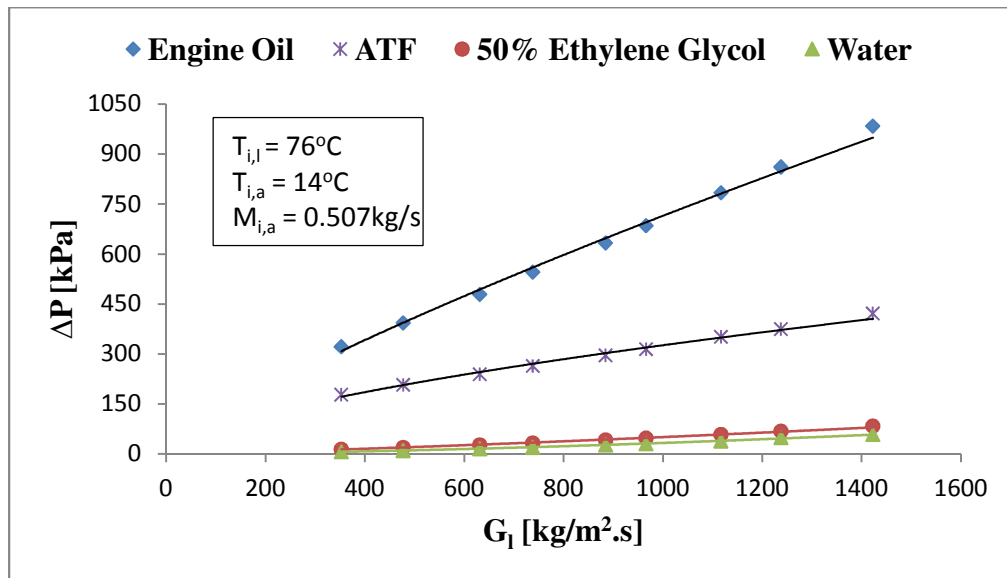
Figure 4.15. Variations of liquid-side pressure drop with liquid mass flux

It is seen that the pressure drop in MICHX for highly viscous fluids is significantly higher than that of the low-viscous fluids. For a particular liquid mass flux of 1423kg/m^{2}s, the liquid-side pressure drop of engine oil is 2.3, 11.80, and 16.9 times higher than the pressure drop of ATF, 50% ethylene glycol, and DI-water respectively.

This necessitates a more powerful pump for potential applications, which makes viscous fluids, especially engine oil unattractive for use in a MICHX.

4.3.5 Liquid-Side Heat Transfer Rate

The variations of liquid-side heat transfer rate ($\dot{Q}_l$) with liquid mass flux (G_l) and liquid-side Reynolds number (Re_l) calculated at a bulk temperature are presented in Figs. 4.16 and Fig. 4.17. From the plots, it is obvious that the heat transfer rate increases with the increase in liquids mass flux as well as Reynolds number. The dependency of liquid-side heat transfer rate on G_l and Re_l could be described by power law with positive exponent.

Figure 4.16 shows that for a particular liquid mass flux, $(Q_l)_{oil} < (Q_l)_{atf} < (Q_l)_g < (Q_l)_w$. However, for a particular liquid-side Reynolds number, $(Q_l)_{oil} > (Q_l)_{atf} > (Q_l)_g > (Q_l)_w$ as shown in Fig. 4.17. These phenomena can play a significant role in performance in potential automotive and other industrial applications.

The plots are steeper at lower mass flux than higher mass flux of liquid. For the mass flux greater than about 1200kg/s, the liquids temperatures drop in all liquids were found very small, which is described in section 4.3.1. Similarly, Fig. 4.16 also shows that for mass flux above 1200kg/s, the heat transfer rate of all liquids are negligible, which specifies their thermally saturated condition at that point.
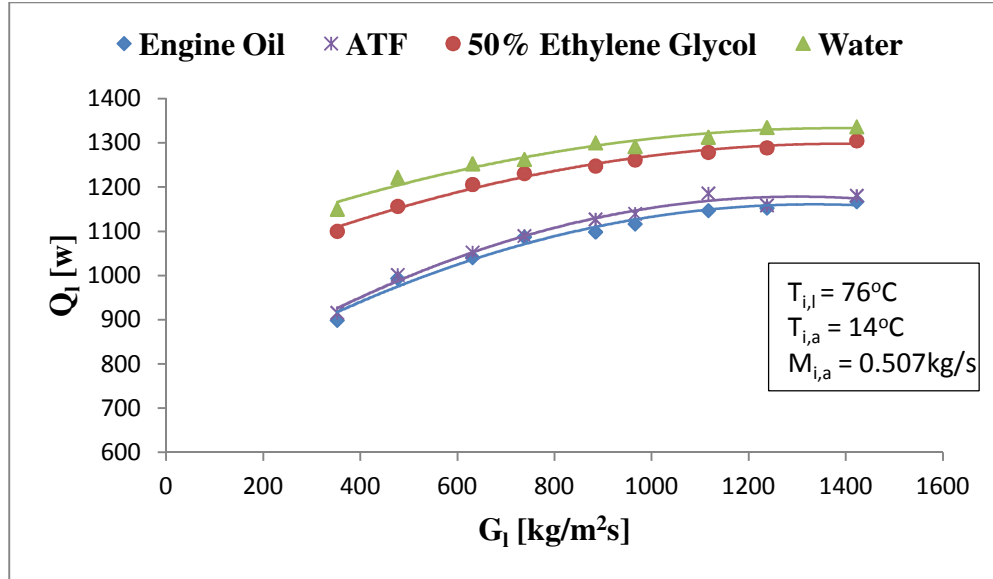
Figure 4.16. Variations of heat transfer rate with liquid mass flux
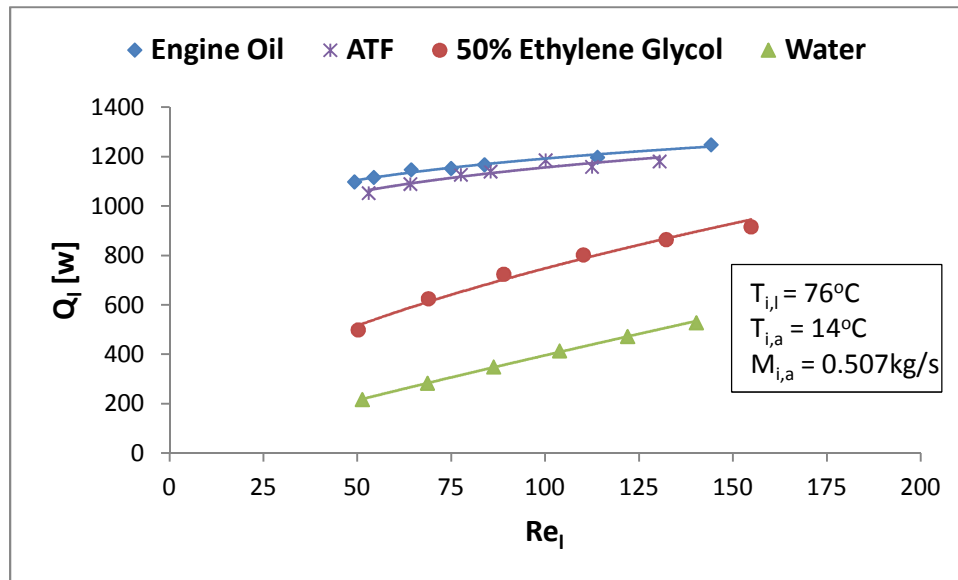
Figure 4.17. Variations of heat transfer rate with liquid-side Reynolds number

4.3.6 Effect of Liquid Mass Flux and Reynolds Number on Brinkman Number

Viscous heating is important for a larger value of Brinkman number. It can directly affect the film temperature (T_f) of the liquid when $Br \geq 1$, which is found in engine oil for Reynolds number greater than 100. The Brinkman numbers (Br) of

different liquids were calculated based on Eq. 3.22. Since Br is directly proportional to the dynamic viscosity of a liquid, it generally becomes higher with highly viscous fluid triggering higher viscous dissipation. Under some situations, viscous dissipation may lead to a significant variation in flow and temperature field, which can be the source of flow instability, hydrodynamic thermal explosion, and oscillatory motion (Bastanjian et al., 1965 and Gruntfest, 1964). Both Fig. 4.18 and 4.19 show that Br_l increases with increasing both G_l and Re_l, which follows a power law relationship.
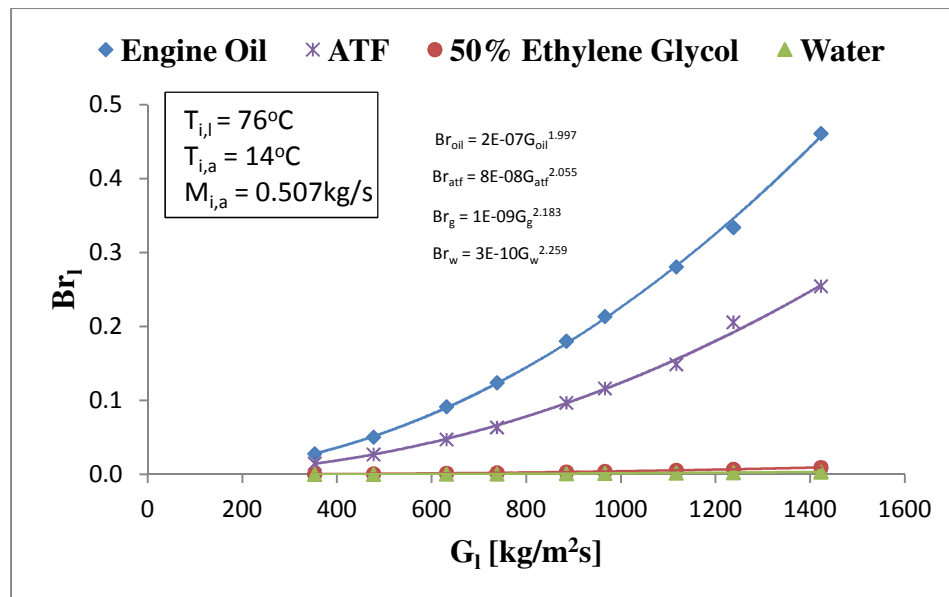
Figure 4.18. Effect of mass fluxes on Brinkman number
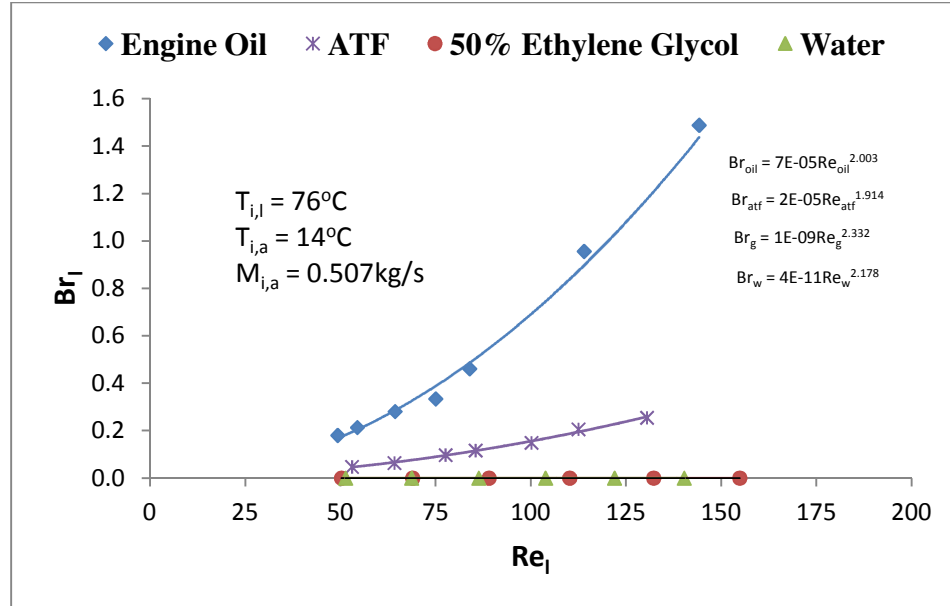
Figure 4.19. Effect of Reynolds number on Brinkman number

In the current study, within the G_l range of 353-1423kg/s, the Br of engine oil, ATF, 50% ethylene glycol, and DI-water varies from $2.8 \times 10^{-02} \sim 4.6 \times 10^{-01}$, $1.5 \times 10^{-02} \sim 2.6 \times 10^{-01}$, $4.5 \times 10^{-04} \sim 9.5 \times 10^{-03}$, and $1.5 \times 10^{-04} \sim 3.5 \times 10^{-03}$, respectively. In this case for $49 \leq Re_{oil} \leq 144$, $53 \leq Re_{atf} \leq 131$, $50 \leq Re_g \leq 155$, and $51 \leq Re_w \leq 140$, the corresponding Br_l of four liquids are $0.2\ to\ 1.5$, $4.7 \times 10^{-02} \sim 0.26$, $8.8 \times 10^{-06} \sim 1.2 \times 10^{-04}$, and $2.1 \times 10^{-07} \sim 1.9 \times 10^{-06}$. A comparative statement of the results obtained from the current study with Tso and Mahulikar (2000) is presented in Table 4.2.

Table 4.2. Comparison of Br_l between current study and others

Study	Working Fluids	B. C.	Re	Brinkman Number
Current study	Engine Oil	T	49-144	$0.2 \sim 1.5$
	ATF	T	53-131	$4.7 \times 10^{-2} \sim 0.26$
	Ethylene Glycol	T	50-155	$8.8 \times 10^{-6} \sim 1.2 \times 10^{-4}$
	DI-water	T	51-140	$2.1 \times 10^{-7} \sim 1.9 \times 10^{-6}$
Tso and Mahulikar (2000)	DI-water	H	80-107	$10^{-8} \sim 10^{-5}$

4.3.7 Liquid-Side Convective Heat Transfer Coefficient

Convective heat transfer coefficient of different liquids for different liquid mass fluxes and Reynolds numbers are shown in Fig 4.20 and 4.21 respectively. From Fig. 4.20, it is evident that at lower fluxes gain in h with increasing flux is greater than higher fluxes. Plot 4.20 also show that for a particular liquid mass flux, $h_{oil} < h_{atf} < h_g < h_w$. It is also obvious that there is no remarkable difference in heat transfer coefficient of ATF and engine oil. Fig. 4.20 shows that for a particular liquid mass flux of 1423kg/m^{2}s, the heat transfer coefficient of water is approximately 22.79%, 63.71%, and 64.44% higher than ethylene glycol, ATF, and engine oil respectively.
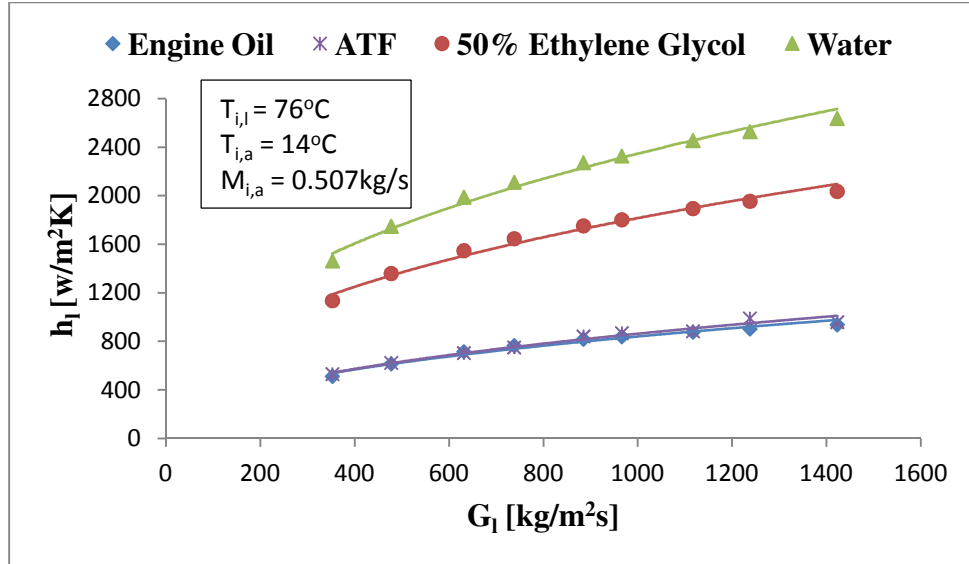
Figure 4.20. Variations of heat transfer coefficient with liquid mass flux
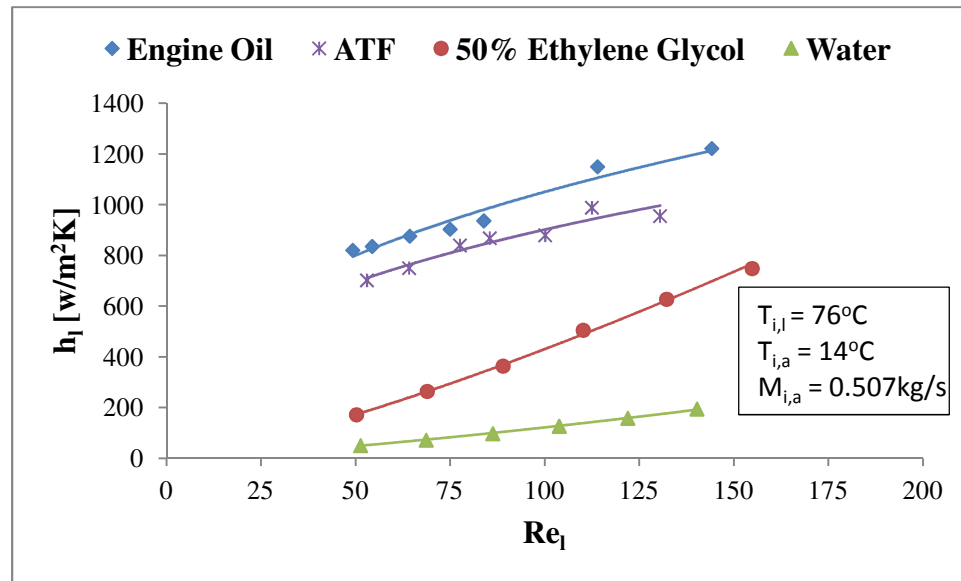
Figure 4.21. Variations of heat transfer coefficient with liquid-side Reynolds number

On the other hand, for a specified Reynolds number, the relationship is $h_{oil} > h_{atf} > h_g > h_w$ as presented in Fig. 4.21. Results show that for a specified Reynolds number of 140, the heat transfer coefficient of engine oil is approximately 21.77%,

38.71%, and 84.05% higher than ATF, ethylene glycol, and DI-water respectively. This is due to the viscous effects of different liquids on convective heat transfer coefficient.

The relationship between the convective heat transfer coefficient and Reynolds number follows the power law as

$$h_{oil} = 171.41 Re_{oil}^{0.394} \tag{4.10}$$

$$h_{atf} = 160.30 Re_{atf}^{0.375} \tag{4.11}$$

$$h_g = 0.98 Re_g^{1.322} \tag{4.12}$$

and

$$h_w = 0.25 Re_w^{1.345} \tag{4.13}$$

4.3.8 Liquid-Side Nusselt Number

Variations of liquid-side Nusselt numbers with respect to mass fluxes and Reynolds numbers are presented in Fig. 4.22 and Fig. 4.23 respectively. Results also show that $Nu_{oil} < Nu_{atf} < Nu_g < Nu_w$, for both constant mass flux and Reynolds number. In this case for $353 \leq G_l \leq 1423 kg/m^2 s$, the Nusselt number of engine oil, ATF, 50% ethylene glycol, and DI-water range from 3.84~7.09, 3.43~6.23, 2.48~4.40 and 2.21~3.96 respectively While, Fig. 4.23 shows, for $50 \leq Re_l \leq 150$, the Nusselt number of engine oil, ATF, 50% ethylene glycol, and DI-water vary from $6.21 \leq Nu_{oil} \leq 9.25$, $4.56 \leq Nu_{atf} \leq 6.23$, $0.38 \leq Nu_g \leq 1.64$, and $0.08 \leq Nu_w \leq 0.30$ respectively.

The relationship between Nusselt number and Reynolds number follows the power law as:

$$Nu_{oil} = 1.29 Re_{oil}^{0.396} \tag{4.14}$$

$$Nu_{atf} = 1.02 Re_{atf}^{0.380} \tag{4.15}$$

$$Nu_g = 2.2 \times 10^{-3} Re_g^{1.315} \tag{4.16}$$

and

$$Nu_w = 4 \times 10^{-4} Re_w^{1.343} \tag{4.17}$$
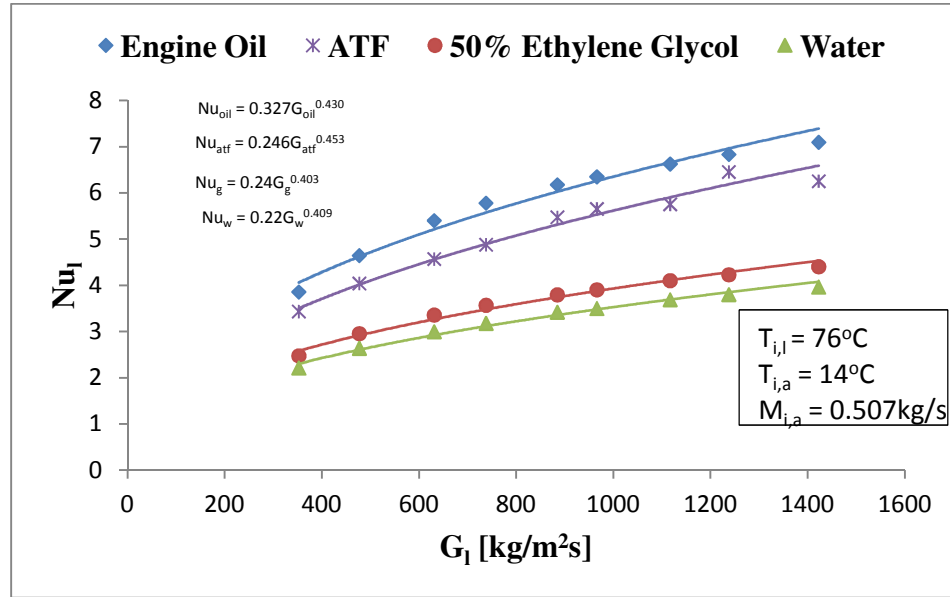
Figure 4.22. Variations of liquid-side Nusselt number with liquid-side mass flux
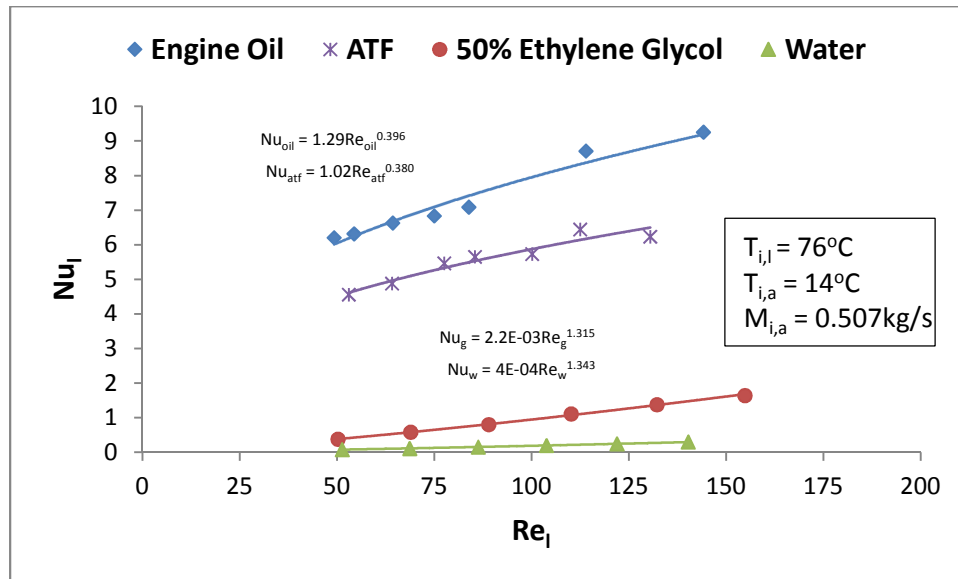
Figure 4.23. Variations of liquid-side Nusselt number with Re_l

4.4 Thermal and Flow Fields in MICHX

To understand the performance of MICHX, the flow and thermal behavior of different liquids in channels are explained in this section.

4.4.1 Centerline Temperature in the First, Middle, and Last Channels

In order to closely study the flow behavior inside the heat exchanger, temperature of engine oil in individual channel is closely examined. The temperature value of interest is at the center-line of the first, middle and last channels. The distribution of this temperature value is shown in Fig. 4.24 for individual channel of both top and bottom slabs. It is important to note that the channels are numbered from 1 to 68 based on the direction of the air cross-flow. This means channel 1 refers to the first channel that is exposed to the cross-flow, and channel 68 is the last. In other word, channel 68 refers to the first one from the liquid inlet boundary, while channel 1 refers to the last. It is evident for all channels that as engine oil are moving forward along the length of each channel, its temperature is decreasing gradually.
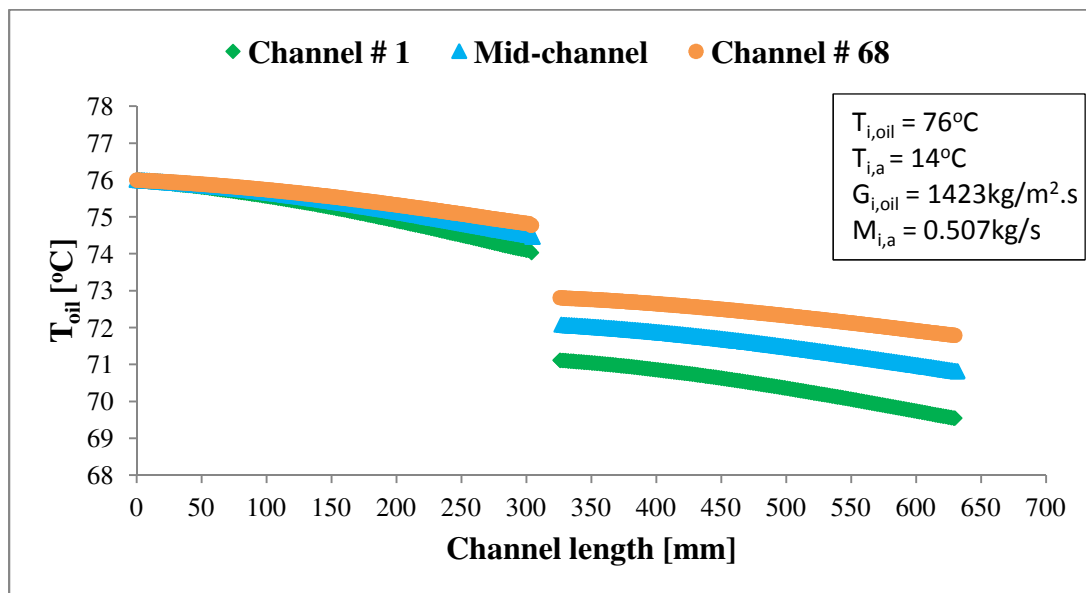
Figure 4.24. Centerline temperature of engine oil in 1st, middle, and last channels

The plot also shows that the temperature of the liquid in the first channel is lower than the temperature of liquid in the middle channel, which is in turn lower than that of the last channel. This is understandable since the cross-flow air will gradually warm as it travels across the channels and hence less effective at cooling the subsequent channels. This effect is more visible as the liquid travels along the channels. As a result, even though there is no temperature difference between the first and the last channel at the entrance of the top slab, the temperature difference between first and last channels is significantly higher in the bottom slab. The temperature difference between inlet and outlet of serpentine is found higher in 1st channel compared with mid-and last channels.

4.4.2 Distributions of Mass Flow Rate in Each Channel

The mass flow rate of liquids, for a constant liquid mass flux of 1423 kg/m^2.s, through all the 68 channels in the multi-port serpentine slabs are shown in Fig. 4.25. As shown in Fig. 4.25, it is obvious that the mass flow rate of liquids is higher in the channels closer to the liquid inlet port than the channels farther to the liquid inlet port. This was previously explained in relation of channel numbers to the direction of the cooling air flow. Results show a little scattered mass flow rate of DI-water, which is speculated to relate to its low viscosity. It is also evident that the distribution of mass flow rate through each channel is more even for highly viscous fluids, such as ATF and engine oil, compared to low-viscous fluids, such as DI-water and ethylene glycol. It is also found that the entrance region effects in mass flow rate for highly viscous fluid especially, engine oil is negligible. These effects are observed significantly higher for DI-water than ethylene glycol, ATF, and engine oil. This behavior can make the performance of highly viscous fluids more predictable.
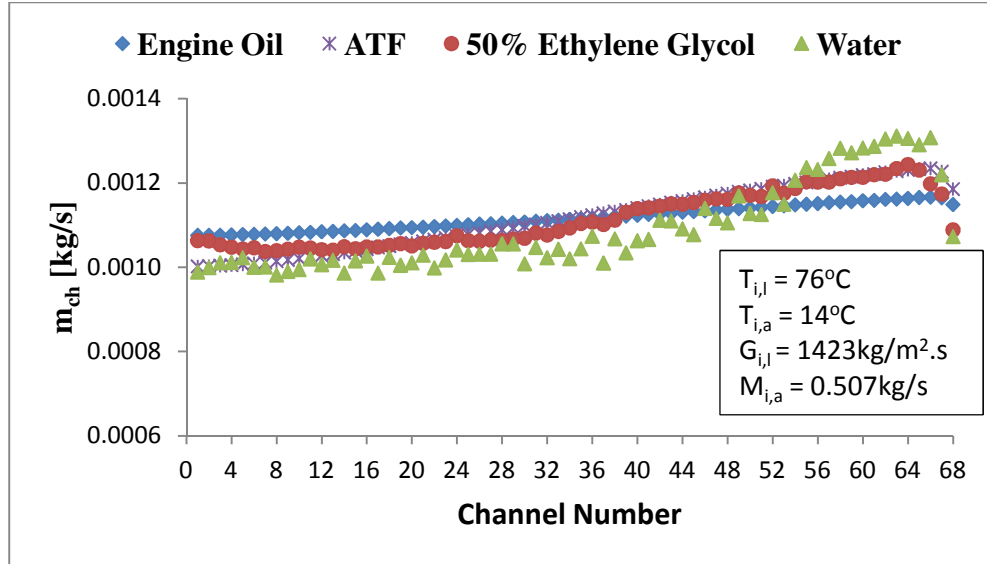
Figure 4.25. Distributions of liquids mass flow rates over 68 channels

4.4.3 Variations of Temperature Drop in Each Channel

The temperature drops of different liquids, for a constant liquid mass flux of 1423 kg/m²s, in all the 68 channels in the MICHX slabs are shown in Fig. 4.26.
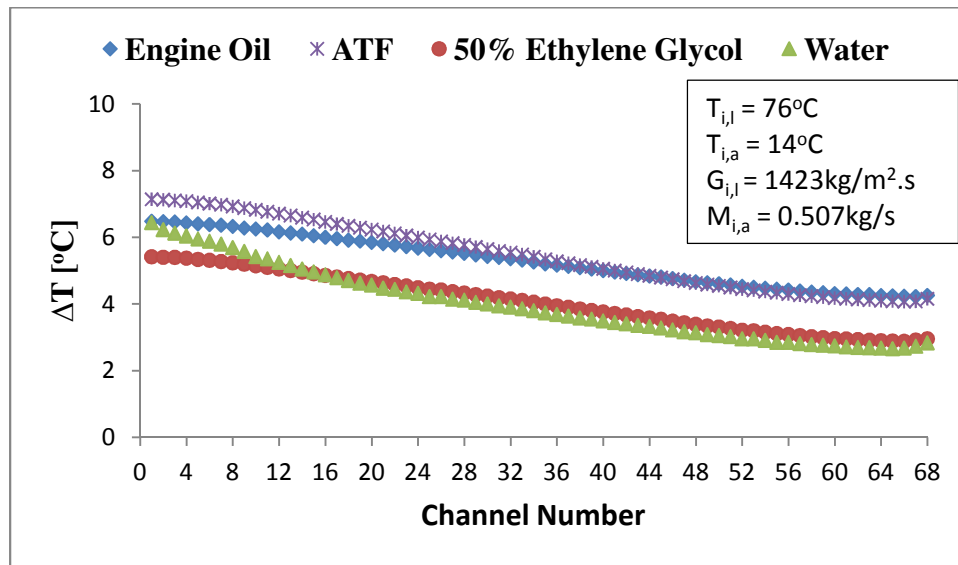
Figure 4.26. Variations of liquid-side temperature drops through 68 channels

It is evident from the figure that the temperature drop (ΔT) decreases in the direction of the cooling air cross flow. The deviations in ΔT between channel # 1 and channel # 68

are 3.61, 2.58, 2.98, and 2.29^{o}C for water, ethylene glycol, ATF, and engine oil respectively.

4.4.4 Variations of Heat Transfer Rate in Each Channel

The liquid-side heat transfer rate, for a constant liquid mass flux of 1423 kg/m^{2}s, in all the 68 channels in the MICHX slabs are shown in Fig. 4.27. It is obvious that the heat transfer rate gradually decrease in the direction of the cooling air cross flow. The respective heat transfer rate of 50% ethylene glycol, ATF, and engine oil are 27%, ---%, and 43% lower than that of DI-water as shown in Fig. 4.26.
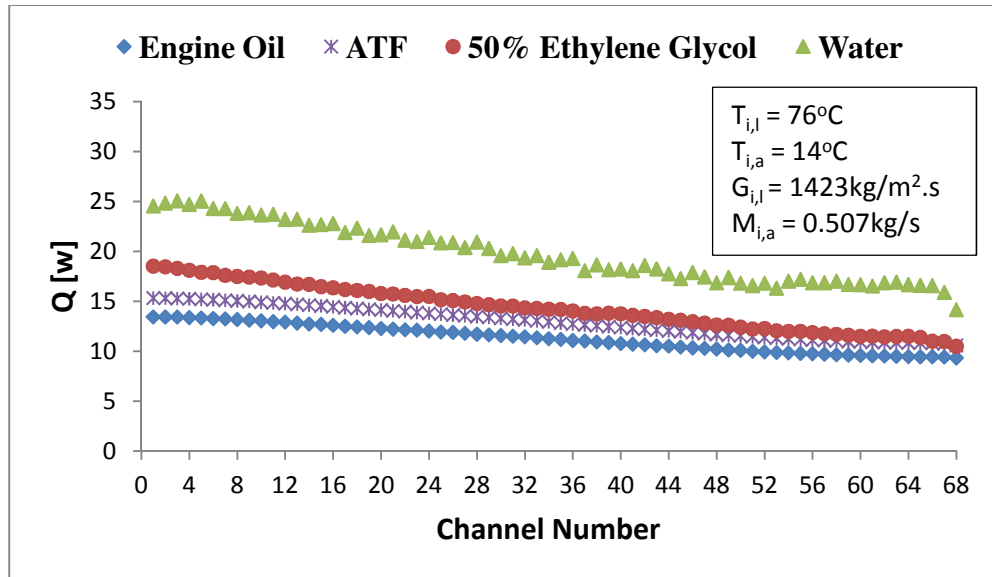
Figure 4.27. Distributions of liquids heat transfer rate through 68 channels

4.4.5 Liquid Velocity along the Centerline of the Mid-Channel (Channel # 35)

The velocity profiles of different liquids along the centerline of the middle channel (channel # 35) are shown in Fig. 4.28.
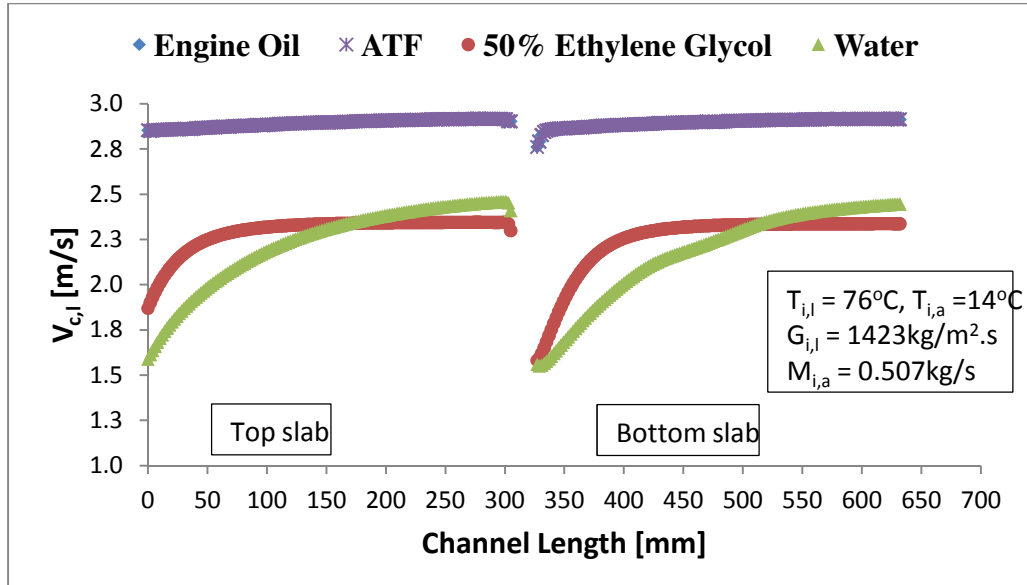
Figure 4.28. Velocity profile along the centerline of the mid-channel (channel # 35)

Figure 4.28 shows the variations of centerline velocity of different liquids along the flow direction for $Re_{oil} = 83.94, Re_{atf} = 130.53, Re_g = 1438.54,$ and $Re_w = 3802.12$. As seen in Fig. 4.28, when liquids flow through the channels, hydrodynamic boundary layers develop along the top and bottom channels. It is found that the hydrodynamic developing length is shorter and flatter in the top slab compared to those in the bottom slab. Results also show that the entrance lengths of highly viscous liquids like engine oil and ATF are shorter than those of low viscous liquids like ethylene glycol and DI-water. Liquid viscosity plays the most important role for these phenomena. This is because Renolds number is a function of viscosity, and for a particular liquid mass flux, $Re_{oil} < Re_{atf} < Re_g < Re_w$. In case of engine oil, ATF, and 50% ethylene glycol, the flow becomes hydrodynamically fully developed before entering to the serpentine bend

from the top slab as well as before leaving from the bottom slab to the outlet header. While DI-water is hydrodynamically developing throuh out the length of the channel. It is also noticeable that the the new entrance length after the serpentine bend is not the same as those of the entry to the channel from the header at the beginning.

4.4.6 Variations of Dimensionless Temperature along the Mid-channel
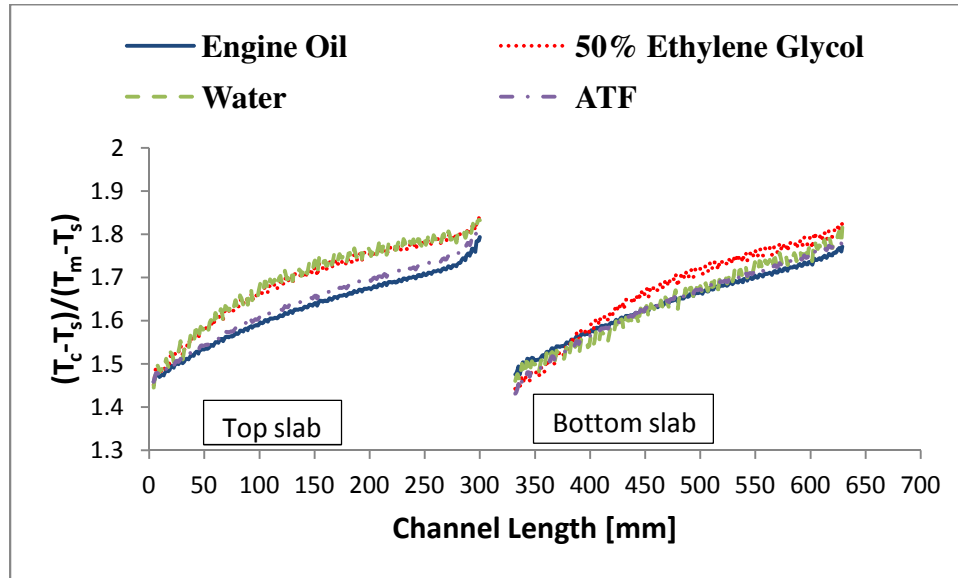
Figure 4.29. Variations of dimensionless temperature along the mid-channel (Ch. # 35)

The variations of liquid-side local dimensionless temperature, $\frac{T_{c,l}-T_s}{T_{m,l}-T_s}$ along the channel length for a particular liquid mass flux of 1423kg/m^{2}s are shown in Fig. 4.29. It is seen that liquids build a new thermal boundary layer when entering to the bottom slab from the serpentine due to the adiabatic serpentine. Since the serpentine is well insulated, and it is isolated from the heat transfer test chamber, no heat is being carried away from the hot fluids. Therefore, the serpentine surfaces are considered adiabatic. At serpentine region, the heat transfer from the hot fluid to the solid walls takes place by axial conduction.

4.4.7 Temperature Distributions along the Mid-channel
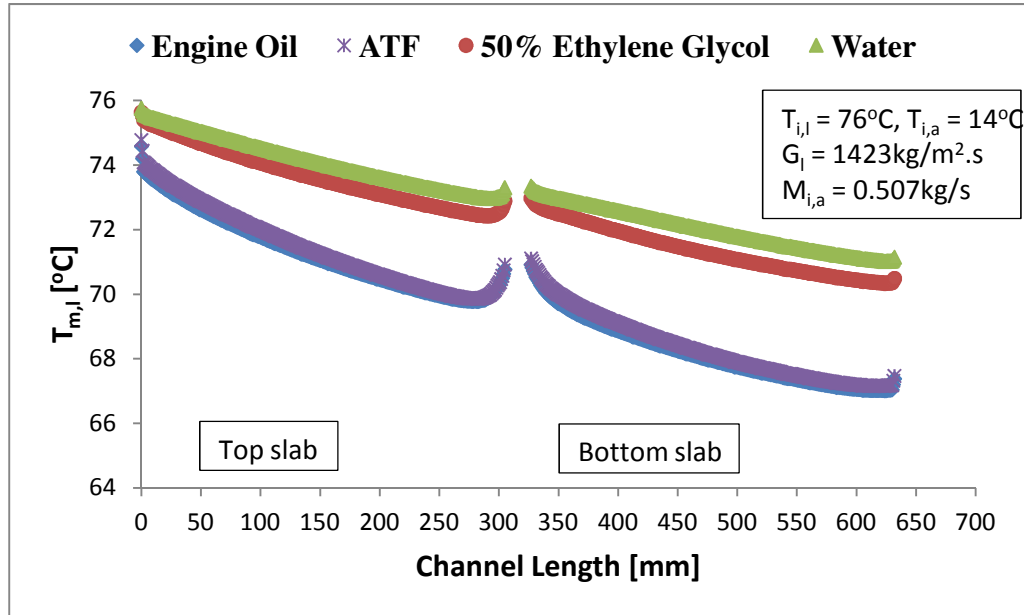
Figure 4.30. Variations of liquid-side local temperature along the mid-channel (Ch. # 35)

Figure 4.30 shows the local fluid mean temperature in the middle channel (channel # 35) channel along the direction of streamlines. Results show that the inlet of the MICHX channels, the temperatures of engine oil, ATF, 50% ethylene glycol, and DI-water are 74.59, 74.79, 75.64, and $75.76^{o}C$ respectively. While a constant inlet temperature of $76^{o}C$ was specified in inlet boundary condition, which is located at the inlet of the inlet manifold. Even though, it was specified that the inlet header and inlet manifold are thermally well insulated and adiabatic, it is evident that temperatures of engine oil, ATF, 50% ethylene glycol, and DI-water drop 1.41, 1.21, 0.36, and $0.24^{o}C$ during traveling this distance due to thermal conduction of aluminum.

The reason of considering inlet boundary condition at the inlet manifold is to match the inlet boundary conditions of numerical simulations with experiment conditions. Another reason is to avoid the complicacy of 68 inlet boundary conditions for 68 channels. Expectedly, results also show that the liquids temperatures decrease due to

the contact of cold air as they pass through the channels. However, the temperature of liquids increase at the serpentine because of the accumulation of heat from the liquids as there is no contact of cold air. The accumulation of heat at the serpentine takes place because the serpentine part is thermally well insulated. The rise of liquid temperature starts at 5-20mm ahead of the serpentine.

It is observed that in the top slab, the temperature falls down into 69.78$^{\mathrm{o}}$C, 69.86$^{\mathrm{o}}$C, 72.43$^{\mathrm{o}}$C, and 72.97$^{\mathrm{o}}$C for engine oil, ATF, 50% ethylene glycol, and DI-water respectively. Then liquid temperature increases up to 70.92$^{\mathrm{o}}$C, 71.11$^{\mathrm{o}}$C, 72.99$^{\mathrm{o}}$C, and 73.35$^{\mathrm{o}}$C in the serpentine region. After that, liquid temperature gradually decreases along the bottom slab and reached to 67.01, 67.16, 70.34, and 71.02$^{\mathrm{o}}$C. Finally, again the temperature of liquid increase a little before leaving from the channel to the adiabatic outlet header. For a particular liquid mass flux, it is evident that temperature drop in highly viscous liquids, such as engine oil and ATF is higher than that of low viscous liquids, such as ethylene glycol and DI-water as $Re_{oil} < Re_{atf} < Re_g < Re_w$. Even though, the flow of engine oil, ATF, and 50% ethylene glycol become hydrodynamically fully developed at some distance, they are still thermally developing throughout the length of channel. It is also evident that the steepness and the entrance length of thermally developing flow are higher in highly viscous liquids compared to those of low viscous liquids.

4.4.8 Variations of Wall (Surface) Temperature along the Mid-channel
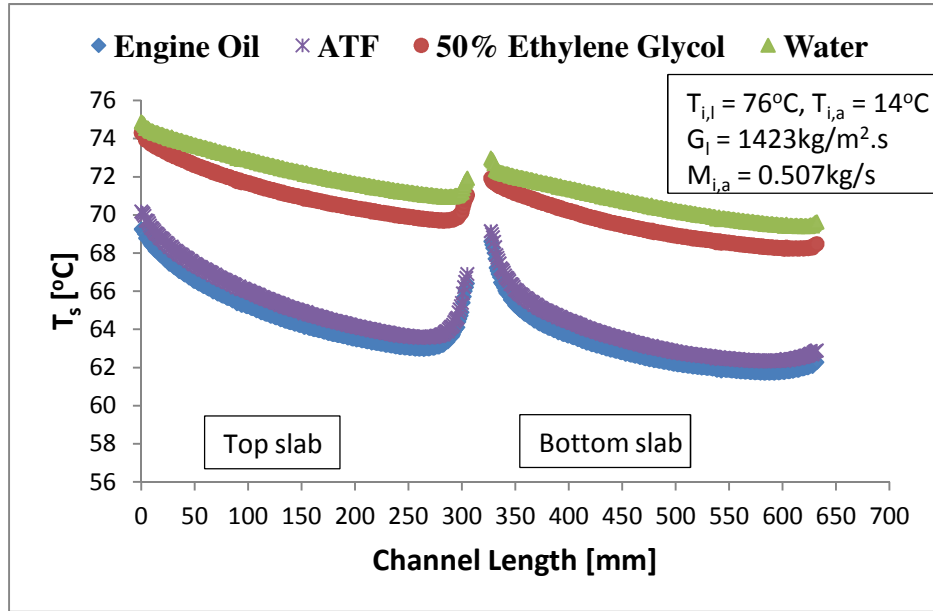
Figure 4.31. Variations of wall temperature along the mid-channel

Figure 4.31 shows the local wall (inner surface of channel) temperature in the middle channel (channel # 35) in the flow direction for same liquid mass flux but various Reynolds number. Behavior of surface temperatures at the inlet of middle channel is observed similar to that of liquid temperature at the same channel. This is due to the axial thermal conduction, which is explained in section 4.4.7.   It is obvious that the surface temperature of the channel decreases as it travels through the channel. Similar to the liquid local mean temperature, the inner surface temperature of channel wall is thermally developing throughout the length of channel.

From Fig. 4.31, it is clear that the entrance condition from the inlet header to the top slab at the beginning differ from the new entry condition from serpentine to the bottom slab. Since the serpentine is well insulated and located at the outside of the test chamber, the outer surface of the MICHX at the serpentine are adiabatic. As a result, the heat is conducted from the hot liquids to the solid walls to become thermally equilibrium,

and the local wall temperature increases at the serpentine region. The surface temperature is higher for low viscous liquids, such as DI-water and 50% ethylene glycol compared to those for highly viscous liquids.

4.4.9 Local Heat Transfer Coefficient of Liquids along the Mid-channel
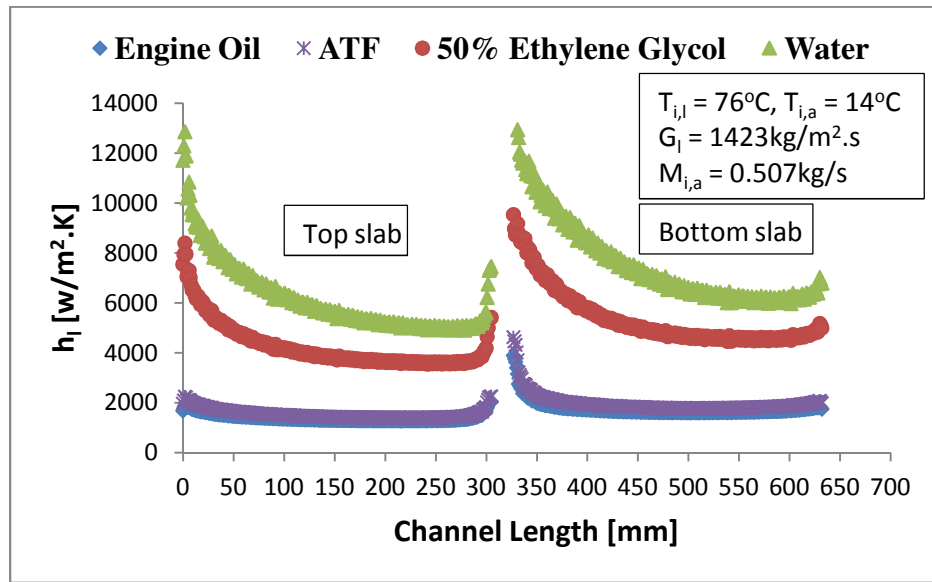
Figure 4.32. Local heat transfer coefficient of liquids through the mid-channel

Figure 4.32 shows the variations of the local heat transfer coefficient of different liquids flowing through the middle channel (channel # 35) for a particular liquid mass flux of 1423kg/m^{2}s, while the Reynolds number are different for different liquids. Even though there is no significant difference between the local heat transfer coefficient ATF and engine oil, the relationship among them are $(h_l)_w > (h_l)_g > (h_l)_{atf} > (h_l)_{oil}$. The nature and steepness of the local heat transfer coefficient for different liquids are different from each other. The steepness of the curves at the entrance to the top slab from the header and to the bottom slab from the serpentine is high. Then the steepness gradually reduces. About 5-20mm before the serpentine, the heat transfer coefficients start increase rapidly.

It was seen that both hydrodynamic and thermal boundary layer break at the serpentine region and generate a new boundary layer at the beginning of the bottom slab. This phenomenon is more obvious for low viscous liquids. Since the serpentine surface of the MICHX is adiabatic, no heat transfer is carried away at this region. The heat is transferred from the hot fluid to the solid walls to become thermally equilibrium. The existence of serpentine significantly enhances the heat transfer coefficient as clearly presented in Fig. 4.32.

4.4.10 Nusselt Number Correlation

The Nusselt number (Nu_l) of different liquids was calculated based on Eq. 3.31. Since the viscosity of working liquids are temperature dependent, the Nu_l was corrected with viscosity ratio as

$$Nu_{lc} = Nu_l \left(\frac{\mu_m}{\mu_f}\right)^n \qquad (4.18)$$

where, Nu_{lc} is the corrected Nusselt number of liquids,

μ_m and μ_f are the dynamic viscosity of liquids at mean and film temperature respectively, and

There is no exact value of exponent n. In the current study, 0.14 was considered because most of the authors including Kumar et al. (2007), Shah and Sekulic (2003), and Kays and London (1998) used n= 0.14 in their researches. The effects of Re_l on Nu_l are shown in Fig. 4.33. The dashed lines represent the corrected Nusselt number (Nu_{lc}) of different liquids. From Fig. 4.33, it is obvious that the Nu_{lc} is slightly lower than Nu_l for high viscosity fluids like ATF and engine oil. However, there is no deviation between Nu_l and Nu_{lc} for low viscosity fluids like water and ethylene glycol. Since the wall temperature is

lower than the fluid mean temperature, the $\mu_f > \mu_m$ This is why the dashed lines are slightly lower than the solid lines of original Nu_l.
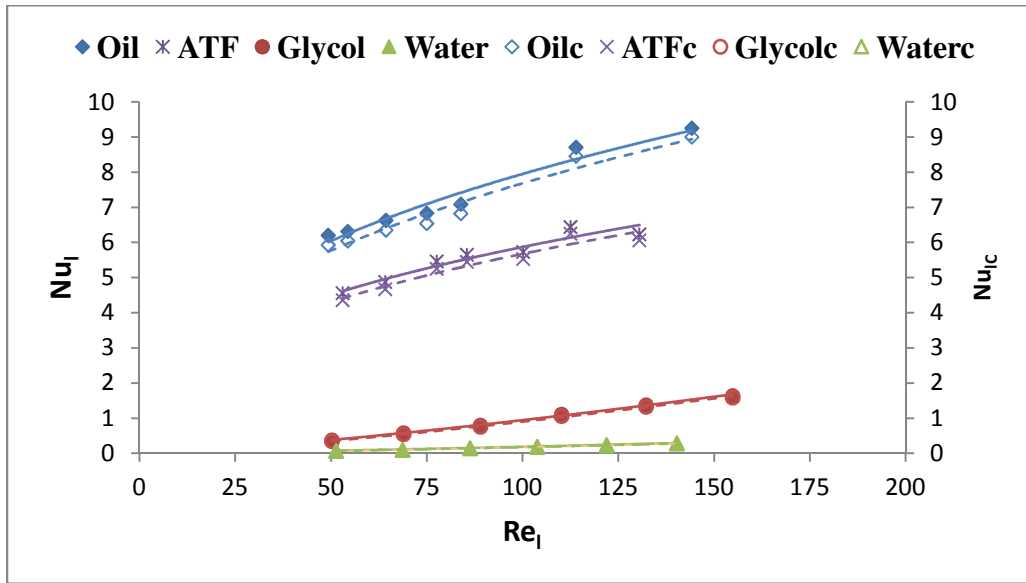
Figure 4.33. Effect of liquid-side Reynolds number on Nusselt number
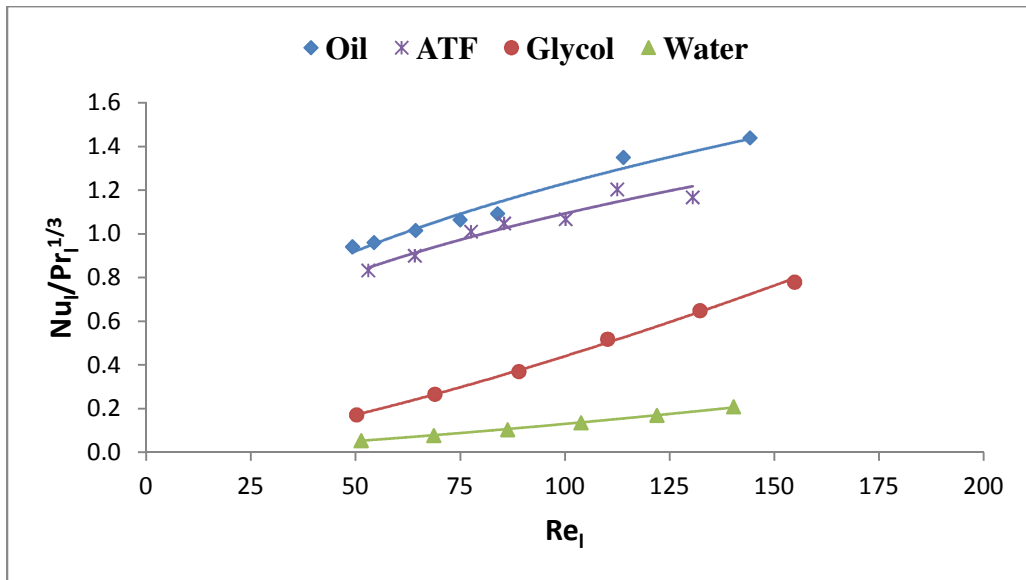
Figure 4.34. $Nu_l - Pr_l - Re_l$ correlation

Nusselt number is also dependent on Reynolds number and Prandtl number. Fig. 4.34 shows the relationship among Nu_l, Re_l, and Pr_l. Since the deviations between

original Nusselt number (Nu_l) and the corrected Nusselt number (Nu_{lc}) are very small, original Nusselt number is used to establish a relationship among the Nu_l, Re_l, and Pr_l. In current study, the heat transfer correlation of engine oil, ATF, 50% ethylene glycol, and DI-water flow for the Reynolds number range from $49 \leq Re_{oil} \leq 144$, $53 \leq Re_{atf} \leq 131$, $50 \leq Re_g \leq 155$, and $51 \leq Re_w \leq 140$ at bulk temperature are obtained. As expected, Nusselt number of liquids increases with increasing Reynolds number, and the curve followed a power-law relationship as

$$Nu_{oil} = 0.18 Re_{oil}^{0.419} \, Pr_{oil}^{1/3} \tag{4.19}$$

$$Nu_{atf} = 0.17 Re_{atf}^{0.406} Pr_{atf}^{1/3} \tag{4.20}$$

$$Nu_g = 8 \times 10^{-4} Re_g^{1.359} Pr_g^{1/3} \tag{4.21}$$

and

$$Nu_w = 3 \times 10^{-4} Re_w^{1.351} Pr_w^{1/3} \tag{4.22}$$

CHAPTER V

CONCLUSIONS AND RECOMMENDATIONS

5.1 Conclusions

In this research, numerical simulations were carried out to investigate the performance of minichannel heat exchanger (MICHX) during cooling of four different viscous fluids, namely engine oil, automatic transmission fluid (ATF), ethylene glycol, and DI-water. For ethylene glycol and DI-water, numerical results were compared with the experimental measured data to validate the model. From the analyses of results obtained from simulation, the following conclusions are made:

1- In case of engine oil, ATF, and 50% ethylene glycol, the flow becomes hydrodynamically fully developed before entering to the serpentine bend from the top slab as well as before leaving from the bottom slab to the outlet header. On the other hand, DI-water is hydrodynamically developing throughout the length of the channel.

2- The steepness and the entrance length of thermally developing flow are higher in highly viscous liquids compared to those of low viscous liquids.

3- The hydrodynamic developing length is shorter and flatter in the top slab compared to those in the bottom slab. Results also show that the entrance lengths of highly viscous liquids like engine oil and ATF are shorter than those of low viscous liquids like ethylene glycol and DI-water. Liquid viscosity plays the most important role for these phenomena.

4- For a specified liquid mass flux, the best heat transfer rate as well as the heat transfer coefficient was found in DI-water, while the worst was observed in engine oil. However, for a specified liquid-side Reynolds number, the result

was found completely reverse. These phenomena can play a significant role in performance in potential automotive and other industrial applications.

5- For liquid mass flux greater than about 1200 kg/m^{2}s, the change in heat transfer rate and temperature drop in all liquids are found very small, which specifies their thermally saturated condition at that point. This suggests that for a specified application, an optimum design may exist where the size of a heat exchanger unit and the size and power rating of a pump is properly balanced.

6- At the adiabatic regions, such as manifolds, headers, and serpentine bend, no heat transfer is carried away by air. The heat is transferred from the hot fluid to the solid walls to become thermal equilibrium. Axial conduction is significant at these regions.

7- The pressure drop in MICHX for engine oil is found extremely high compared to other fluids, which necessitates a more powerful pump for potential applications of high-viscosity fluids.

8- On the other hand, the distribution of temperature, mass flow rate, and heat transfer rate through each channel are more even for high-viscosity fluids compared to low-viscosity fluids.

9- The entrance region effects in mass flow rate, temperature, and heat transfer rate for high-viscosity fluids are negligible. These effects are observed significantly higher for low-viscosity fluids.

10- The existence of adiabatic serpentine bend in MICHX slab changes the flow direction and creates a new temperature profile after the bend which enhances the heat transfer coefficient at the entrance of the bottom slab.

11- Finally, it was observed that the existence of serpentine bend in multi-port flat slab enhances heat transfer rate at the expense of low pressure drop penalty. The pressure drop in the serpentine is relatively small as compared to the pressure drop at the inlet header.

5.2 Recommendations

The numerical simulations and analysis of results were made systematically and very carefully to find out the most important thermal and flow behaviors of different viscous fluids. However, there are still many other heat transfer parameters which were not provided in current study.

1- For a specified Reynolds number, a better heat transfer has been detected in MICHX for cooling of high-viscosity fluids compared to low-viscosity fluids. However, the necessity of further investigations is realized to find out the optimal channel size that would permit higher mass flow rate for such types of high-viscous fluids.

2- Further research on high-viscosity fluids is required to characterize heat transfer and flow behaviors due to axial heat conduction, viscous heating, and thermal interaction.

3- Due to the limitations of processor speed and inadequacy of RAM, current study was carried out only on two slabs, which include only one serpentine. Thorough investigation on multiple slabs is required to find out the optimum number as well as the length and size of slabs in a MICHX for specific purposes. To do this, a higher speed and capacity computer is suggested, which is under process of procurement.

APPENDICES

APPENDIX A

<u>A. Devices and Instruments</u>

Numerous researches have been conducted by Khan, M. G. (2012), Asker, S. (2011), Dasgupta, E. S, (2011), and Siddiqui, F. A. (2011) using the test facilities related to the current study, which is known as "Integrated Thermal Management Research Laboratory" (ITMRL) in the department of Mechanical Automotive and Materials Engineering (MAME), University of Windsor. The devices and instruments included in the experimental setup are presented below:
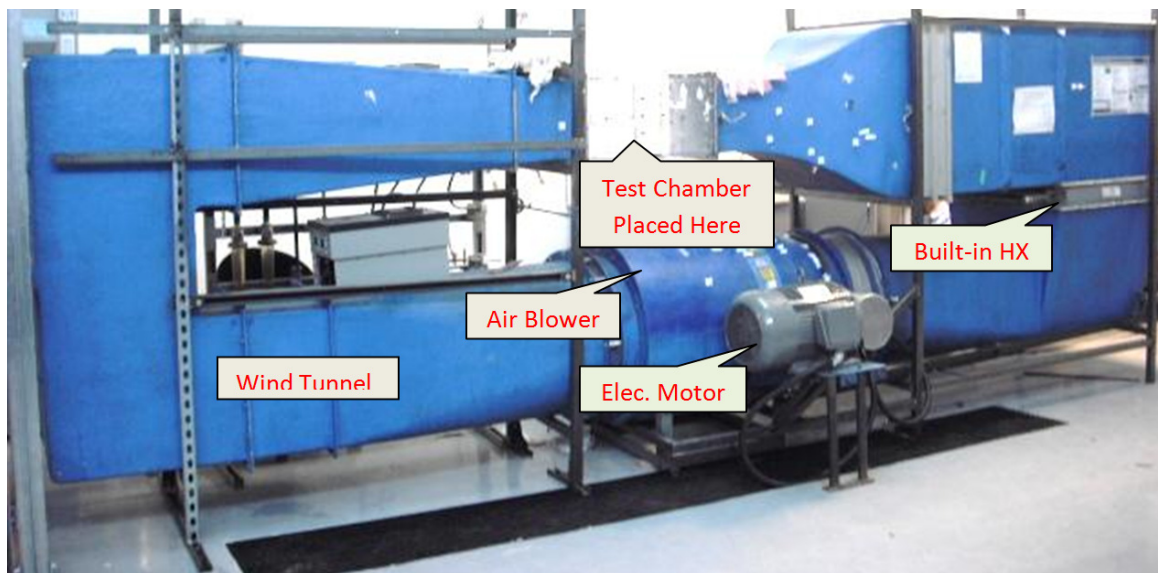
Figure A.1. Closed loop wind tunnel for heat transfer research
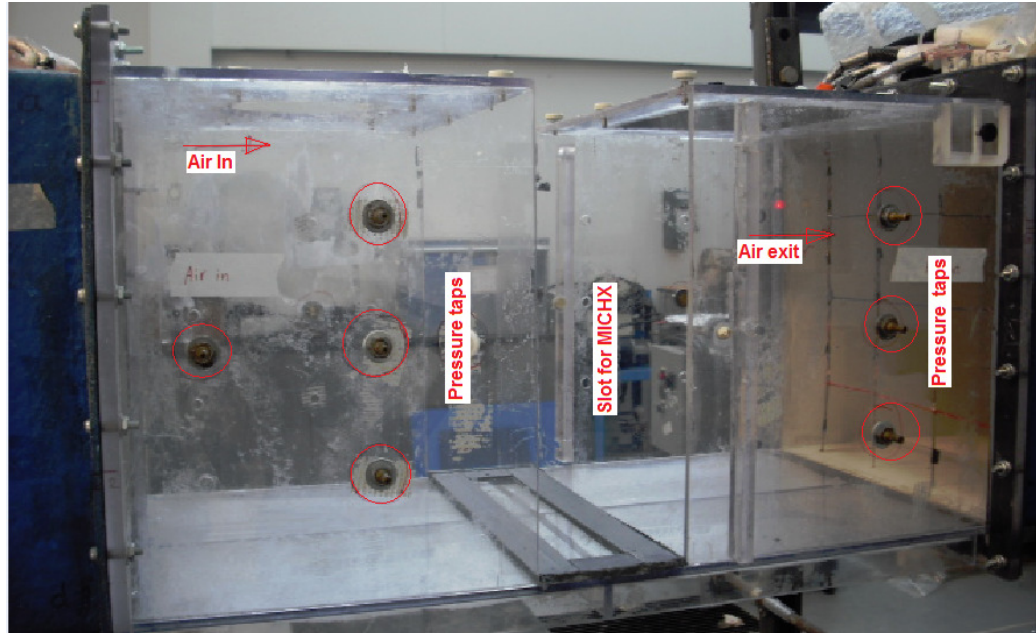
Figure A.2. Test Chamber

Figure A.3. Electric Heater
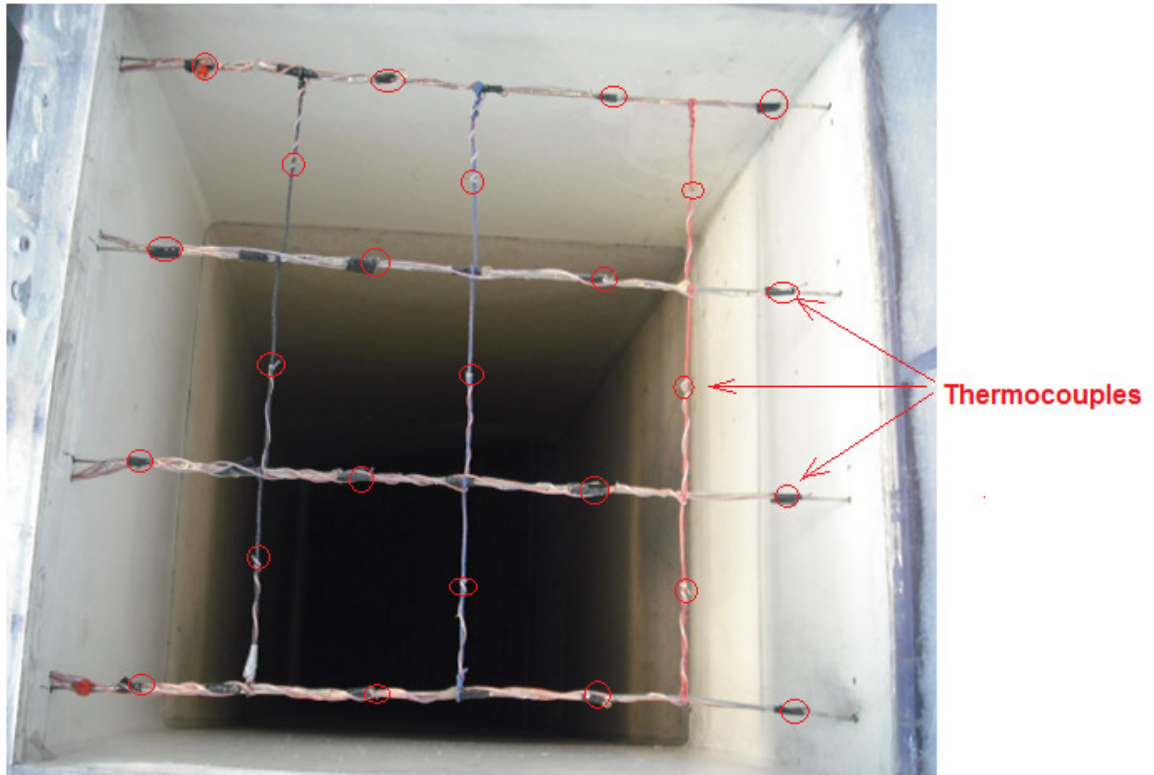
Figure A.4a. T-type thermocouples (total 25) at the inlet location of the test chamber
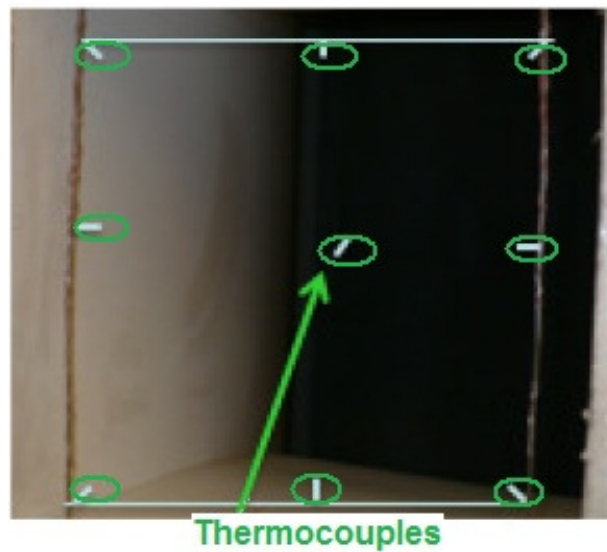
Figure A.4b. T-type thermocouples (total 9) at the outlet location of the test chamber
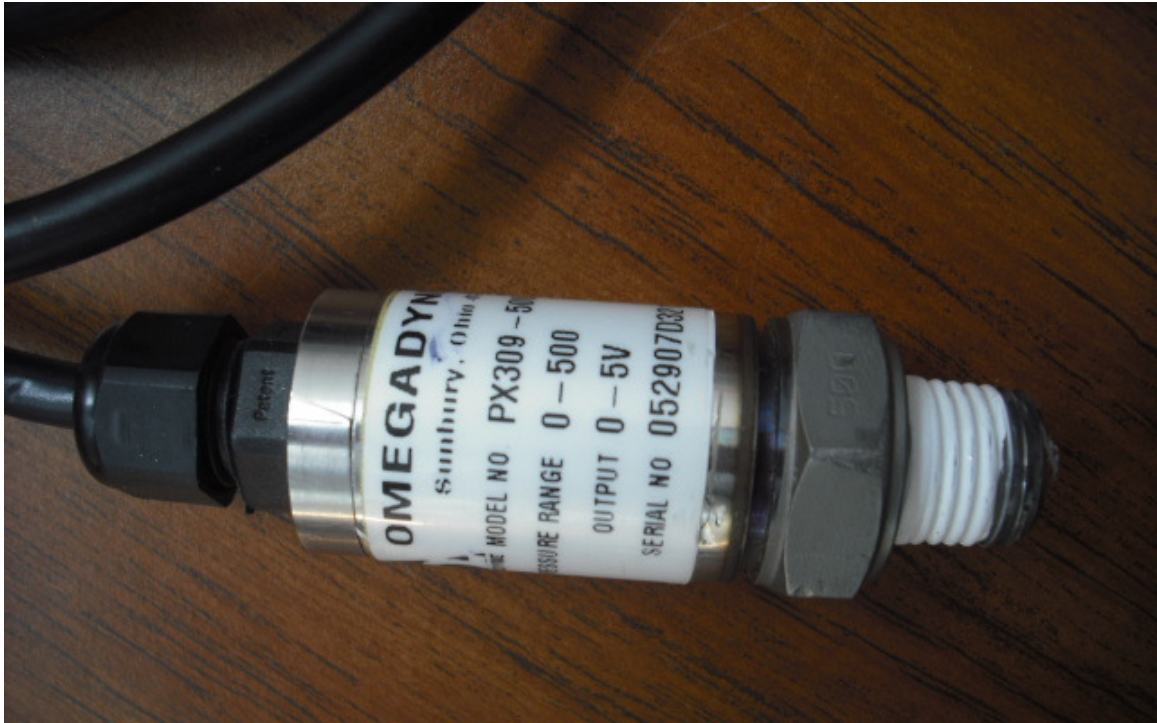
Figure A.5. Pressure Transducer (PTD)

Figure A.6. Resistance Temperature Detector (RTD)
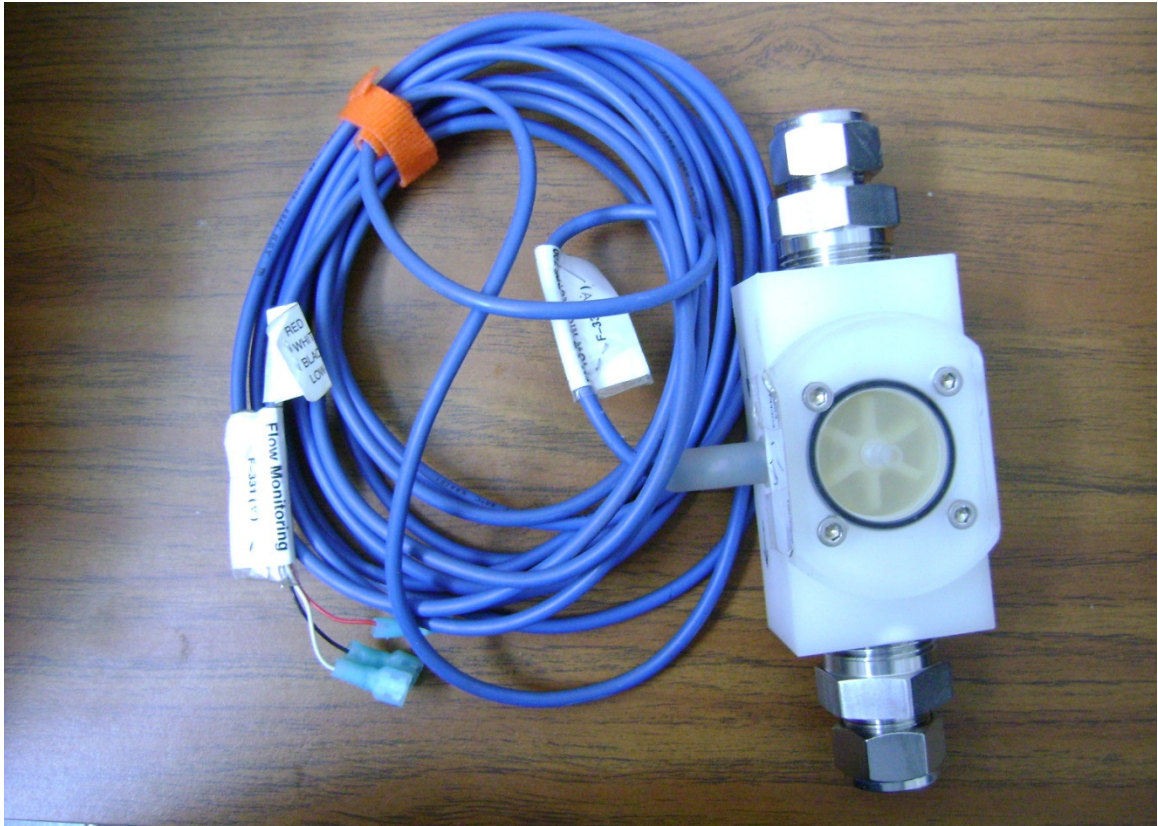
Figure A.7. White Flow Meter
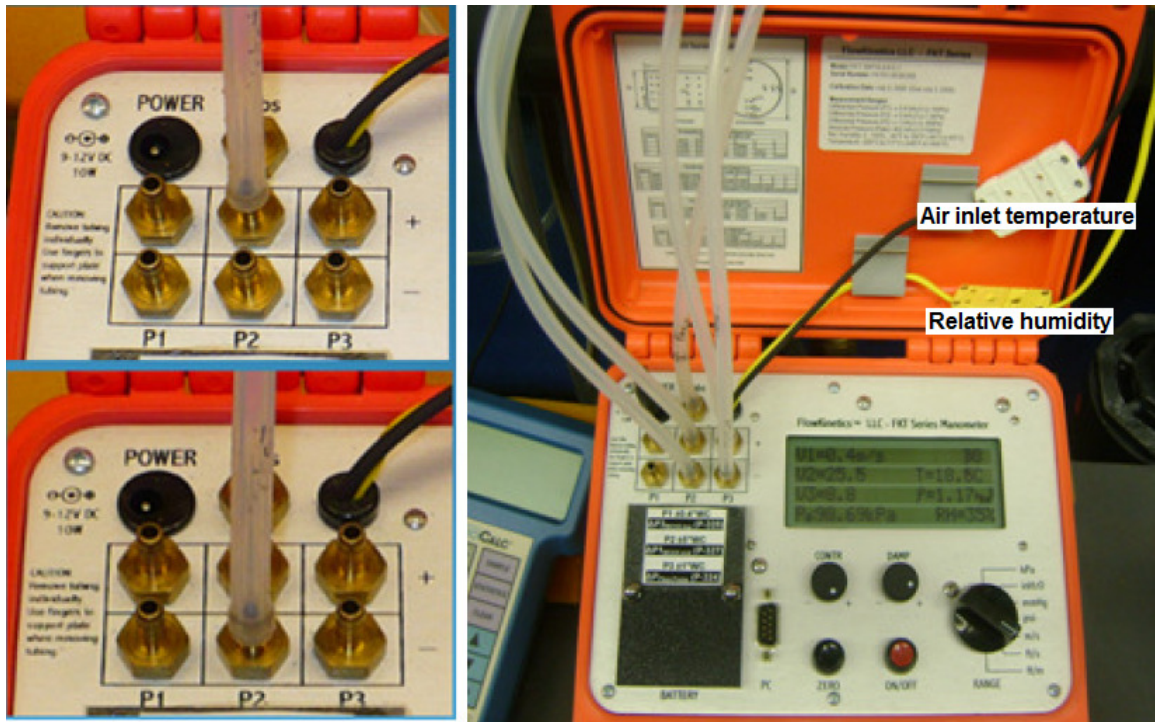
Figure A.7a. FlowKinetics FKT series
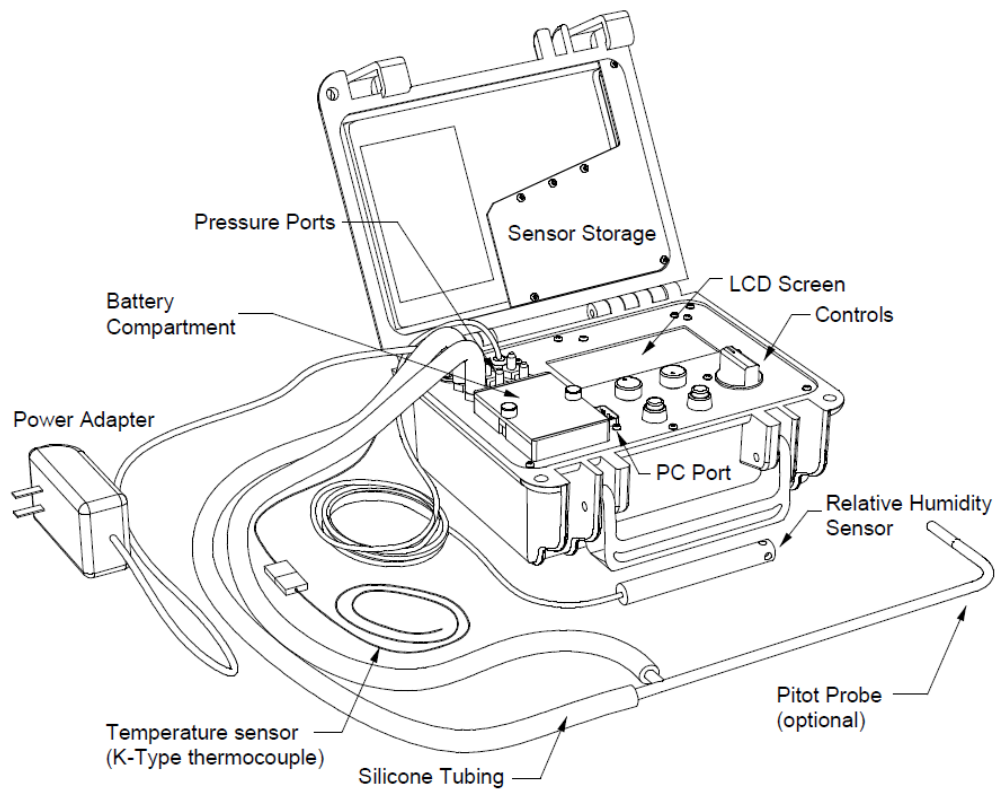
Figure A.7b. Schematic FlowKinetics FKT series

APPENDIX B

B. Data Sheet of Numerical Results

Data obtained from numerical simulations, which were used in analysis of results under chapter 4 are appended in Tables B.1-B.9.

| Table B.1.		Liquid Mass Flux, Reynolds Number, and Error in Mass Balance					
Inlet Temp. (Liquid)	Inlet Temp. (Air)	Mass Flow Rate (Liquid)	Mass Flow Rate (Air)	Liquid Mass flux (Channel Inlet)	Liquid Re (Channel Inlet)	Liquid Mass flow (Outlet)	Error in Mass Balance
$T_{i,oil}$	$T_{i,a}$	$M_{i,oil}$	M_a	G_{oil}	Re_{oil}	$M_{o,oil}$	(%MB)
^{o}C	^{o}C	kg/s	kg/s	kg/m^{2}s		kg/s	
76	14	0.018837	0.5069	352.70	16.60	0.018837	-0.002
76	14	0.025488	0.5069	477.25	24.16	0.025493	-0.018
76	14	0.033724	0.5069	631.45	33.41	0.033718	0.017
76	14	0.039421	0.5069	738.12	39.90	0.039422	-0.003
76	14	0.047257	0.5069	884.84	49.29	0.047251	0.011
76	14	0.051604	0.5069	966.24	54.44	0.051596	0.015
76	14	0.059660	0.5069	1117.08	64.38	0.059656	0.006
76	14	0.066112	0.5069	1237.89	75.02	0.066104	0.013
76	14	0.075989	0.5069	1422.83	83.94	0.075982	0.009
76	14	0.101377	0.5069	1898.19	114.01	0.101358	0.018
76	14	0.126721	0.5069	2372.74	144.24	0.126722	0.000
$T_{i,atf}$	$T_{i,a}$	$M_{i,atf}$	M_a	G_{atf}	Re_{atf}	$M_{o,atf}$	(%MB)
^{o}C	^{o}C	kg/s	kg/s	kg/m^{2}s		kg/s	
76	14	0.018837	0.5069	352.70	26.72	0.018837	-0.001
76	14	0.025488	0.5069	477.25	38.18	0.025489	-0.003
76	14	0.033724	0.5069	631.45	53.06	0.033727	-0.010
76	14	0.039421	0.5069	738.12	64.18	0.039421	0.000
76	14	0.047257	0.5069	884.84	77.62	0.047224	0.069
76	14	0.051604	0.5069	966.24	85.51	0.051600	0.007
76	14	0.059660	0.5069	1117.08	100.19	0.059647	0.021
76	14	0.066112	0.5069	1237.89	112.54	0.066114	-0.003
76	14	0.075989	0.5069	1422.83	130.53	0.075982	0.010
$T_{i,g}$	$T_{i,a}$	$M_{i,g}$	M_a	G_g	Re_g	$M_{o,g}$	(%MB)
^{o}C	^{o}C	kg/s	kg/s	kg/m^{2}s		kg/s	
76	14	0.003899	0.5069	73.00	50.28	0.003898	0.032
76	14	0.005199	0.5069	97.34	68.98	0.005200	-0.029
76	14	0.006498	0.5069	121.67	89.04	0.006498	0.009
76	14	0.007798	0.5069	146.01	110.23	0.007795	0.041
76	14	0.009097	0.5069	170.34	132.28	0.009095	0.029
76	14	0.010397	0.5069	194.67	154.88	0.010401	-0.034
76	14	0.018837	0.5069	352.70	311.13	0.018834	0.014
76	14	0.025488	0.5069	477.25	439.90	0.025485	0.013

76	14	0.033724	0.5069	631.45	600.87	0.033722	0.006
76	14	0.039421	0.5069	738.12	713.09	0.039407	0.035
76	14	0.047257	0.5069	884.84	868.17	0.047260	-0.008
76	14	0.051604	0.5069	966.24	953.93	0.051614	-0.019
76	14	0.059660	0.5069	1117.08	1113.96	0.059636	0.041
76	14	0.066112	0.5069	1237.89	1242.04	0.066090	0.034
76	14	0.075989	0.5069	1422.83	1438.54	0.075967	0.029

$T_{i,w}$	$T_{i,a}$	$M_{i,w}$	M_a	G_w	Re_w	$M_{o,w}$	(%MB)
^oC	^oC	kg/s	kg/s	kg/m^{2}s		kg/s	
76	14	0.000882	0.5069	16.52	34.12	0.000880	0.248
76	14	0.001323	0.5069	24.78	51.38	0.001323	0.051
76	14	0.001764	0.5069	33.04	68.73	0.001767	-0.129
76	14	0.002206	0.5069	41.30	86.34	0.002212	-0.291
76	14	0.002647	0.5069	49.56	103.88	0.002650	-0.117
76	14	0.003088	0.5069	57.82	122.01	0.003090	-0.067
76	14	0.003529	0.5069	66.08	140.32	0.003534	-0.146
76	14	0.018837	0.5069	352.70	877.32	0.018836	0.005
76	14	0.025488	0.5069	477.25	1213.63	0.025477	0.045
76	14	0.033724	0.5069	631.45	1634.50	0.033720	0.013
76	14	0.039421	0.5069	738.12	1926.46	0.039438	-0.044
76	14	0.047257	0.5069	884.84	2326.87	0.047241	0.032
76	14	0.051604	0.5069	966.24	2550.71	0.051622	-0.035
76	14	0.059660	0.5069	1117.08	2964.09	0.059645	0.025
76	14	0.066112	0.5069	1237.89	3294.11	0.066104	0.013
76	14	0.075989	0.5069	1422.83	3802.12	0.075974	0.020

Table B.2.	Error in Heat Balance							
Inlet Temp. (Liquid)	Inlet Temp. (Air)	Mass Flow Rate Air	Liquid Mass flux (Channel Inlet)	Liquid Re (Channel Inlet)	Heat Transfer Rate Air	Heat Transfer Rate (Liquid)	Average Heat Transfer	Error in Heat Balance
$T_{i,oil}$	$T_{i,a}$	M_a	G_{oil}	Re_{oil}	Q_a	Q_{oil}	Q_{avg}	(%HB)
^{o}C	^{o}C	kg/s	kg/m^{2}s		w	w	w	
76	14	0.5069	352.70	16.60	892.45	898.72	895.58	0.700
76	14	0.5069	477.25	24.16	986.79	993.69	990.24	0.696
76	14	0.5069	631.45	33.41	1051.78	1041.05	1046.42	-1.025
76	14	0.5069	738.12	39.90	1089.79	1087.40	1088.60	-0.220
76	14	0.5069	884.84	49.29	1108.35	1098.49	1103.42	-0.893
76	14	0.5069	966.24	54.44	1105.43	1116.64	1111.03	1.009
76	14	0.5069	1117.08	64.38	1148.59	1147.14	1147.86	-0.126
76	14	0.5069	1237.89	75.02	1153.96	1152.72	1153.34	-0.107
76	14	0.5069	1422.83	83.94	1165.22	1167.56	1166.39	0.201
76	14	0.5069	1898.19	114.01	1179.71	1197.59	1188.65	1.504
76	14	0.5069	2372.74	144.24	1232.14	1248.84	1240.49	1.3467
$T_{i,atf}$	$T_{i,a}$	M_a	G_{atf}	Re_{atf}	Q_a	Q_{atf}	Q_{avg}	(%HB)
^{o}C	^{o}C	kg/s	kg/m^{2}s		w	w	w	
76	14	0.5069	352.70	26.72	915.41	915.94	915.68	0.058
76	14	0.5069	477.25	38.18	998.81	1001.62	1000.22	0.281
76	14	0.5069	631.45	53.06	1048.11	1052.60	1050.36	0.427
76	14	0.5069	738.12	64.18	1089.37	1089.74	1089.56	0.034
76	14	0.5069	884.84	77.62	1124.36	1127.24	1125.80	0.256
76	14	0.5069	966.24	85.51	1140.06	1139.89	1139.97	-0.015
76	14	0.5069	1117.08	100.19	1177.38	1185.94	1181.66	0.725
76	14	0.5069	1237.89	112.54	1154.98	1159.10	1157.04	0.356
76	14	0.5069	1422.83	130.53	1173.48	1180.81	1177.15	0.623
$T_{i,g}$	$T_{i,a}$	M_a	G_g	Re_g	Q_a	Q_g	Q_{avg}	(%HB)
^{o}C	^{o}C	kg/s	kg/m^{2}s		w	w	w	
76	14	0.5069	73.00	50.28	496.14	499.18	497.66	0.610
76	14	0.5069	97.34	68.98	625.15	625.32	625.23	0.028
76	14	0.5069	121.67	89.04	724.00	724.53	724.27	0.073
76	14	0.5069	146.01	110.23	798.42	802.69	800.55	0.533
76	14	0.5069	170.34	132.28	863.90	864.67	864.28	0.089
76	14	0.5069	194.67	154.88	917.92	916.41	917.16	-0.165
76	14	0.5069	352.70	311.13	1105.85	1100.29	1103.07	-0.504
76	14	0.5069	477.25	439.90	1150.04	1156.81	1153.42	0.587

$T_{i,w}$	$T_{i,a}$	M_a	G_w	Re_w	Q_a	Q_w	Q_{avg}	(%HB)
76	14	0.5069	631.45	600.87	1210.00	1206.14	1208.07	-0.319
76	14	0.5069	738.12	713.09	1227.89	1230.95	1229.42	0.249
76	14	0.5069	884.84	868.17	1249.56	1247.91	1248.73	-0.132
76	14	0.5069	966.24	953.93	1269.34	1261.72	1265.53	-0.602
76	14	0.5069	1117.08	1113.96	1281.59	1278.84	1280.22	-0.215
76	14	0.5069	1237.89	1242.04	1293.36	1289.07	1291.22	-0.332
76	14	0.5069	1422.83	1438.54	1302.49	1305.07	1303.78	0.1978

$T_{i,w}$	$T_{i,a}$	M_a	G_w	Re_w	Q_a	Q_w	Q_{avg}	(%HB)
^oC	^oC	kg/s	kg/m^2s		w	w	w	
76	14	0.5069	16.52	34.12	-150.74	150.36	150.55	-0.253
76	14	0.5069	24.78	51.38	-216.55	217.08	216.82	0.247
76	14	0.5069	33.04	68.73	-281.66	283.59	282.62	0.683
76	14	0.5069	41.30	86.34	-349.01	349.23	349.12	0.062
76	14	0.5069	49.56	103.88	-414.45	414.31	414.38	-0.035
76	14	0.5069	57.82	122.01	-469.71	472.23	470.97	0.535
76	14	0.5069	66.08	140.32	-525.50	527.90	526.70	0.455
76	14	0.5069	352.70	877.32	-1149.55	1150.38	1149.96	0.072
76	14	0.5069	477.25	1213.63	-1215.03	1222.13	1218.58	0.582
76	14	0.5069	631.45	1634.50	-1245.28	1253.09	1249.18	0.625
76	14	0.5069	738.12	1926.46	-1268.99	1262.86	1265.93	-0.484
76	14	0.5069	884.84	2326.87	-1304.24	1300.46	1302.35	-0.290
76	14	0.5069	966.24	2550.71	-1301.08	1292.00	1296.54	-0.700
76	14	0.5069	1117.08	2964.09	-1310.15	1313.11	1311.63	0.226
76	14	0.5069	1237.89	3294.11	-1335.57	1334.98	1335.27	-0.044
76	14	0.5069	1422.83	3802.12	-1331.97	1336.59	1334.28	0.346

Inlet Temp. (Liquid)	Inlet Temp. (Air)	Mass Flow-rate (Air)	Liquid Mass flux (Channel Inlet)	Liquid Re (Channel Inlet)	Liquid Outlet Temp.	Liquid Temp. Drop	Air Outlet Temp.	Air Temp. Rise

Table B.3. $T_{o,l}$, $T_{o,a}$, ΔT_l, and ΔT_a

| $T_{i,oil}$ | $T_{i,a}$ | M_a | G_{oil} | Re_{oil} | $T_{o,oil}$ | ΔT_{oil} | $T_{o,a}$ | ΔT_a |
^oC	^oC	kg/s	kg/m^{2}s		^oC	^oC	^oC	^oC
76	14	0.5069	352.70	16.60	52.19	23.81	15.75	1.75
76	14	0.5069	477.25	24.16	56.43	19.57	15.93	1.93
76	14	0.5069	631.45	33.41	60.37	15.63	16.06	2.06
76	14	0.5069	738.12	39.90	61.94	14.06	16.14	2.14
76	14	0.5069	884.84	49.29	64.02	11.98	16.17	2.17
76	14	0.5069	966.24	54.44	64.79	11.21	16.17	2.17
76	14	0.5069	1117.08	64.38	65.93	10.07	16.25	2.25
76	14	0.5069	1237.89	75.02	66.79	9.21	16.26	2.26
76	14	0.5069	1422.83	83.94	67.77	8.23	16.28	2.28
76	14	0.5069	1898.19	114.01	70.46	5.54	16.31	2.31
76	14	0.5069	2372.74	144.24	71.37	4.63		

| $T_{i,atf}$ | $T_{i,a}$ | M_a | G_{atf} | Re_{atf} | $T_{o,atf}$ | ΔT_{atf} | $T_{o,a}$ | ΔT_a |
^oC	^oC	kg/s	kg/m^{2}s		^oC	^oC	^oC	^oC
76	14	0.5069	352.70	26.72	52.96	23.04	15.79	1.79
76	14	0.5069	477.25	38.18	57.45	18.55	15.96	1.96
76	14	0.5069	631.45	53.06	61.31	14.69	16.05	2.05
76	14	0.5069	738.12	64.18	63.02	12.98	16.14	2.14
76	14	0.5069	884.84	77.62	64.02	11.98	16.37	2.37
76	14	0.5069	966.24	85.51	64.84	11.16	16.23	2.23
76	14	0.5069	1117.08	100.19	66.70	9.30	16.31	2.31
76	14	0.5069	1237.89	112.54	67.80	8.20	16.30	2.30
76	14	0.5069	1422.83	130.53	68.74	7.26	16.30	2.30

| $T_{i,g}$ | $T_{i,a}$ | M_a | G_g | Re_g | $T_{o,g}$ | ΔT_g | $T_{o,a}$ | ΔT_a |
^oC	^oC	kg/s	kg/m^{2}s		^oC	^oC	^oC	^oC
76	14	0.5069	73.00	50.28	37.99	38.01	14.97	0.97
76	14	0.5069	97.34	68.98	40.31	35.69	15.23	1.23
76	14	0.5069	121.67	89.04	42.95	33.05	15.42	1.42
76	14	0.5069	146.01	110.23	45.52	30.48	15.56	1.56
76	14	0.5069	170.34	132.28	47.88	28.12	15.69	1.69
76	14	0.5069	194.67	154.88	49.93	26.07	15.80	1.80
76	14	0.5069	352.70	311.13	58.78	17.22	16.17	2.17
76	14	0.5069	477.25	439.90	62.64	13.36	16.25	2.25

$T_{i,w}$	$T_{i,a}$	M_a	G_w	Re_w	$T_{o,w}$	ΔT_w	$T_{o,a}$	ΔT_a
76	14	0.5069	631.45	600.87	65.48	10.52	16.37	2.37
76	14	0.5069	738.12	713.09	66.83	9.17	16.41	2.41
76	14	0.5069	884.84	868.17	68.24	7.76	16.45	2.45
76	14	0.5069	966.24	953.93	68.81	7.19	16.49	2.49
76	14	0.5069	1117.08	1113.96	69.72	6.28	16.51	2.51
76	14	0.5069	1237.89	1242.04	70.29	5.71	16.54	2.54
76	14	0.5069	1422.83	1438.54	70.97	5.03	16.55	2.55
$T_{i,w}$	$T_{i,a}$	M_a	G_w	Re_w	$T_{o,w}$	ΔT_w	$T_{o,a}$	ΔT_a
^{o}C	^{o}C	kg/s	kg/m^{2}s		^{o}C	^{o}C	^{o}C	^{o}C
76	14	0.5069	16.52	34.12	35.62	40.38	14.30	0.30
76	14	0.5069	24.78	51.38	36.06	39.94	14.42	0.42
76	14	0.5069	33.04	68.73	36.51	39.49	14.55	0.55
76	14	0.5069	41.30	86.34	37.16	38.84	14.68	0.68
76	14	0.5069	49.56	103.88	37.50	38.50	14.81	0.81
76	14	0.5069	57.82	122.01	38.37	37.63	14.92	0.92
76	14	0.5069	66.08	140.32	39.18	36.82	15.03	1.03
76	14	0.5069	352.70	877.32	60.98	15.02	16.25	2.25
76	14	0.5069	477.25	1213.63	64.22	11.78	16.38	2.38
76	14	0.5069	631.45	1634.50	66.87	9.13	16.44	2.44
76	14	0.5069	738.12	1926.46	68.10	7.90	16.49	2.49
76	14	0.5069	884.84	2326.87	69.25	6.75	16.56	2.56
76	14	0.5069	966.24	2550.71	69.83	6.17	16.55	2.55
76	14	0.5069	1117.08	2964.09	70.60	5.40	16.57	2.57
76	14	0.5069	1237.89	3294.11	71.04	4.96	16.62	2.62
76	14	0.5069	1422.83	3802.12	71.68	4.32	16.61	2.61

Table B.4. $T_{b,l}, T_{s,l}, T_{ser}$, and Dimensionless Temperature								
Inlet Temp. (Liq.)	Inlet Temp. (Air)	Mass Flow Rate (Air)	Liquid Mass Flux	Liquid Re	Liquid Bulk Temp.	Inner Surface Temp.	Dimen-sionless Temp.	Serpen-tine Temp.
$T_{i,oil}$	$T_{i,a}$	M_a	G_{oil}	Re_{oil}	$T_{b,oil}$	$T_{s,oil}$	$(\Delta T_l/\Delta T_{max})_{oil}$	$(T_{ser})_{oil}$
^oC	^oC	kg/s	kg/m^{2}s		^oC	^oC		^oC
76	14	0.5069	352.70	16.60	64.09	50.63	0.38	55.84
76	14	0.5069	477.25	24.16	66.22	53.83	0.32	60.27
76	14	0.5069	631.45	33.41	68.18	57.02	0.25	64.04
76	14	0.5069	738.12	39.90	68.97	58.06	0.23	65.41
76	14	0.5069	884.84	49.29	70.01	59.70	0.19	67.04
76	14	0.5069	966.24	54.44	70.39	60.19	0.18	67.57
76	14	0.5069	1117.08	64.38	70.97	60.92	0.16	68.37
76	14	0.5069	1237.89	75.02	71.39	61.60	0.15	68.97
76	14	0.5069	1422.83	83.94	71.89	62.33	0.13	69.71
76	14	0.5069	1898.19	114.01	73.23	65.30	0.09	70.88
76	14	0.5069	2372.74	144.24	73.69	65.90	0.07	71.40
$T_{i,atf}$	$T_{i,a}$	M_a	G_{atf}	Re_{atf}	$T_{b,atf}$	$T_{s,atf}$	$(\Delta T_l/\Delta T_{max})_{atf}$	$(T_{ser})_{atf}$
^oC	^oC	kg/s	kg/m^{2}s		^oC	^oC		^oC
76	14	0.5069	352.70	26.72	64.48	51.24	0.37	57.23
76	14	0.5069	477.25	38.18	66.73	54.39	0.30	61.53
76	14	0.5069	631.45	53.06	68.66	57.18	0.24	64.52
76	14	0.5069	738.12	64.18	69.51	58.37	0.21	65.78
76	14	0.5069	884.84	77.62	70.01	59.73	0.19	67.11
76	14	0.5069	966.24	85.51	70.42	60.35	0.18	67.73
76	14	0.5069	1117.08	100.19	71.35	61.05	0.15	68.49
76	14	0.5069	1237.89	112.54	71.90	62.92	0.13	69.95
76	14	0.5069	1422.83	130.53	72.37	62.92	0.12	69.95
$T_{i,g}$	$T_{i,a}$	M_a	G_g	Re_g	$T_{b,g}$	$T_{s,g}$	$(\Delta T_l/\Delta T_{max})_g$	$(T_{ser})_g$
^oC	^oC	kg/s	kg/m^{2}s		^oC	^oC		^oC
76	14	0.5069	73.00	50.28	56.99	34.80	0.61	28.66
76	14	0.5069	97.34	68.98	58.15	40.01	0.58	36.07
76	14	0.5069	121.67	89.04	59.47	44.21	0.53	42.10
76	14	0.5069	146.01	110.23	60.76	48.61	0.49	46.81
76	14	0.5069	170.34	132.28	61.94	51.38	0.45	50.56
76	14	0.5069	194.67	154.88	62.96	53.57	0.42	53.49
76	14	0.5069	352.70	311.13	67.39	59.96	0.28	63.43

76	14	0.5069	477.25	439.90	69.32	62.79	0.22	66.78
76	14	0.5069	631.45	600.87	70.74	64.76	0.17	69.00
76	14	0.5069	738.12	713.09	71.42	65.68	0.15	69.98
76	14	0.5069	884.84	868.17	72.12	66.65	0.13	70.96
76	14	0.5069	966.24	953.93	72.40	67.03	0.12	71.35
76	14	0.5069	1117.08	1113.96	72.86	67.68	0.10	71.95
76	14	0.5069	1237.89	1242.04	73.14	68.09	0.09	72.32
76	14	0.5069	1422.83	1438.54	73.49	68.57	0.08	72.75
$T_{i,w}$	$T_{i,a}$	M_a	G_w	Re_w	$T_{b,w}$	$T_{s,w}$	$(\Delta T_l/\Delta T_{max})_w$	$(T_{ser})_w$
^oC	^oC	kg/s	kg/m^{2}s		^oC	^oC		^oC
76	14	0.5069	16.52	34.12	55.81	20.37	0.65	14.35
76	14	0.5069	24.78	51.38	56.03	23.16	0.64	15.48
76	14	0.5069	33.04	68.73	56.26	26.31	0.64	17.54
76	14	0.5069	41.30	86.34	56.58	29.17	0.63	20.35
76	14	0.5069	49.56	103.88	56.75	31.76	0.62	23.36
76	14	0.5069	57.82	122.01	57.18	34.43	0.61	26.62
76	14	0.5069	66.08	140.32	57.59	36.85	0.59	29.78
76	14	0.5069	352.70	877.32	68.49	62.46	0.24	65.36
76	14	0.5069	477.25	1213.63	70.11	64.75	0.19	68.12
76	14	0.5069	631.45	1634.50	71.43	66.60	0.15	70.11
76	14	0.5069	738.12	1926.46	72.05	67.46	0.13	70.99
76	14	0.5069	884.84	2326.87	72.62	68.23	0.11	71.78
76	14	0.5069	966.24	2550.71	72.91	68.66	0.10	72.16
76	14	0.5069	1117.08	2964.09	73.30	69.20	0.09	72.66
76	14	0.5069	1237.89	3294.11	73.52	69.47	0.08	72.95
76	14	0.5069	1422.83	3802.12	73.84	69.96	0.07	73.35

Table B.5.		Liquid-side Pressure Drop				
Inlet Temp. (Liquid)	Inlet Temp. (Air)	Mass Flow-rate (Air)	Liquid Mass flux (Channel Inlet)	Liquid Re (Channel Inlet)	Liquid-side Pressure Drop	Liquid-side Pressure Drop
$T_{i,oil}$	$T_{i,a}$	M_a	G_{oil}	Re_{oil}	ΔP_{oil}	ΔP_{oil}
^{o}C	^{o}C	kg/s	kg/m^{2}s		kPa	psi
76	14	0.5069	352.70	16.60	321.46	46.62
76	14	0.5069	477.25	24.16	393.34	57.05
76	14	0.5069	631.45	33.41	478.82	69.45
76	14	0.5069	738.12	39.90	545.70	79.15
76	14	0.5069	884.84	49.29	633.31	91.85
76	14	0.5069	966.24	54.44	685.33	99.40
76	14	0.5069	1117.08	64.38	784.14	113.73
76	14	0.5069	1237.89	75.02	861.38	124.93
76	14	0.5069	1422.83	83.94	984.27	142.76
76	14	0.5069	1898.19	114.01	1306.38	189.48
76	14	0.5069	2372.74	144.24	1648.51	239.10
$T_{i,atf}$	$T_{i,a}$	M_a	G_{atf}	Re_{atf}	$\Delta patf$	$\Delta patf$
^{o}C	^{o}C	kg/s	kg/m^{2}s		kPa	psi
76	14	0.5069	352.70	26.72	177.82	25.79
76	14	0.5069	477.25	38.18	207.16	30.05
76	14	0.5069	631.45	53.06	239.04	34.67
76	14	0.5069	738.12	64.18	263.79	38.26
76	14	0.5069	884.84	77.62	295.62	42.88
76	14	0.5069	966.24	85.51	314.45	45.61
76	14	0.5069	1117.08	100.19	351.33	50.96
76	14	0.5069	1237.89	112.54	374.73	54.35
76	14	0.5069	1422.83	130.53	421.59	61.15
$T_{i,g}$	$T_{i,a}$	M_a	G_g	Re_g	ΔP_g	ΔP_g
^{o}C	^{o}C	kg/s	kg/m^{2}s		kPa	psi
76	14	0.5069	73.00	50.28	4.58	0.66
76	14	0.5069	97.34	68.98	5.42	0.79
76	14	0.5069	121.67	89.04	6.10	0.88
76	14	0.5069	146.01	110.23	6.80	0.99
76	14	0.5069	170.34	132.28	7.51	1.09
76	14	0.5069	194.67	154.88	8.28	1.20
76	14	0.5069	352.70	311.13	13.92	2.02
76	14	0.5069	477.25	439.90	19.26	2.79

$T_{i,w}$	$T_{i,a}$	M_a	G_w	Re_w	ΔP_w	ΔP_w
76	14	0.5069	631.45	600.87	26.87	3.90
76	14	0.5069	738.12	713.09	32.69	4.74
76	14	0.5069	884.84	868.17	41.75	6.05
76	14	0.5069	966.24	953.93	47.40	6.87
76	14	0.5069	1117.08	1113.96	58.20	8.44
76	14	0.5069	1237.89	1242.04	68.06	9.87
76	14	0.5069	1422.83	1438.54	83.38	12.09
$T_{i,w}$	$T_{i,a}$	M_a	G_w	Re_w	ΔP_w	ΔP_w
^{o}C	^{o}C	kg/s	kg/m^{2}s		kPa	psi
76	14	0.5069	16.52	34.12	0.43	0.06
76	14	0.5069	24.78	51.38	0.61	0.09
76	14	0.5069	33.04	68.73	0.78	0.11
76	14	0.5069	41.30	86.34	0.94	0.14
76	14	0.5069	49.56	103.88	1.07	0.16
76	14	0.5069	57.82	122.01	1.18	0.17
76	14	0.5069	66.08	140.32	1.30	0.19
76	14	0.5069	352.70	877.32	6.50	0.94
76	14	0.5069	477.25	1213.63	9.98	1.45
76	14	0.5069	631.45	1634.50	15.26	2.21
76	14	0.5069	738.12	1926.46	19.66	2.85
76	14	0.5069	884.84	2326.87	26.68	3.87
76	14	0.5069	966.24	2550.71	30.63	4.44
76	14	0.5069	1117.08	2964.09	38.53	5.59
76	14	0.5069	1237.89	3294.11	49.04	7.11
76	14	0.5069	1422.83	3802.12	58.14	8.43

Table B.6. Liquid Dynamic Viscosity and Correction Factor							
Inlet Temp. (Liquid)	Inlet Temp. (Air)	Mass Flow-rate (Air)	Liquid Mass flux (Channel Inlet)	Liquid Re Channel	Liquid Dynamic Viscosity	Liquid Viscosity at $T_{i,s}$	Vicsosity Correction Factor
$T_{i,oil}$	$T_{i,a}$	M_a	G_{oil}	Re_{oil}	$\mu_{b,oil}$	$\mu_{s,oil}$	$(\mu_b/\mu_s)_{oil}^{0.14}$
^oC	^oC	kg/s	kg/m^{2}s		kg/ms	kg/ms	
76	14	0.5069	352.70	16.60	0.02125	0.03265	0.94164
76	14	0.5069	477.25	24.16	0.01975	0.02950	0.94538
76	14	0.5069	631.45	33.41	0.01890	0.02658	0.95341
76	14	0.5069	738.12	39.90	0.01850	0.02587	0.95414
76	14	0.5069	884.84	49.29	0.01795	0.02475	0.95602
76	14	0.5069	966.24	54.44	0.01775	0.02425	0.95726
76	14	0.5069	1117.08	64.38	0.01735	0.02350	0.95841
76	14	0.5069	1237.89	75.02	0.01650	0.02260	0.95691
76	14	0.5069	1422.83	83.94	0.01695	0.02225	0.96263
76	14	0.5069	1898.19	114.01	0.01665	0.02050	0.97130
76	14	0.5069	2372.74	144.24	0.01645	0.02000	0.97301
$T_{i,atf}$	$T_{i,a}$	M_a	G_{atf}	Re_{atf}	$\mu_{b,atf}$	$\mu_{s,atf}$	$(\mu_b/\mu_s)_{atf}^{0.14}$
^oC	^oC	kg/s	kg/m^{2}s		kg/ms	kg/ms	
76	14	0.5069	352.70	26.72	0.01320	0.01940	0.94752
76	14	0.5069	477.25	38.18	0.01250	0.01770	0.95247
76	14	0.5069	631.45	53.06	0.01190	0.01630	0.95691
76	14	0.5069	738.12	64.18	0.01150	0.01570	0.95735
76	14	0.5069	884.84	77.62	0.01140	0.01510	0.96141
76	14	0.5069	966.24	85.51	0.01130	0.01470	0.96384
76	14	0.5069	1117.08	100.19	0.01115	0.01440	0.96482
76	14	0.5069	1237.89	112.54	0.01100	0.01360	0.97073
76	14	0.5069	1422.83	130.53	0.01090	0.01330	0.97252
Inlet Temp. Liquid	Inlet Temp. Air	Mass Flow-rate Air	Liquid Mass flux Channel_in	Liquid Re Channel_in	Liquid Dynamic Viscosity	Liquid Viscosity at Ti,s	Vicsosity Correction Factor
$T_{i,g}$	$T_{i,a}$	M_a	G_g	Re_g	$\mu_{b,g}$	$\mu_{s,g}$	$(\mu_b/\mu_s)_g^{0.14}$
^oC	^oC	kg/s	kg/m^{2}s		kg/ms	kg/ms	
76	14	0.5069	73.00	50.28	0.00145	0.00258	0.92274
76	14	0.5069	97.34	68.98	0.00141	0.00224	0.93716
76	14	0.5069	121.67	89.04	0.00137	0.00201	0.94751
76	14	0.5069	146.01	110.23	0.00132	0.00179	0.95855

$T_{i,w}$	$T_{i,a}$	M_a	G_w	Re_w	$\mu_{b,w}$	$\mu_{s,w}$	$(\mu_b/\mu_s)_w^{0.14}$
76	14	0.5069	170.34	132.28	0.00129	0.00167	0.96425
76	14	0.5069	194.67	154.88	0.00126	0.00158	0.96844
76	14	0.5069	352.70	311.13	0.00113	0.00135	0.97580
76	14	0.5069	477.25	439.90	0.00108	0.00126	0.97905
76	14	0.5069	631.45	600.87	0.00105	0.00120	0.98105
76	14	0.5069	738.12	713.09	0.00104	0.00118	0.98192
76	14	0.5069	884.84	868.17	0.00102	0.00115	0.98288
76	14	0.5069	966.24	953.93	0.00101	0.00114	0.98322
76	14	0.5069	1117.08	1113.96	0.00100	0.00113	0.98390
76	14	0.5069	1237.89	1242.04	0.00100	0.00112	0.98434
76	14	0.5069	1422.83	1438.54	0.00099	0.00110	0.98479
$T_{i,w}$	$T_{i,a}$	M_a	G_w	Re_w	$\mu_{b,w}$	$\mu_{s,w}$	$(\mu_b/\mu_s)_w^{0.14}$
^oC	^oC	kg/s	kg/m^{2}s		kg/ms	kg/ms	
76	14	0.5069	16.52	34.12	0.00048	0.00097	0.90748
76	14	0.5069	24.78	51.38	0.00048	0.00091	0.91549
76	14	0.5069	33.04	68.73	0.00048	0.00084	0.92437
76	14	0.5069	41.30	86.34	0.00048	0.00079	0.93194
76	14	0.5069	49.56	103.88	0.00048	0.00075	0.93883
76	14	0.5069	57.82	122.01	0.00047	0.00071	0.94522
76	14	0.5069	66.08	140.32	0.00047	0.00068	0.95079
76	14	0.5069	352.70	877.32	0.00040	0.00044	0.98813
76	14	0.5069	477.25	1213.63	0.00039	0.00042	0.98964
76	14	0.5069	631.45	1634.50	0.00039	0.00041	0.99080
76	14	0.5069	738.12	1926.46	0.00038	0.00041	0.99132
76	14	0.5069	884.84	2326.87	0.00038	0.00040	0.99175
76	14	0.5069	966.24	2550.71	0.00038	0.00040	0.99203
76	14	0.5069	1117.08	2964.09	0.00038	0.00040	0.99235
76	14	0.5069	1237.89	3294.11	0.00038	0.00040	0.99246
76	14	0.5069	1422.83	3802.12	0.00037	0.00039	0.99280

Table B.7.		Liquid Density, Conductivity, Specific Heat, and Prandtl Number						
Inlet Temp. (Liquid)	Inlet Temp. (Air)	Mass Flow-rate (Air)	Liquid Mass flux (Channel Inlet)	Liquid Re (Channel Inlet)	Liquid Density	Liquid Thermal Conductivity	Liquid Specific Heat	Liquid Pr
$T_{i,oil}$	$T_{i,a}$	M_a	G_{oil}	Re_{oil}	$\rho_{b,oil}$	$k_{b,oil}$	$Cp_{b,oil}$	$Pr_{b,oil}$
°C	°C	kg/s	kg/m²s		kg/m³	w/mK	j/kgK	
76	14	0.5069	352.70	16.60	829.20	0.13279	2088	334.14
76	14	0.5069	477.25	24.16	827.60	0.13262	2097	312.29
76	14	0.5069	631.45	33.41	826.60	0.13247	2106	300.48
76	14	0.5069	738.12	39.90	826.00	0.13236	2109	294.78
76	14	0.5069	884.84	49.29	825.40	0.13234	2113	286.61
76	14	0.5069	966.24	54.44	825.10	0.13229	2117	284.05
76	14	0.5069	1117.08	64.38	824.60	0.13223	2119	278.05
76	14	0.5069	1237.89	75.02	824.40	0.13219	2122	264.88
76	14	0.5069	1422.83	83.94	823.70	0.13216	2125	272.55
76	14	0.5069	1898.19	114.01	823.40	0.13207	2127	268.16
76	14	0.5069	2372.74	144.24	823.20	0.13205	2129	265.22
$T_{i,atf}$	$T_{i,a}$	M_a	G_{atf}	Re_{atf}	$\rho_{b,atf}$	$k_{b,atf}$	$Cp_{b,atf}$	$Pr_{b,atf}$
°C	°C	kg/s	kg/m²s		kg/m³	w/mK	j/kgK	
76	14	0.5069	352.70	26.72	839.70	0.15465	2109	179.97
76	14	0.5069	477.25	38.18	838.20	0.15425	2116	171.43
76	14	0.5069	631.45	53.06	837.00	0.15405	2124	164.07
76	14	0.5069	738.12	64.18	836.60	0.15385	2128	159.06
76	14	0.5069	884.84	77.62	836.10	0.15375	2132	158.08
76	14	0.5069	966.24	85.51	835.60	0.15365	2133	156.87
76	14	0.5069	1117.08	100.19	835.40	0.15355	2135	155.03
76	14	0.5069	1237.89	112.54	835.00	0.15350	2138	153.18
76	14	0.5069	1422.83	130.53	834.70	0.15335	2140	152.11
$T_{i,g}$	$T_{i,a}$	M_a	G_g	Re_g	$\rho_{b,g}$	$k_{b,g}$	$Cp_{b,g}$	$Pr_{b,g}$
°C	°C	kg/s	kg/m²s		kg/m³	w/mK	j/kgK	
76	14	0.5069	73.00	50.28	1035.40	0.45313	3367	10.79
76	14	0.5069	97.34	68.98	1034.80	0.45384	3370	10.48
76	14	0.5069	121.67	89.04	1034.10	0.45464	3373	10.14
76	14	0.5069	146.01	110.23	1033.40	0.45541	3376	9.82
76	14	0.5069	170.34	132.28	1032.80	0.45611	3379	9.54
76	14	0.5069	194.67	154.88	1032.20	0.45670	3381	9.31
76	14	0.5069	352.70	311.13	1029.80	0.45922	3392	8.37
76	14	0.5069	477.25	439.90	1028.80	0.46027	3396	8.01

$T_{i,w}$	$T_{i,a}$	M_a	G_w	Re_w	$\rho_{b,w}$	$k_{b,w}$	$Cp_{b,w}$	$Pr_{b,w}$
76	14	0.5069	631.45	600.87	1028.10	0.46104	3400	7.75
76	14	0.5069	738.12	713.09	1027.70	0.46140	3402	7.63
76	14	0.5069	884.84	868.17	1027.30	0.46177	3403	7.51
76	14	0.5069	966.24	953.93	1027.20	0.46192	3404	7.46
76	14	0.5069	1117.08	1113.96	1026.90	0.46216	3405	7.39
76	14	0.5069	1237.89	1242.04	1026.80	0.46230	3406	7.34
76	14	0.5069	1422.83	1438.54	1026.60	0.46248	3407	7.29

| $T_{i,w}$ | $T_{i,a}$ | M_a | G_w | Re_w | $\rho_{b,w}$ | $k_{b,w}$ | $Cp_{b,w}$ | $Pr_{b,w}$ |
^oC	^oC	kg/s	kg/m^{2}s		kg/m^3	w/mK	j/kgK	
76	14	0.5069	16.52	34.12	984.96	0.65001	4066	3.03
76	14	0.5069	24.78	51.38	984.85	0.65024	4066	3.02
76	14	0.5069	33.04	68.73	984.74	0.65045	4066	3.00
76	14	0.5069	41.30	86.34	984.59	0.65077	4066	2.99
76	14	0.5069	49.56	103.88	984.50	0.65093	4066	2.98
76	14	0.5069	57.82	122.01	984.29	0.65135	4066	2.96
76	14	0.5069	66.08	140.32	984.08	0.65175	4066	2.94
76	14	0.5069	352.70	877.32	978.23	0.66148	4067	2.47
76	14	0.5069	477.25	1213.63	977.29	0.66279	4067	2.41
76	14	0.5069	631.45	1634.50	976.52	0.66383	4067	2.37
76	14	0.5069	738.12	1926.46	976.15	0.66431	4067	2.35
76	14	0.5069	884.84	2326.87	975.81	0.66475	4067	2.33
76	14	0.5069	966.24	2550.71	975.63	0.66497	4067	2.32
76	14	0.5069	1117.08	2964.09	975.40	0.66526	4068	2.30
76	14	0.5069	1237.89	3294.11	975.27	0.66543	4068	2.30
76	14	0.5069	1422.83	3802.12	975.07	0.66567	4068	2.29

Table B.8. Br_l, h_l, and Nu_l

Inlet Temp. (Liquid)	Inlet Temp. (Air)	Mass Flow-rate (Air)	Liquid Mass flux (Channel Inlet)	Liquid Re (Channel Inlet)	Liquid Br	Liquid h	Liquid Nu
$T_{i,oil}$	$T_{i,a}$	M_a	G_{oil}	Re_{oil}	Br_{oil}	$h_{b,oil}$	$Nu_{b,oil}$
^{o}C	^{o}C	kg/s	kg/m^{2}s				
76	14	0.5069	352.70	16.60	2.81E-02	511	3.84
76	14	0.5069	477.25	24.16	5.06E-02	614	4.63
76	14	0.5069	631.45	33.41	9.17E-02	719	5.43
76	14	0.5069	738.12	39.90	1.24E-01	766	5.78
76	14	0.5069	884.84	49.29	1.80E-01	821	6.21
76	14	0.5069	966.24	54.44	2.14E-01	836	6.32
76	14	0.5069	1117.08	64.38	2.81E-01	877	6.63
76	14	0.5069	1237.89	75.02	3.34E-01	904	6.84
76	14	0.5069	1422.83	83.94	4.61E-01	937	7.09
76	14	0.5069	1898.19	114.01	9.56E-01	1150	8.71
76	14	0.5069	2372.74	144.24	1.49E+00	1222	9.25
$T_{i,atf}$	$T_{i,a}$	M_a	G_{atf}	Re_{atf}	Br_{atf}	$h_{b,atf}$	$Nu_{b,atf}$
^{o}C	^{o}C	kg/s	kg/m^{2}s				
76	14	0.5069	352.70	26.72	1.49E-02	531	3.43
76	14	0.5069	477.25	38.18	2.71E-02	622	4.03
76	14	0.5069	631.45	53.06	4.74E-02	702	4.56
76	14	0.5069	738.12	64.18	6.37E-02	751	4.88
76	14	0.5069	884.84	77.62	9.70E-02	840	5.47
76	14	0.5069	966.24	85.51	1.16E-01	869	5.65
76	14	0.5069	1117.08	100.19	1.49E-01	880	5.73
76	14	0.5069	1237.89	112.54	2.06E-01	989	6.44
76	14	0.5069	1422.83	130.53	2.55E-01	956	6.23
$T_{i,g}$	$T_{i,a}$	M_a	G_g	Re_g	Br_g	$h_{b,g}$	$Nu_{b,g}$
^{o}C	^{o}C	kg/s	kg/m^{2}s				
76	14	0.5069	73.00	50.28	8.81E-06	172	0.38
76	14	0.5069	97.34	68.98	1.97E-05	264	0.58
76	14	0.5069	121.67	89.04	3.25E-05	364	0.80
76	14	0.5069	146.01	110.23	5.72E-05	506	1.11
76	14	0.5069	170.34	132.28	8.63E-05	628	1.38
76	14	0.5069	194.67	154.88	1.23E-04	749	1.64
76	14	0.5069	352.70	311.13	4.47E-04	1139	2.48
76	14	0.5069	477.25	439.90	8.85E-04	1356	2.95

$T_{i,w}$	$T_{i,a}$	M_a	G_w	Re_w	Br_w	$h_{b,w}$	$Nu_{b,w}$
76	14	0.5069	631.45	600.87	1.63E-03	1551	3.36
76	14	0.5069	738.12	713.09	2.29E-03	1645	3.56
76	14	0.5069	884.84	868.17	3.40E-03	1754	3.80
76	14	0.5069	966.24	953.93	4.10E-03	1808	3.91
76	14	0.5069	1117.08	1113.96	5.62E-03	1898	4.11
76	14	0.5069	1237.89	1242.04	7.02E-03	1958	4.24
76	14	0.5069	1422.83	1438.54	9.46E-03	2034	4.40

| $T_{i,w}$ | $T_{i,a}$ | M_a | G_w | Re_w | Br_w | $h_{b,w}$ | $Nu_{b,w}$ |
°C	°C	kg/s	kg/m^{2}s				
76	14	0.5069	16.52	34.12	1.02E-07	33	0.05
76	14	0.5069	24.78	51.38	2.11E-07	51	0.08
76	14	0.5069	33.04	68.73	3.64E-07	72	0.11
76	14	0.5069	41.30	86.34	6.44E-07	98	0.15
76	14	0.5069	49.56	103.88	9.65E-07	127	0.20
76	14	0.5069	57.82	122.01	1.31E-06	159	0.24
76	14	0.5069	66.08	140.32	1.86E-06	195	0.30
76	14	0.5069	352.70	877.32	1.49E-04	1463	2.21
76	14	0.5069	477.25	1213.63	2.99E-04	1744	2.63
76	14	0.5069	631.45	1634.50	5.70E-04	1984	2.99
76	14	0.5069	738.12	1926.46	8.14E-04	2117	3.19
76	14	0.5069	884.84	2326.87	1.21E-03	2276	3.42
76	14	0.5069	966.24	2550.71	1.49E-03	2336	3.51
76	14	0.5069	1117.08	2964.09	2.05E-03	2452	3.69
76	14	0.5069	1237.89	3294.11	2.54E-03	2530	3.80
76	14	0.5069	1422.83	3802.12	3.48E-03	2635	3.96

Inlet Temp. (Liquid)	Inlet Temp. (Air)	Mass Flow-rate (Air)	Liquid Mass flux (Channel Inlet)	Liquid Re (Channel Inlet)	Corrected Nusselt Number	Corrected $Nu/Pr^{1/3}$
$T_{i,oil}$	$T_{i,a}$	M_a	G_{oil}	Re_{oil}	$Nu_{c,oil}$	$(Nu/Pr^{1/3})_{c,oil}$
^{o}C	^{o}C	kg/s	kg/m^{2}s			
76	14	0.5069	352.70	16.60	3.62	0.52
76	14	0.5069	477.25	24.16	4.37	0.64
76	14	0.5069	631.45	33.41	5.18	0.77
76	14	0.5069	738.12	39.90	5.52	0.83
76	14	0.5069	884.84	49.29	5.93	0.90
76	14	0.5069	966.24	54.44	6.05	0.92
76	14	0.5069	1117.08	64.38	6.36	0.97
76	14	0.5069	1237.89	75.02	6.54	1.02
76	14	0.5069	1422.83	83.94	6.82	1.05
76	14	0.5069	1898.19	114.01	8.46	1.31
76	14	0.5069	2372.74	144.24	9.00	1.40
$T_{i,atf}$	$T_{i,a}$	M_a	G_{atf}	Re_{atf}	$Nu_{c,atf}$	$(Nu/Pr^{1/3})_{c,atf}$
^{o}C	^{o}C	kg/s	kg/m^{2}s			
76	14	0.5069	352.70	26.72	3.25	0.58
76	14	0.5069	477.25	38.18	3.84	0.69
76	14	0.5069	631.45	53.06	4.36	0.80
76	14	0.5069	738.12	64.18	4.67	0.86
76	14	0.5069	884.84	77.62	5.25	0.97
76	14	0.5069	966.24	85.51	5.45	1.01
76	14	0.5069	1117.08	100.19	5.53	1.03
76	14	0.5069	1237.89	112.54	6.25	1.17
76	14	0.5069	1422.83	130.53	6.06	1.14
$T_{i,g}$	$T_{i,a}$	M_a	G_{g}	Re_{g}	$Nu_{c,g}$	$(Nu/Pr^{1/3})_{c,g}$
^{o}C	^{o}C	kg/s	kg/m^{2}s			
76	14	0.5069	73.00	50.28	0.35	0.16
76	14	0.5069	97.34	68.98	0.55	0.25
76	14	0.5069	121.67	89.04	0.76	0.35
76	14	0.5069	146.01	110.23	1.06	0.50
76	14	0.5069	170.34	132.28	1.33	0.63
76	14	0.5069	194.67	154.88	1.59	0.76
76	14	0.5069	352.70	311.13	2.42	1.19
76	14	0.5069	477.25	439.90	2.88	1.44

Table B.9.   Corrected Liquid-side Nusselt Number

$T_{i,w}$	$T_{i,a}$	M_a	G_w	Re_w	$Nu_{c,w}$	$(Nu/Pr^{1/3})_{c,w}$
76	14	0.5069	631.45	600.87	3.30	1.67
76	14	0.5069	738.12	713.09	3.50	1.78
76	14	0.5069	884.84	868.17	3.73	1.91
76	14	0.5069	966.24	953.93	3.85	1.97
76	14	0.5069	1117.08	1113.96	4.04	2.07
76	14	0.5069	1237.89	1242.04	4.17	2.15
76	14	0.5069	1422.83	1438.54	4.33	2.23
$T_{i,w}$	$T_{i,a}$	M_a	G_w	Re_w	$Nu_{c,w}$	$(Nu/Pr^{1/3})_{c,w}$
^{o}C	^{o}C	kg/s	kg/m^{2}s			
76	14	0.5069	16.52	34.12	0.05	0.03
76	14	0.5069	24.78	51.38	0.07	0.05
76	14	0.5069	33.04	68.73	0.10	0.07
76	14	0.5069	41.30	86.34	0.14	0.10
76	14	0.5069	49.56	103.88	0.18	0.13
76	14	0.5069	57.82	122.01	0.23	0.16
76	14	0.5069	66.08	140.32	0.28	0.20
76	14	0.5069	352.70	877.32	2.19	1.62
76	14	0.5069	477.25	1213.63	2.60	1.94
76	14	0.5069	631.45	1634.50	2.96	2.22
76	14	0.5069	738.12	1926.46	3.16	2.38
76	14	0.5069	884.84	2326.87	3.40	2.56
76	14	0.5069	966.24	2550.71	3.49	2.63
76	14	0.5069	1117.08	2964.09	3.66	2.77
76	14	0.5069	1237.89	3294.11	3.77	2.86
76	14	0.5069	1422.83	3802.12	3.93	2.98

REFERENCES

Adams, T. M., Abdel-Khalik, S. I., Jeter, S. M. & Qureshis, Z. H., (1998). An experimental investigation of single-phase forced convection in microchannels. International Journal of Heat and Mass transfer, 41(6-7), 851-857.

Albakhit, H. & Fakheri, A., (2005, July). A hybrid approach for full numerical simulation of heat exchangers, ASME Conference Proceedings, Heat Transfer Summer Conference (HT), San Francisco, CA, USA.

Ashrae. (1997). *Ashrae handbook : Fundamentals*. American Society of Heating, Refrigerating and Air-Conditioning Engineers. Atlanta, GA.

Bagalagel, S. M. & Sahin, A. Z., (2002). Design optimization of heat exchangers with high-viscosity fluids. International Journal of Energy Research, 26(10), 867–880.

Bahrami, M., Yovanovich, M. M. & Culham, J. R., (2007). A novel solution for pressure drop in singly connected microchannels of arbitrary cross-section. International Journal of Heat and Mass Transfer, 50(13-14), 2492–2502.

Bastanjian, S.A., Merzhanov, A.G. & Xudiaev, S.I., (1965). On hydrodynamic thermal explosion, Sov. Phys. Docl. 163, 133–136.

Bintoro, J. S., Akbarzadeh, A. & Mochizuki, M., (2005). A closed-loop electronics cooling by implementing single phase, impinging jet and mini channels heat exchanger. Applied Thermal Engineering, 25(17-18), 2740–2753.

Borrajo-Peláez, R., Ortega-Casanova, J. & Cejudo-López, J. M., (2010). A three-dimensional numerical study and comparison between the air side model and the air/water side model of a plain fin-and-tube heat exchanger. Applied Thermal Engineering, 30(13), 1608-1615.

Brandner, J. J., Anurjew, E., Buhn, L., Hansjosten, E., Henning, T., Schygulla, U., Wenka, A. & Schubert, K., (2006). Concept and realization of microstructure heat exchangers for enhanced heat transfer. Experimental Thermal and Fluid Science, 30(8), 801-809.

Can-Am Instruments Limited, 2851 Brighton Road, Oakville, Ontario, L6H 6C9

Cao, H., Chen, G. & Yuan, Q., (2010). Thermal performance of crossflow microchannel heat exchangers. Industrial & Engineering Chemistry Research, 49(13), 6215–6220.

Carluccio, E., Starace, G., Ficarella, A. & Laforgia, D., (2005). Numerical analysis of a cross-flow compact heat exchanger for vehicle applications, Applied Thermal Engineering, 25(13), 1995–2013.

Chen, C. S., (2009). The effects of temperature on heat transfer in microchannel flows. Modern Physics Letters B, 23(3), 265-268.

Chen, Y., Zhang, C., Shi, M. & Wu, J., (2009). Three-dimensional numerical simulation of heat and fluid flow in noncircular microchannel heat sinks. International Communications in Heat and Mass Transfer, 36(9), 917–920.

Cheng, Y. J., (2007). Numerical simulation of stacked microchannel heat sink with mixing-enhanced passive structure. International Communications in Heat and Mass Transfer, 34(3), 295–303.

Cole, K. D. & Çetin, B., (2011). The effect of axial conduction on heat transfer in a liquid microchannel flow. International Journal of Heat and Mass Transfer, 54(11–12), 2542–2549.

Dang, T. & Teng, J.-T., (2011). Comparisons of the heat transfer and pressure drop of the microchannel and minichannel heat exchangers. Heat and Mass Transfer, 47(10), 1311–1322.

Dasgupta, E. S., Siddiqui, F. A. & Fartaj, A., (2011). Experimental study on air side heat transfer and fluid flow characteristics of microchannel heat exchanger. SAE International Journal of Materials and Manufacturing, 4(1), 1198-1210.

Dehghandokht, M., Khan, M. G., Fartaj, A. & Sanaye, S., (2011). Flow and heat transfer characteristics of water and ethylene glycol-water in a multi-port serpentine meso-channel heat exchanger. International Journal of Thermal Sciences, 50(8), 1615-1627.

Dehghandokht, M., Khan, M. G., Fartaj, A. & Sanaye, S., (2011). Numerical study of fluid flow and heat transfer in a multi-port serpentine meso-channel heat exchanger. Applied Thermal Engineering, 31(10), 1588-1599.

Gamrat, G., Favre-Marinet, M. & Asendrych, D., (2005). Conduction and entrance effects on laminar liquid flow and heat transfer in rectangular microchannels. International Journal of Heat and Mass Transfer, 48(14), 2943–2954.

Gamrat, G., Favre-Marinet, M. & Asendrych, D., (2004, June). Numerical modeling of heat transfer in rectangular microchannels. ASME 2004 2nd International Conference on Microchannels and Minichannels (ICMM2004), Rochester, New York, USA.

Garimella, S., Dowling, W. J., Veen, M. D. V. & Killion, J. D., (2001). The effect of simultaneously developing flow on heat transfer in rectangular tubes. Heat Transfer Engineering, 22(6), 12-25.

Gruntfest,J., Young, J.P. & Johnson, N.L., (1964). Temperatures generated by the flow of liquids in pipers, Journal of Applied Physics. 35(1), 18–23.

Harms, T. M., Kazmierczak, M. J. & Gerner, F. M., (1999). Developing convective heat transfer in deep rectangular microchannels. International Journal of Heat and Fluid Flow, 20(2), 149-157.

Hetsroni, G., Mosyak, A., Pogrebnyak, E. & Yarin, L. P., (2005). Heat transfer in micro-channels: Comparison of experiments with theory and numerical results. International Journal of Heat and Mass Transfer, 48(25-26), 5580–5601.

Hettiarachchi, H. D. M., Golubovic, M., Worek, W. M. & Minkowycz, W. J., (2008). Three-dimensional laminar slip-flow and heat transfer in a rectangular microchannel with constant wall temperature. International Journal of Heat and Mass Transfer, 51(21-22), 5088–5096.

Ji, Y., Yuan, K. & Chung, J. N., (2006). Numerical simulation of wall roughness on gaseous flow and heat transfer in a microchannel. International Journal of Heat and Mass Transfer, 49(7-8), 1329–1339.

Jokar, A., Eckels, S. J. & Hosni, M. H., (2010). Single-phase flow in meso-channel compact heat exchangers for air conditioning applications. Heat Transfer Engineering, 31(1), 3–16.

Junqi, D., Jiangping, C., Zhijiu, C., Yimin, Z. & Wenfeng, Z., (2007). Heat transfer and pressure drop correlations for the wavy fin and flat tube heat exchangers. Applied Thermal Engineering, 27(11-12), 2066–2073.

Kahalerras, H. & Targui, N., (2008). Numerical analysis of heat transfer enhancement in a double pipe heat exchanger with porous fins. International Journal of Numerical Methods for Heat & Fluid Flow,18(5), 593-617.

Kandlikar, S. G., (2002). Fundamental issues related to flow boiling in minichannels and microchannels. Experimental Thermal and Fluid Science, 26(2-4), 389–407.

Kandlikar, S. G., (2006). Effect of liquid-vapor phase distribution on the heat transfer mechanisms during flow boiling in minichannels and microchannels. Heat Transfer Engineering, 27(1), 4–13.

Kandlikar, S. G., Joshi, S. & Tian, S., (2003). Effect of surface roughness on heat transfer and fluid flow characteristics at low Reynolds numbers in small diameter tubes. Heat Transfer Engineering, 24(3), 4-16.

Kays, W. M., and London, A. L., (1998). Compact heat exchangers: Third edition. Krieger Publishing Company, Florida.

Kemp, S. and Linden, J., (1990). Physical and chemical properties of a typical Automatic transmission fluid. SAE Technical Paper 902148, DOI: 10.4271/902148.

Khan, M. G. & Fartaj, A., (2011). A review on microchannel heat exchangers and potential applications. International Journal of Energy Research, 35(7), 553–582.

Khan, M. G. (2011). *Experimental investigation of heat transfer and pressure drop characteristics of water and glycol-water mixture in multi-port serpentine microchannel slab heat exchangers*. (Doctoral dissertation, University of Windsor).

Khan, M. G., Fartaj, A. & Ting, D., (2004). An experimental characterization of cross-flow cooling of air via an in-line elliptical tube array. International Journal of Heat and Fluid Flow, 25(4): 636–648.

Kim, N.-Y. Kim, D.-Y. & Byun, H.-W., (2011). Effect of inlet configuration on the refrigerant distribution in a parallel flow minichannel heat exchanger. International Journal of Refrigeration, 34(5), 1209-1221.

Koo, J. & Kleinstreuer, C., (2004). Viscous dissipation effects in microtubes and microchannels. International Journal of Heat and Mass Transfer, 47(14-16), 3159–3169.

Koo, J. & Kleinstreuer, C., (2004). Viscous dissipation effects in microtubes and microchannels. International Journal of Heat and Mass Transfer, 47(14-16), 3159–3169.

Kumar, V., Gupta, P., and Nigam, K. D. P., (2007). Fluid flow and heat transfer in curved tubes with temperature-dependent properties. Industrial & Engineering Chemistry Research., 46(10), 3226-3236.

Li, J., Wang, S., Cai, W. & Zhang, W., (2010). Numerical study on air-side performance of an integrated fin and micro-channel heat exchanger. Applied Thermal Engineering, 30(17-18), 2738-2745.

Liao, Q. & Jen, T. C., (2008). Numerical simulation of fluid flow and heat transfer in a curved square duct by using the lattice Boltzmann method. Numerical Heat Transfer, Part A, 54(5), 451–480.

Liu, J.-T., Peng, X.-F. & Yan, W.-M., (2007). Numerical study of fluid flow and heat transfer in microchannel cooling passages. International Journal of Heat and Mass Transfer, 50(9-10), 1855–1864.

Mahulikar, S. P. & Herwig, H., (2005). Theoretical investigation of scaling effects from macro-to-microscale convection due to variations in incompressible fluid properties. American Institute of Physics, Applied Physics Letters, 86 (1), 014105.

Mahulikar, S. P. & Herwig, H., (2006). Physical effects in laminar micro-convection due to variations in incompressible fluid properties. American Institute of Physics, Physics of Fluids, 18(7), 073601.

Mala, G. M. & Li, D., (1999). Flow characteristics of water in microtubes. International Journal of Heat and Fluid Flow, 20(2), 142–148.

Mala, G. M., Li, D., Werner, C., Jacobasch, H.-J. & Ning, Y. B., (1997). Flow characteristics of water through a microchannel between two parallel plates with electrokinetic effects. International Journal of Heat and Fluid Flow, 18(5), 489–496.

Maranzana, G., Perry, I. & Maillet, D., (2004). Mini- and micro-channels: Influence of axial conduction in the walls. International Journal of Heat and Mass Transfer, 47(17–18), 3993–4004.

Mehendale, S. S., Jacobi, A. M. & Shah, R. K., (2000). Fluid flow and heat transfer at micro- and meso-scales with applications to heat exchanger design. Applied Mechanics Reviews, 53(7), 175-193.

Mukherjee, A., Kandlikar, S. G. & Edel, Z. J., (2011). Numerical study of bubble growth and wall heat transfer during flow boiling in a microchannel. International Journal of Heat and Mass Transfer, 54(16-17), 3702–3718.

Nellis, G. F., (2003). A heat exchanger model that includes axial conduction, parasitic heat loads, and property variations. Cryogenics, 43(9), 523–538.

Ng, E. Y. K., Tso, C. P., Wen, Z. M. & Choo, K. F., (1999). Numerical simulation of flow and conjugate heat transfer in a microchannel for electronics cooling. Journal of Electronics Manufacturing, 9(2): 141-153, 1999.

Ngo, T. L., Kato, Y., Nikitin, K. & Ishizuka, T., (2007). Heat transfer and pressure drop correlations of microchannel heat exchanger with S-shaped and zigzag fins for carbon dioxide cycles, Experimental Thermal and Fluid Science, 32(2): 560-570, November 2007.

Nield, D. A., (2006). A Note on a Brinkman–Brinkman forced convection problem. Transport in Porous Media, 64(2), 185–188.

Nield, D. A., Kuznetsov, A. V. & Xiong, M., (2003). Thermally developing forced convection in a porous medium: Parallel plate channel with walls at uniform temperature, with axial conduction and viscous dissipation effects. International Journal of Heat and Mass Transfer, 46, 643–651.

Nield, D. A., Kuznetsov, A. V. & Xiong, M., (2004). Effects of viscous dissipation and flow work on forced convection in a channel filled by a saturated porous medium. Transport in Porous Media, 56(3), 351–367.

Nuntaphan, A., Kiatsiriroat, T., & Wang, C. C., (2005). Air side performance at low Reynolds number of cross-flow heat exchanger using crimped spiral fins. International Communications in Heat and Mass Transfer, 32(1-2), 151–165.

Oliet, C., Oliva, A., Castro, J. & Perez-Segarra, C.D., (2007), Parametric studies on automotive radiators. Applied Thermal Engineering, 27(11-12), 2033–2043.

Owhaib, W. & Palm, B., (2004). Experimental investigation of single-phase convective heat transfer in circular microchannels. Experimental Thermal and Fluid Science, 28(2-3), 105–110.

Paeng, J. G., Kim, K. H. & Hwan, Y., (2009). Experimental measurement and numerical computation of the air side convective heat transfer coefficients in a plate fin-tube heat exchanger. Journal of Mechanical Science and Technology, 23(2), 536~543.

Park, H. S., (2007). Dependency of heat transfer rate on the Brinkman number in microchannels. Dans 13th International Worshop on Thermal Investigations of ICs and Systems - Therminic 2007, Budapest, Hongrie.

Park, Y.-G. & Jacobi, A. M., (2009, Septermber). The air-side thermal-hydraulic performance of flat-tube heat exchangers with louvered, wavy, and plain fins under dry and wet conditions. Journal of Heat Transfer, 131(6), 061801.

Peiro, J., & Sherwin, S., (2005). Finite difference, finite element and finite volume methods for partial differential equations. (S. Yip ed., Vol. 1, pp. 1-32). Netherlands: Springer.

Peng, W., Jiang, P.-X., Wang, Y.-P. & Wei, B.-Y., (2011). Experimental and numerical investigation of convection heat transfer in channels with different types of ribs. Applied Thermal Engineering, 31(14-15), 2702-2708.

Qu, W. & Mudawa, I., (2002). Analysis of three-dimensional heat transfer in micro-channel heat sinks. International Journal of Heat and Mass Transfer, 45(19), 3973–3985.

Qu, W. & Mudawar, I., (2002). Experimental and numerical study of pressure drop and heat transfer in a single-phase micro-channel heat sink. International Journal of Heat and Mass Transfer, 45, 2549–2565.

Qu, W. Mudawar I., Lee, S. & Wereley, S. T., (2006). Experimental and computational investigation of flow development and pressure drop in a rectangular micro-channel. Journal of Electronic Packaging, 128(1), 1-9.

Ryu, J. H., Choi, D. H. & Kim, S. J., (2002). Numerical optimization of the thermal performance of a microchannel heat sink. International Journal of Heat and Mass Transfer, 45(13), 2823-2827.

Saitoh, S., Daiguji, H. & Hihara, E., (2005). Effect of tube diameter on boiling heat transfer of R-134a in horizontal small-diameter tubes. International Journal of Heat and Mass Transfer 48(23-24), 4973–4984.

Saitoh, S., Daiguji, H. & Hihara, E., (2007). Correlation for boiling heat transfer of R-134a in horizontal tubes including effect of tube diameter. International Journal of Heat and Mass Transfer, 50(25-26), 5215–5225.

Shah, R. K, and Sekulic, D. P., (2003). Fundamentals of heat exchanger design. John Wiley & Sons, Inc., USA.

Shang, Z. & Chen, S., (2011). Numerical investigation of diameter effect on heat transfer of supercritical water flows in horizontal round tubes. Applied Thermal Engineering, 31(4), 573-581.

Shell Nederland Verkoopmaatschappij B.V., Rivium Boulevard 156, 2909 LB, Capelle a/d Ijssel.

Shih, Y. C., (2003). Numerical study of heat transfer performance on the air side of evaporator for a domestic refrigerator, Numerical Heat Transfer, Part A, 44(8), 851–870.

Siddiqui, A., Dasgupta, E. S. & Fartaj, A., (2012). Experimental investigation of air side heat transfer and fluid flow performances of multi-port serpentine cross-flow mesochannel heat exchanger. International Journal of Heat and Fluid Flow, 33(1), 207–219.

Sobhan, C. B. & Garimella, S. V., (2011). A comparative analysis of studies on heat transfer and fluid flow in microchannels. Microscale Thermophysical Engineering, 5(4), 293–311.

Stignor, C. H., Sunden, B. & Fahlen, P., (2009). An experimental study of liquid-phase heat transfer in multiport minichannel tubes. Heat Transfer Engineering, 30(12), 941-951.

Taler, D. (2005). Prediction of heat transfer correlations for compact heat exchangers. Forschung im Ingenieurwesen, 69(3), 137–150.

Tang, L. H., Zeng, M. & Wang, Q. W., (2009). Experimental and numerical investigation on air-side performance of fin-and-tube heat exchangers with various fin patterns. Experimental Thermal and Fluid Science, 33(5): 818–827.

Tang, S. & Yang, K.-T., (2005). Thermal performance of a single-row fin-and-tube heat exchanger. Journal of Thermal Science, 14 (2), 172-180.

Tao, Y. B., He, Y. L., Huang, J., Wu, Z. G. & Tao, W. Q., (2007). Numerical study of local heat transfer coefficient and fin efficiency of wavy fin-and-tube heat exchangers. International Journal of Thermal Sciences, 46(8), 768–778.

Tian, L., He, Y., Tao, Y. & Tao, W., (2009). A comparative study on the air-side performance of wavy fin-and-tube heat exchanger with punched delta winglets in staggered and in-line arrangements. International Journal of Thermal Sciences, 48(9), 1765–1776.

Tso, C. P. & Mahulikar, S. P., (1998). The use of the Brinkman number for single phase forced convective heat transfer in microchannels. International Journal of Heat and Mass Transfer, 41(12), 1759-1769.

Tso, C. P. & Mahulikar, S. P., (1999). The role of the Brinkman number in analysing flow transitions in microchannels. International Journal of Heat and Mass Transfer, 42(10), 1813-1833.

Tso, C. P. & Mahulikar, S. P., (2000). Experimental verification of the role of Brinkman number in microchannels using local parameters. International Journal of Heat and Mass Transfer, 43(10), 1837-1849.

Tuckerman, D. B. & Pease, R. F. W., (1981). High-performance heat sinking for VLSI. IEEE Electron Device Letters, EDL-2(5).

van Rij, J., Ameel, T. & Harman, T., (2009). The effect of viscous dissipation and rarefaction on rectangular microchannel convective heat transfer. International Journal of Thermal Sciences, 48(2), 271–281.

Wang, C.-C. & Chi, K-Y., (2000). Heat transfer and friction characteristics of plain fin-and-tube heat exchangers, part I: new experimental data. International Journal of Heat and Mass Transfer, 43(15), 2681-2691.

Wang, C.-C., Chi, K.-Y. & Chang, C.-J., (2000). Heat transfer and friction characteristics of plain fin-and-tube heat exchangers, part II: Correlation. International Journal of Heat and Mass Transfer, 43(15), 2693-2700.

Wang, C.-C., Lee, C.-J., Chang, C.-T. & Lin, S.-P., (1998). Heat transfer and friction correlation for compact louvered fin-and-tube heat exchangers. International Journal of Heat and Mass Transfer, 42(11), 1945-1956.

Wu, H. Y. & Cheng, P., (2003). An experimental study of convective heat transfer in silicon microchannels with different surface conditions. International Journal of Heat and Mass Transfer, 46(14), 2547–2556.

Yataghene, M., Fayolle, F. & Legrand, J., (2009). Experimental and numerical analysis of heat transfer including viscous dissipation in a scraped surface heat exchanger. Chemical Engineering and Processing, 48(10), 1445–1456.

Zeldovich, Y.B., Barenblatt, G.I., Librovich, V.B., & Maxhviladse, G.M., (1985). Mathematical theory of combustion and explosion, Plenum, New York.

Zhang, T., Jia, L., Yang, L. & Jaluria, Y., (2010). Effect of viscous heating on heat transfer performance in microchannel slip flow region. International Journal of Heat and Mass Transfer, 53(21-22), 4927–4934.

Zhuo, L., Wen-Quan, T. & Ya-Ling, H., (2006). A numerical study of laminar convective heat transfer in microchannel. International Journal of Thermal Sciences, 45(12), 1140–1148.

VITA AUCTORIS

Name	Mohammed Ismail
Place of Birth	Debidwar, Comilla, Bangladesh
Year of Birth	1968
Education	1977. Completed elementary school education from Kutumbapur Govt. Primary School, Comilla, Bangladesh and promoted to Grade VI.
	1983. Completed Secondary School Certificate (SSC) from Gumta Ishaquia High School, Comilla, Bangladesh.
	1985. Completed Higher Secondary School Certificate (HSC) from Comilla Victoria Govt. College, Bangladesh
	1993. Received the Degree of Bachelor of Science (B.Sc.) in Mechanical Engineering from Bangladesh University of Engineering & Technology (BUET), Dhaka, Bangladesh.
	2011. Received the Degree of Master of Engineering (MEng) in Mechanical Engineering from University of Windsor, Ontario, Canada.
Experience	1994-2006. Worked as a mechanical engineer in Bangladesh
Current	2012. A candidate for the Degree of Master of Applied Science (M.A.Sc.) in Mechanical Engineering at the University of Windsor, ON, Canada